Fluorescence lifetime imaging at video rate – a new technique in photosynthesis research

vorgelegt von
Diplom - Physiker
Oliver Holub
aus Hannover

von der Fakultät II (Mathematik und Naturwissenschaften)
der Technischen Universität Berlin
zur Erlangung des akademischen Grades

Doktor der Naturwissenschaften
(Dr. rer. nat.)

genehmigte Dissertation

Promotionsausschuß:

Vorsitzende:	Prof. Dr. Karola Rück-Braun, TU Berlin
Berichter:	Prof. Dr. Gernot Renger, TU Berlin
Berichter:	Prof. Dr.-Ing. Hans Joachim Eichler, TU Berlin

Tag der wissenschaftlichen Aussprache: 15. April 2003

Berlin 2003
D 83

1 Introduction

Fluorescence is the tool of choice for a year by year increasing number of biophysical and biochemical applications. While the development of new fluorescent dyes and their chemical linkage to selected molecules allow specific direct fluorescence staining (Haugland 2001), living organisms can even produce their own fluorescent probes at controlled molecular locations through genetic approaches (Conn 1999). Improvements in instrumentation have made it possible to measure properties of fluorescence, including spectral excitation, emission, polarization and lifetime down to the level of a single molecule (Eggeling *et al.* 2001; Rigler and Elson 2001).

The measurement of the lifetime of fluorescence has become an important standard technique for cuvette-based experiments over the past decades. By measuring the lifetime of fluorescence, it is possible to obtain information about the environment of the fluorophores, the geometry and dynamic of their excited states and their movements in solution (Cundall and Dale 1983; Jameson *et al.* 1984; McGown and Bright 1984).

Fluorescence Lifetime Imaging (FLI) has, therefore, received much attention since it was proven feasible ten years ago (Clegg *et al.* 1992; Lakowicz *et al.* 1992; Wang *et al.* 1992; Gadella Jr. *et al.* 1993). This interest in FLI can be attributed to the quantitative information only obtainable from dynamic measurements, and to unique properties such as lifetime's independence of fluorophore concentration or excitation light intensity and its sensitivity to the local environment of the fluorophore (as pH, polarity or temperature). The importance of these properties is evident when one considers that the fluorophore concentration is not controllable in most imaging applications and thereby quantification is not possible. In addition, many applications deal with sample geometries that prevent homogeneous illumination and/or contain a variety of inhomogeneous local environments (for example, the organelles in a cell). Furthermore, there is a need for imaging applications to resolve the local distribution of different fluorescent species, which have a spectral overlap, or for specific Förster Fluorescence Resonance Energy Transfer (FRET) studies, in which the lifetime provides information about proximity relationships between donor- and acceptor-labeled molecules in biological specimens (Bastiaens and Squire 1999).

When biological samples are being investigated, the amount of time that a measurement takes is often extremely important. Image acquisition, analysis and display of a fluorescence lifetime image usually take several minutes. Faster lifetime measurements are indispensable

when resolving fast dynamic processes, (e.g. fluorescence transients of photosynthetic systems), sample screening, medical fluorescence diagnostics and a variety of other applications. For this reason, an instrument was developed to enable continuous mode fluorescence lifetime imaging at video-rate with concurrent image acquisition, analysis and visualization.

The first part of this work describes the development and construction of this instrument, and the important improvements, procedures and parameters that have been found useful for its operation. The second part demonstrates how the instrument is used in the observation of photosynthetic processes, and answers several questions posed in the current research in this field. In contrast to applications in which fluorescent probes have to be applied artificially, chlorophyll molecules, which harvest the sunlight in plants to drive photochemistry for carbon fixation, are intrinsically fluorescent. Their changing fluorescence during illumination, (called the fluorescence transient), mainly monitors the kinetics of electron transfer during photochemistry, but the complex process of light harvesting is influenced by a number of additional factors, which can be revealed partially through lifetime measurements. Fast fluorescence measurements are required to record the changes of such kinetic processes. Under intense irradiation, plants and photosynthetic algae activate photoprotection mechanisms to dissipate potentially harmful energy that exceeds their photosynthetic capacity. The so-called xanthophyll-cycle is known to be involved in photoprotection (Demmig-Adams *et al.* 1996). Therefore two xanthophyll-cycle mutants have been studied in this work.

After a short literature overview, which summarizes the theoretical and experimental foundations of fluorescence lifetime measurements in part 2.1 and about photoprotection during photosynthesis in part 2.2, the experimental work is presented in section 3. In 3.1.1 the instrumental components are described and discussed in their functional context. This is followed, in 3.1.2, by a detailed presentation of the custom designed software developments. Part 3.2 offers a description of the application of the FLIM instrument, as mentioned above: Lifetime images of non-photochemical quenching mutant cells of the green alga *Chlamydomonas reinhardtii* allow a direct comparison of fluorescence quenching in the different mutants. Inter- and intracellular lifetime heterogeneities of single alga cells and cell ensembles are presented. Finally a new (non-imaging) method for photosynthetic samples is introduced: The measurement of the Fluorescence Lifetime Transient. Part 4 contains a summary while part 5 contains the Appendix with bibliography, a list of abbreviations, some commentaries and methods developed specifically for the analysis of the algae measurements.

2 Theory and literature overview

2.1 Fluorescence lifetime

2.1.1 Fundamental concepts and definitions

When molecules or atoms absorb light, the equivalent of this energy has to reappear in another form. It can manifest itself as kinetic energy of the particles and their vibrational modes, which can be transferred to other particles by collision (heat) or as chemical energy to drive an endothermic chemical reaction, which plays an important role in photosynthesis. But the absorbed energy can also again be emitted as luminescence-light. Such photoluminescence can be divided further in fluorescence and phosphorescence. For organic compounds the fluorescence is the important process, which shall be of main interest for this work. Characteristic for the absorbing matter, the photoluminescence is polarized and has a spectral distribution, which is independent of the excitation light. Another important matter-dependent characteristic of this light is a certain inertia. It does not start or stop immediately with the exciting irradiation, but follows with a certain delay, which, although short, is drastically longer than the oscillation time of the light. A measure for such delay is its mean decay time. When the excitation with a constant intensity or with a pulse of light stops at the time $t = 0$, the fluorescence intensity decays with a certain function in time $F(t)$ down to 0. As the mean decay time τ one defines the mean value, which this function forms with the time passed:

$$\tau = \frac{\int_0^\infty F(t)\, t\, dt}{\int_0^\infty F(t)\, dt} \tag{2.1}$$

Such general definition (see also Förster 1951) is valid for any form of the decay. Because the process of absorption itself is so fast that it takes place in about the oscillation time of the light, the fluorescence decay can be understood to be the result of the return of excited molecules back into their ground state, after a certain dwell time in their excited state. τ is then the mean lifetime of a fluorescent state of the ensemble of molecules created by irradiation. The statistical return of excited molecules in an ensemble of the same species into the ground state, which is accompanied by the emission of a fluorescence photon for each return, can lead to a single exponential decay of the fluorescence intensity:

$$F(t) = a' \, e^{-\frac{t}{\tau}} \tag{2.2}$$

The fluorescence lifetime τ here is the time after which the intensity has decayed to $1/e$ (≈ 37 %) of its starting value a'.

2.1.2 Dependency of environmental parameters

If all molecules return to the ground state by fluorescence alone [corresponding to a fluorescence quantum yield $\Phi_f = 1$; the quantum yield is the quotient of emitted to absorbed quanta; compare also equation (2.9)], the time constant $\tau = \tau_0$ of the single-exponential decay (the intrinsic radiative lifetime of the excited state) does correspond to the reciprocal transition rate constant k_F from the excited to the ground state[1]:

$$\tau_0 = \frac{1}{k_F} \tag{2.3}$$

τ_0 of fluorescent organic molecules is usually around 10^{-9} to 10^{-8} s. But most fluorescent systems can return to the ground state via additional nonradiative deactivation pathways, which can be pictured in an energy level diagram, called Jabłoński-diagram[2] (Fig. 1):

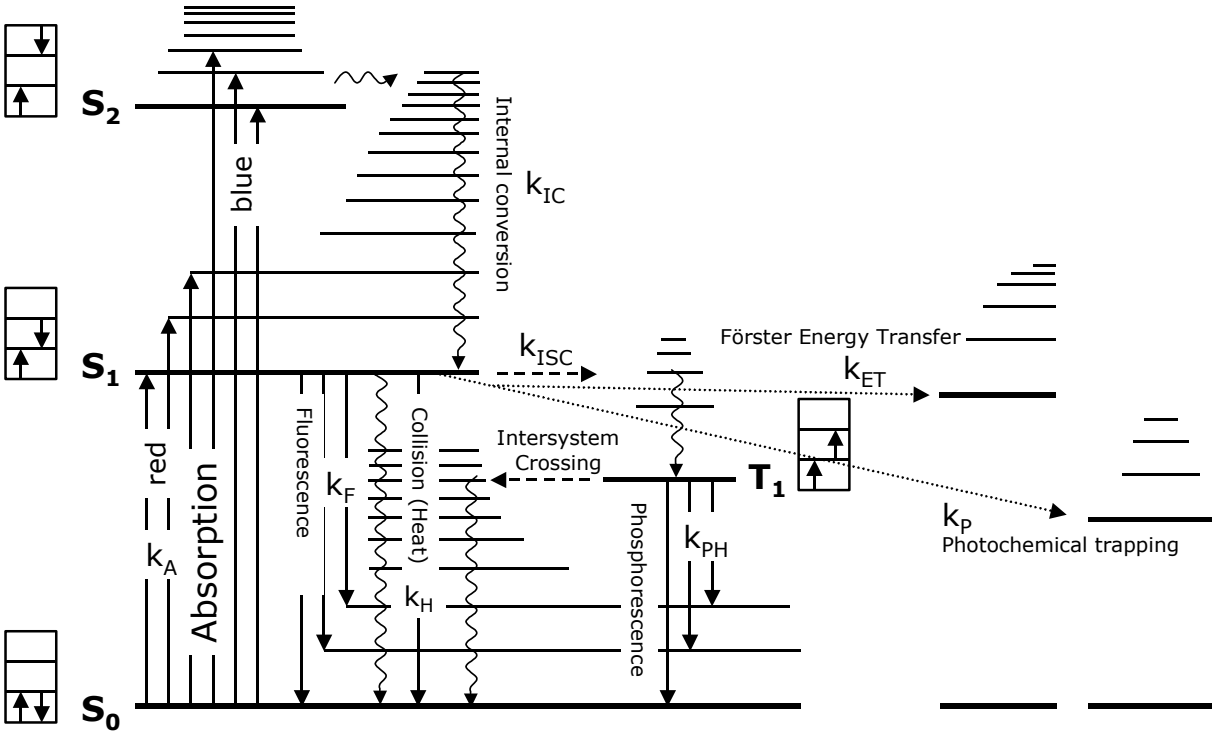

Fig. 1: Jabłoński-diagram (energy level diagram)
The different deactivation pathways, through which an excited molecule can return to its ground-state, are labeled with the corresponding rate constants: Fluorescence k_F, internal conversion k_{IC}, intersystem crossing k_{ISC}, phosphorescence k_{PH}, Förster energy transfer k_{ET}, collisional dynamic quenching k_H (heat) and (for photosynthetic samples) photochemical trapping k_P.

The energy of a molecule is not constituted only by its electronic energy, but also by its nucleic vibrations and rotations. The broad spectral distribution of molecular absorption and fluorescence is the result of varying amounts of kinetic nucleic energy, which are transferred during electronic transitions in addition to the fixed amount of electronic excitation energy. Through **absorption**, a process which is orders of magnitude faster than fluorescence ($\tau_A = 1/k_A \approx 10^{-15}$ s), a fluorescent molecule gets from the singlet electronic ground state S_0 to a higher vibrational state of the excited state S_1. For certain fluorophores the vibronic modes of S_2 and even higher electronic states can be excited, as is the case for example for chlorophyll molecules during absorption of blue light. From these excited states - the Franck-Condon states[3] - relaxation to the lowest vibrational state of S_1 occurs by fast **internal conversion** ($\tau_{IC} \leq 10^{-12}$ s), during which the excess energy is transferred to surrounding solvent molecules by collision and charge induced molecular movements (heat). This explains why the wavelength for excitation and emission is not necessarily identical as seen for electronic transitions in simple atomic systems. The energy loss by internal conversion is the reason, why the emission is in general shifted to longer wavelength. This redshift is also called the Stokes shift[4] (Stokes 1852a, b).

If for the relaxation from one state to the other nonradiative internal conversion or emission of radiation dominates, depends mainly on two factors: First the energy difference between the states and second the interaction with the surrounding molecules, as for example the solvent molecules[5]. Due to the small energy differences between S_1 and S_2 (and higher singlet states) deactivation here is dominated by internal conversion to S_1, so that fluorescence in general only occurs from the lowest excited state. This is referred to as Kasha's rule[6] (Kasha 1950). Relaxation from S_1 to S_0 by internal conversion also occurs, but because the energy difference to the ground state is in general large this transition is drastically slower (rate constant similar to fluorescence).

Intersystem crossing from S_1 allows the occupation of the triplet state T_1, although the transition $S_1 \rightarrow T_1$ is as spin-forbidden as $S_0 \leftrightarrow T_1$ according to the spin selection rules, because they involve a spin flip ($k_{ISC} \approx 10^4$-10^{12} s^{-1} strongly depending on solvent). Such violation of the $\Delta S = 0$ selection rule, which applies absolutely only for pure electric dipole transitions, is made possible by growing coupling between singlet and triplet state, lower energy difference between S_1 and T_1 and spin-orbit coupling (Henry and Siebrand 1973; Siebrand 1976). Nevertheless transitions, which violate the selection rules, are apt to be slow. Heavy atoms in the molecule or its surrounding favor the intersystem crossing due to stronger spin-orbit coupling. From T_1 the molecule can return to S_0 by emission of a phosphorescence

photon ($k_{PH} \approx 10^{-1}$-10^{3} s^{-1}), by additional intersystem crossing[7] or by internal conversion. From T_1 the occupation of higher excited triplet states is also possible. The relative long lifetime of the triplet state predestinates this state for energy transfer and charge transfer processes. Energy transfer from the triplet state of most tetrapyrroles to ground-state oxygen for example is an efficient source for the generation of singlet-state oxygen, a very photodamaging species.

During **bimolecular fluorescence quenching** (or **dynamic quenching**) the energy of the excited state is transferred to another molecule by collision. In contrast to internal conversion the excited fluorophore and the quenching partner in its ground state form a quenching complex, which is called excimer if the quenching partner is a molecule of the same species or exciplex otherwise (Weller 1968). This complex has different energy levels and can therefore emit fluorescence of different wavelength, but the energy can also be transferred further as heat. The rate of this process is depending on the concentration of the quencher [Q]. Usually $k_H = k_q$ [Q], with the diffusion controlled bimolecular rate constant $k_q = 10^9 – 10^{10}$ M^{-1} sec^{-1} (Stern and Volmer 1919). It should be stated at this point that another very common quenching is the static quenching of fluorescence. But this type of quenching does not deactivate the excited state. The quencher forms a ground state complex with the fluorophore and thereby simply makes the fluorophore non-fluorescent. In most cases one will find a combination of dynamic and static quenching (Webber 1997; Lakowicz 1999).

Förster fluorescence resonance energy transfer (Perrin 1927; Förster 1946, 1948) is a radiationless intermolecular energy transfer over large intermolecular distances (usually 1 - 10 nm). Under favorable dipole orientation, distance ($k_{ET} \sim 1/\text{distance}^6$) and spectral overlap between an excited donor molecule and an acceptor molecule in its ground state the excitation energy can be transferred radiationless due to long-range dipol-dipol coupling (see e.g. Wieb van der Meer *et al.* 1995). This process is of main importance for the light-harvesting during photosynthesis, where the energy migrates over many chlorophyll molecules to be channeled to reaction centers to drive photochemistry. But Förster-energy-transfer is also an important tool for controlled stereo-chemical studies (see e.g. Clegg 1996; Holub 1996). If donor and acceptor get in close proximity so that their electron systems start to overlap (at distances smaller than 1 nm), additional **electron exchange** becomes important for this kind of energy transfer (Dexter 1953).

The absorbed energy can also be used to drive **chemical reactions**. **Photochemical trapping** during photosynthesis, the production of glucose and oxygen from carbondioxide and water in its photochemical reactions, is an important example.

All mentioned processes are in kinetic competition and the more efficient they deactivate the excited state (the higher their rate constants), the shorter will be the real lifetime of the excited state:

$$\tau = \frac{1}{k_F + k_{nr}} \leq \tau_0 \tag{2.4}$$

Here k_{nr} denotes the sum of all additional deactivation rates except fluorescence (*nr* for non-radiative).

At steady state measurements the fluorophores are irradiated continuously with constant excitation intensity. Then the time change of the number of excited particles *N(t)* is determined by the number *E(t)=const.=E* of photons absorbed per time unit and deactivation through the different relaxation processes:

$$\frac{dN(t)}{dt} = E - \left(k_F + k_{nr}\right) N(t) \tag{2.5}$$

where $(k_F + k_{nr}) N(t)$ is the number of deactivated molecules per time unit and

$$F(t) = k_F \; N(t) \tag{2.6}$$

the number of emitted photons per time unit.

For steady state measurements the quasi-stationary equilibrium state is reached after a short time and the concentration of excited particles stays constant (*dN(t)/dt=0*):

$$E = \left(k_F + k_{nr}\right) N \tag{2.7}$$

The number *N* of excited molecules does not change any more with time, due to continuous light absorption and relaxation at the same time. $k_F \; N$ is the number of fluorescence transitions per time unit. The fluorescence quantum yield Φ_f, the quotient of quanta emitted as fluorescence to absorbed quanta, can then be written:

$$\Phi_f = \frac{F}{E} = \frac{k_F \; N}{E} \tag{2.8}$$

And with (2.7) and (2.4), (2.3) one obtains the rate constant and lifetime formulation:

$$\Phi_f = \frac{k_F}{k_F + k_{nr}} = \tau \; k_F = \frac{\tau}{\tau_0} \tag{2.9}$$

The direct relation between lifetime and quantum yield reveals its importance in every case of quantitative fluorescence intensity measurements. The knowledge of the lifetime allows the investigation of the direct molecular environment of the fluorophore, which in this case acts

like a molecular probe and reveals valuable information especially of - in general quite inhomogeneous - biological samples.

2.1.3 Historical introduction to lifetime measurements

100 years ago Abraham and Lemoine opened the way for phase fluorometry by investigating the low inertia of the electro-optical Kerr-cell (Abraham and Lemoine 1899). Lord Rayleigh (1904) realized that their instrumentation could be used to measure the very short decay times of fluorescence, which was attempted by Wood (1921) and Gottling (1923). But the first fluorometer - a term he coined - was build by Gaviola in 1926 and used for the first precise direct[8] lifetime measurements of fluorescence (Gaviola 1926a; 1926b; 1927). Contrary to his predecessors he was modulating the excitation light continuously by driving the Kerr-cell with a high frequency (HF) of 16 MHz. The fluorescence signal of a sample is then also modulated with the same frequency but undergoes a lifetime-dependent phase shift and reduction in amplitude (demodulation). Gaviola send the fluorescence through a second Kerr-cell driven from the same frequency source and measured its intensity. This measurements he repeated after changing the pathlength the fluorescence light had to travel - a way to determine its phase. He obtained the lifetime by comparing the phase of the fluorescence with the phase of reflected light by replacing the fluorescent sample with a mirror.

Important technical and conceptional improvements have been undertaken since Gaviola's time, but the basic methodology he introduced still lies at the heart of phase fluorometry and is employed by the instrument presented in this work. Phase changes and light detection nowadays are obtained electronically and the whole measurement and analysis is automated, while Gaviola still had to rely on visual detection of the fluorescence. His approach of measuring the periodic fluorescence signal during continuous periodic excitation is nowadays called the phase and modulation method (it is operating in the frequency domain). The second important method for lifetime determinations is the direct measurement of the fluorescence decay after a short pulse of light (time domain).

Both methods have their specific advantages depending on the experimental conditions. While the time domain especially in combination with time-correlated single photon counting (see e.g. Wahl 1975; Badea and Brand 1979) allows sensitive measurements even at low fluorophore concentrations, the frequency domain allows fast measurements if a sufficient number of photons is at hand.

Gaviola used the same frequency for excitation modulation and emission detection in order to obtain access to the not directly measurable HF modulation. This procedure is called

homodyning and will be discussed in more detail later, because it is also employed in this work.

Hundred years of phase fluorometry left a considerable literature. An excellent review, which includes an overview of the early history of phase fluorometry, has been given by Teale (1983). Jameson (2001) gives a comprehensive overview of the developments of Gregorio Weber and his influences in this field, his utilization of the principle of cross-correlation (heterodyning) instead of the homodyning approach (Spencer and Weber 1969), which laid the basis for Gratton's multifrequency cross-correlation phase and modulation fluorometer in 1978 (Gratton and Limkeman 1983; for a classical review on multifrequency fluorometry see Jameson *et al.* 1984). A good general introduction can also be found in the second edition of Lakowicz's standard volume of fluorescence spectroscopy (Lakowicz 1999).

2.1.4 Fluorescence lifetime-resolved imaging (FLI)

The same two methods used for fluorometry – frequency- or time-domain – can also be applied for lifetime imaging - independent of how the image is obtained, either by full field caption with high-speed two-dimensional detectors (e.g. charge-coupled device (CCD) cameras) or scanning techniques (see e.g. vandeVen and Gratton 1992).

In the beginning of 1990 several groups started to develop FLI-systems, when necessary electronic devices like CCD-cameras, high-speed gate-able image-intensifiers and necessary computation power became easily available (utilizing the time domain: Cubeddu *et al.* 1991; Kohl *et al.* 1993; Minami and Hirayama 1990; Ni and Melton 1991; Oida *et al.* 1993; Schneckenburger *et al.* 1993; Wang *et al.* 1991; and utilizing the frequency domain: Clegg *et al.* 1992; Gadella Jr. *et al.* 1993; Gratton *et al.* 1990; Lakowicz and Berndt 1991; Marriott *et al.* 1991; Morgan *et al.* 1990; Piston *et al.* 1992; Wang *et al.* 1989). Confocal (Buurman *et al.* 1992; Morgan *et al.* 1992), two-photon (Piston *et al.* 1992; So *et al.* 1995; Sytsma *et al.* 1998) and pump-probe systems (Dong *et al.* 1995; Buist *et al.* 1997; Dong *et al.* 1997; Buehler *et al.* 2000) for lifetime imaging have been constructed. For general reviews on FLI see e.g. (Wang *et al.* 1992; Clegg *et al.* 1996; Gadella Jr. 1999).

Every technique, imaging or non-imaging, must allow averaging of the fluorescent signal for a good signal to noise ratio (S/N). This is usually unproblematic for the non-imaging techniques, which allow the insertion of the fluorescent sample in a cuvette. In the frequency domain the lifetime-dependent phase shift and demodulation of the fluorescence signal are therefore measured at many (usually about 20) different modulation frequencies of the excitation light (10-200 MHz for fluorescent lifetimes of 0.1-20 ns), which allow the

determination of multi-exponential decay components or their distributions. For each frequency the fluorescence signal is averaged until a good S/N is reached resulting in final measurement times of 15-20 minutes for all frequencies. In the time domain the measurement times are of the same order, counting the times between emission and detection of single photons (time-correlated single-photon counting).

For a number of imaging applications in biology such long measurement times are not acceptable. Often the processes of interest are on a much faster time scale and also sample movements or photobleaching in the thin plane of observation make fast measurements desirable. Restriction to a single frequency (and its fundamental harmonic component) in the frequency domain or measurement of the fluorescence decay in only two time windows of a gated image intensifier in the time domain (Wang *et al.* 1992) allow faster measurements and are therefore and for reasons of technical practicability often used for imaging applications. The drawback of this restriction is the reduction of the lifetime analysis to the case of a single exponential decay, although one is recognizing a multi-exponential decay in the frequency domain, because the apparent single lifetime calculated from the demodulated fluorescence signal (τ_{mod}) is in this case longer than the apparent lifetime calculated from the phase shift (τ_{phase}). In some cases the use of additional information, like known lifetime components (Weber 1981) or identical lifetime components at different pixels of the image (Verveer *et al.* 2000), can also allow to resolve more than one lifetime component even in the case of a single frequency measurement.

The endeavor of all new instrumentational developments for FLI is to obtain better resolution (spatially and temporal) in as short a measurement and data processing time as possible. Lifetime imaging setups using new technical developments like 200 ps gated image intensifiers with 100 MHz repetition rates (Dowling *et al.* 1998; Straub and Hell 1998) and delay-line micro-channel plate photomultiplier tube detectors for simultaneous time- and space-correlated single photon counting (Kemnitz *et al.* 1997) allow high precision imaging of many lifetime components with a measurement time (without data processing) of about 10 minutes or simultaneous lifetime and wavelength determination (Bergmann *et al.* 1998).

Instrumentation, which allowed fast measurements of restricted component resolution in combination with fast data processing and display (called real-time or quasi real-time setups), was developed in the middle of the 90's. Periasamy *et al.* (1996) presented a time domain setup with < 2 s measurement time and 2 to 5 s processing and display time for 1000 x 1000 pixel. Schneider and Clegg (1997) presented a frequency domain instrument for fast FLI, which allowed a display of 5-7 lifetime-resolved normalized difference images per second

(256 x 256 pixel) in different applications (microscopy, endoscopy and array scanning). Cubeddu *et al.* (1997; 1999) described a time domain setup displaying lifetime images with 1 fps (512 x 512 pixels) for tumor detection. Dowling *et al.* (Dowling *et al.* 1998) have demonstrated lifetime displays of 3 s using a fast gate-able image intensifier and their system allows multi-exponential resolution if the measurement is performed for several minutes as mentioned above. Mizeret *et al.* (1999) presented a FLI system for endoscopy, which can display lifetime images (32 x 32 pixel) calculated from 3 phase images (40 ms integration time per image) at a rate of 25 fps. New instrumentations like gain modulated framing cameras also seem to be very promising for fast lifetime imaging (Itoh *et al.* 1997).

The instrument, which is described in (Holub *et al.* 2000) together with the improvements presented in this work, is the first of its kind, which allows user-interactive, concurrent image acquisition, analysis and 3D-visualization of lifetime images (320 x 240 pixel) at video-rate (26 fps).

2.1.5 General description of time-resolved luminescence

Mathematically luminescence emission can be described as the convolution integral of the excitation function *E(t)*, which shall describe the number of photons absorbed per time unit, with the δ-function response curve $F_\delta(t)$ of the luminescent system:

$$F(t) = \int_0^t E(t')\, F_\delta(t - t')\, dt' \tag{2.10}$$

F(t) is the number of photons emitted per time unit and therefore directly proportional to the measured fluorescence[9] intensity, which is also effected by instrumentation parameters. The δ-function response curve $F_\delta(t)$ in this description is the signal, which would follow an infinitesimal short excitation pulse at each time point. Here an ensemble of molecules shall be excited, so that the single stochastic processes of the spontaneous emission become a continuous decay function.

After a (δ-function) light pulse the excited state S_1 gets occupied with N^0 particles. Here

$$N^0 = \sum_{s=1}^{S} n_s^0 \propto \sum_{s=1}^{S} c_s \varepsilon_s \tag{2.11}$$

can represent the total number of absorbed photons or the total number of excited molecules. A number of different molecular species *S* be in solution. How many molecules n^0 of each species get excited depends on their concentration *c* and absorption coefficient ε. With time

the number of excited molecules decreases due to fluorescence and the various additional deactivation processes. Equation (2.5) with *E(t)=0* describes this case:

$$\sum_{s=1}^{S} \frac{d\, n_s(t)}{dt} = -\sum_{s=1}^{S} \left(k_{F,s} + k_{nr,s} \right) n_s(t) \tag{2.12}$$

Integration of the differential equation with the condition $n_s(t=0) = n_s^0$ gives the solution:

$$N(t) = \sum_{s=1}^{S} n_s^0 \; e^{-\left(k_{F,s}+k_{nr,s}\right) t} = \sum_{s=1}^{S} n_s^0 \; e^{-\frac{t}{\tau_s}} \tag{2.13}$$

the relation (2.6) then gives for the fluorescence

$$F_\delta(t) = \sum_{s=1}^{S} k_{F,s} \; n_s^0 \; e^{-\frac{t}{\tau_s}} = \sum_{s=1}^{S} \frac{1}{\tau_{0,s}} n_s^0 \; e^{-\frac{t}{\tau_s}} =: \sum_{s=1}^{S} a'_s \; e^{-\frac{t}{\tau_s}} \tag{2.14}$$

This equation can also be understood as a definition of the amplitude $a'_s := k_{F,s}\; n_s^0$, which is weighting the s^{th} lifetime component τ_s. The amplitudes are therefore dependent on concentration, absorption coefficient and rate k_F for each species. In general the amplitudes a'_s of (2.14) are given as relative amplitudes a_s in normalized form:

$$a_s = \frac{a'_s}{\sum_{s=1}^{S} a'_s} \quad \Rightarrow \quad \sum_{s=1}^{S} a_s = 1 \tag{2.15}$$

Summation in (2.14) is performed over all *S* lifetime components. These components can be chemically different species with different lifetimes or molecules of the same species in different states. The states can differ electronically (e.g. singlet or triplet) or can be the result of different molecular environments (e.g. dynamical quenching, see above). But very often the components do not correspond directly to the number of species in solution. In case of a continuous lifetime distribution[10] the sum in (2.14) has to be replaced with the corresponding integral.

The total number N^{tot} of photons emitted as fluorescence is the integral over $F_\delta(t)$:

$$N^{tot} = \int_0^\infty \sum_{s=1}^{S} \frac{n_s^0}{\tau_{0,s}} e^{-\frac{t}{\tau_s}} \, dt = \sum_{s=1}^{S} a_s \tau_s = \sum_{s=1}^{S} \frac{\tau_s}{\tau_{0,s}} n_s^0 = \sum_{s=1}^{S} \Phi_{f,s} \; n_s^0 \tag{2.16}$$

$\tau_{0,s}$ is the lifetime, which one would observe at a quantum yield $\Phi_f = 1$, defined as $\tau_0 = 1/k_f$ in equation (2.3) and τ_s is the really observable lifetime $\tau = 1/(k_f+k_{nr})$, (2.4). A change in the observed lifetime can therefore originate in a frequency change of the radiative transition as well as in changes of the competing non-radiative processes. Because k_f to a good part is

determined by the molecular structure of the fluorophore, in general k_{nr} will be the variable, which changes most at environmental changes like temperature or solvent changes. An increase in the non-radiative deactivation processes (as for example by stronger dynamical quenching) results in a proportional decrease of fluorescence lifetime and quantum yield, that means the decay takes place faster and the total number of photons is reduced from (τ x *constant factor*) to (τ_{quenched} x *constant factor*). But nevertheless changes in τ_0 (as for example induced by stimulated emission) as well as τ do change the quantum yield and thereby the total number of emitted photons. Only in the absence of any non-radiative deactivation processes (in the case of $\tau = \tau_0$, that is $\Phi_f = 1$) a change in τ_0 does not change the total number of photons but affects only the speed of the decay process.

Measurements, which are based on fluorescence intensity comparisons alone, as it is very common for fluorescence microscopy, very often do not take into account that molecular identical fluorophores can have different lifetimes at different image locations, which will result in different fluorescence intensities, even if the concentrations are identical.

2.1.6 Frequency domain theory: Signal

In general, the fluorescence decay of a sample following a single short excitation pulse (i.e. on the time scale of the excited state lifetime) is not intense enough and the time scale too short to be recorded experimentally with sufficient accuracy. Therefore all methods (including the time domain) use repetitive excitation and average the signal of many repetitions. In the frequency domain the excitation light is modulated at radio-frequencies. At this point we want to present a short theoretical description of the phase and modulation method.[11] Although any kind of repetitive excitation signal can be used[12], the description shall be restricted to the important case of purely sinusoidal excitation with regard to the constructed instrument.

The sinusoidally modulated intensity of the excitation light can be described as

$$\begin{aligned} E(t) &= E_0 + E_t \, 2\cos(\omega\, t + \phi^E) \\ &= E_0 \, [\, 1 + M_E \, 2\cos(\omega\, t + \phi^E)] \end{aligned} \tag{2.17}$$

where E_0 denotes the time-independent offset, the average excitation intensity (DC_E), $2 \cdot E_t$ the amplitude of the time-dependent intensity variation (AC_E). The arbitrary phase ϕ^E of the sinusoidal excitation modulation is given by the instrumental setup. M_E is the quotient of the amplitudes of the alternating and direct part

$$M_E = \frac{E_t}{E_0} = \frac{AC_E}{DC_E} \tag{2.18}$$

the modulation depth of the excitation at given angular frequency ω. The repetition frequency $f = \omega/2\pi$ of the sinusoidal intensity changes is usually between 10-100 MHz and therefore orders of magnitude smaller than the frequency of the used light itself.

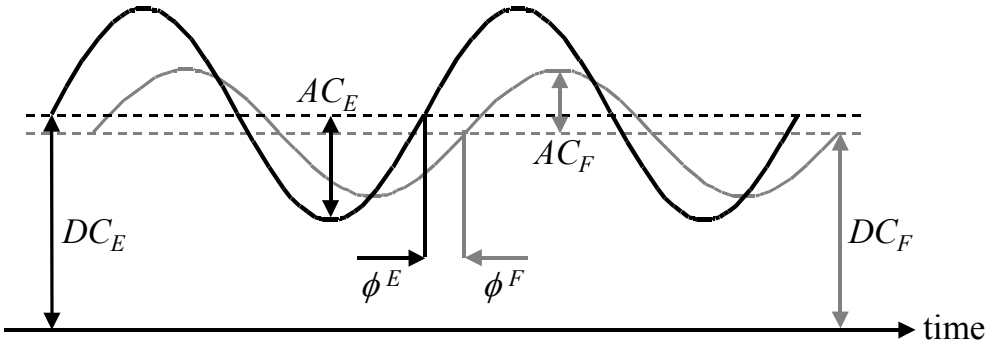

Fig. 2: Excitation and fluorescence emission in the frequency domain
A fluorophore is excited with intensity modulated excitation radiation of radial frequency ω. The emitted fluorescence signal has the same frequency, but undergoes a phase shift Φ and amplitude demodulation M with respect to the excitation radiation depending on the fluorescence lifetimes. This results in two potentially different lifetime estimates τ_{phase} and τ_{mod}, the apparent single lifetimes. AC and DC are the amplitudes of the alternating and direct part of the excitation (*E*) or fluorescence emission (*F*) signal. The modulation depth of the excitation radiation is described by $M_E = AC_E / DC_E$ and of the emission radiation by $M_F = AC_F / DC_F$ respectively. The modulation is then defined as $M = M_F / M_E$ and the phase as $\Phi = \phi^E - \phi^F$. In the case of a mono-exponential decay (a single lifetime component) $M = 1/\sqrt{1+(\omega\tau_{mod})^2}$ and $\Phi = \arctan(\omega\tau_{phase})$ and $\tau_{phase} = \tau_{mod}$, but for more complex lifetime compositions $\tau_{phase} < \tau_{mod}$.

The fluorescence emission *F(t)* can be obtained by integration of (2.10), if (2.17) is used for sinusoidal excitation and an exponential δ-function response as given in (2.14) is assumed. In Fig. 2 it can be seen that in the case of sinusoidal excitation *E(t)* the fluorescence emission *F(t)* is also sinusoidally modulated,

$$\begin{aligned} F(t) &= F_0 + F_t\, 2\cos(\omega\, t + \phi^E - \Phi) \\ &= E_0 \sum_{s=1}^{S} a_s\, \tau_s + E_t\, (\sum_{s=1}^{S} a_s\, \tau_s)\, M\, 2\cos(\omega\, t + \phi^E - \Phi) \\ &= F_0\, [\, 1 + M\, M_E\, 2\cos(\omega\, t + \phi^E - \Phi)] \end{aligned} \tag{2.19}$$

with a direct component F_0 given as,

$$F_0 = E_0 \sum_{s=1}^{S} a_s\, \tau_s \tag{2.20}$$

but the fluorescence emission exhibits the phase lag

$$\boxed{\Phi = \arctan\left[\sum_{s=1}^{S} \frac{a_s \tau_s\, \omega\tau_s}{1+(\omega\tau_s)^2} \Big/ \sum_{s=1}^{S} \frac{a_s \tau_s}{1+(\omega\tau_s)^2}\right]} \tag{2.21}$$

and a decrease of the modulation depth by a factor of

$$M = \frac{M_F}{M_E} = \frac{F_t/F_0}{E_t/E_0} = \sqrt{\left(\sum_{s=1}^{S} \frac{a_s\tau_s \Big/ \sum_{s=1}^{S} a_s\tau_s}{1+(\omega\tau_s)^2} \right)^2 + \left(\sum_{s=1}^{S} \frac{\left(a_s\tau_s \Big/ \sum_{s=1}^{S} a_s\tau_s \right) \cdot \omega\tau_s}{1+(\omega\tau_s)^2} \right)^2} \tag{2.22}$$

compared to the excitation light. These are the two basic relations of phase fluorometry. Phase shift Φ and modulation M are the parameters measured in the phase and modulation method and then used for the lifetime determinations. It should be noted that they are not dependent any more on the excitation intensity (E_0 and E_t). For the case of a single lifetime component (S=1) they reduce to

$$\Phi = \arctan(\omega\tau) \tag{2.23}$$

$$M = \frac{1}{\sqrt{1+(\omega\tau)^2}} \tag{2.24}$$

In analogy to (2.18) the modulation depth of the fluorescence signal has been used

$$M_F = \frac{F_t}{F_0} = \frac{AC_F}{DC_F} \tag{2.25}$$

Some important characteristics of the phase and modulation method are contained in equation (2.19):

1) Static measurements, when the fluorescence intensities are measured using constant excitation ($\Rightarrow F_t$=0), are described in equation (2.19) by the direct component F_0 [compare (2.20) with (2.14)]. Except of the amplitudes a_s, which describe absorption properties and are proportional to the fluorophore concentration [see (2.14)], and the excitation intensity E_0 the steady state fluorescence intensity depends on the lifetimes of the fluorophores τ_s. In imaging applications each of these three parameters can vary at every position of the image. While the excitation intensity for each pixel of the image can be determined, equation (2.20) clarifies why quantitative concentration determinations and pixel comparisons, especially of biological samples with highly heterogenous environments, will only be possible, if the lifetimes at each image location are known.

2) Equation (2.20) further shows that in the static case the amplitudes a_s are weighted by the lifetimes. Therefore from two molecular species with identical number of fluorophores and identical absorption properties, but different lifetimes, the component with the shorter

lifetime contributes less to the overall fluorescence signal. But the same weighting does not only apply to the direct part F_0 . The alternating part F_t is weighted in the same manner [see (2.22)].

3) But the amplitude of the alternating part 2 F_t , which is mainly determined by the modulation M as given in (2.22), in addition contains the lifetime τ_s in the form of the product $\omega\tau_s$ in the denominators and the numerator of the second term. Therefore different lifetime components contribute to the overall fluorescence signal sensitively depending on the frequency of the light modulation. This effect can be seen in the grey curve of Fig. 3, which plots the modulation M against $\omega\tau$ for the case of a single lifetime component [equation (2.24)], and in Fig. 4, which shows the first derivative. Changes in lifetime components around $\omega\tau_s = 1/\sqrt{2} \approx 1$ sensitively are reflected in modulation changes, while the sensitivity for long or short lifetime components diminishes. Long lifetime components ($\omega\tau_s$>>1) do not contribute much to the overall modulation depth. They completely demodulate the fluorescence signal. Very short lifetime components ($\omega\tau_s$<<1) on the other hand do not demodulate at all, so that the fluorescence follows directly the excitation light. They have a deep modulation depth, but which is not very sensitive to lifetime changes.

4) Next to the modulation M also the phase shift Φ as given in (2.21) is a function of the lifetime components and the modulation frequency. This is displayed by the black curve of Fig. 3 for a single lifetime component [equation (2.23)]. In contrast to the modulation, changes of short lifetime components are sensitively reflected in phase changes as can be seen in Fig. 4. But similar to the modulation, the sensitivity decreases for very long lifetimes. Optimal sensitivity in the combination of both, phase and modulation, for a certain lifetime component can be found at $\omega\tau = 1/2$.[13]

5) The relation between phase/modulation and the lifetime of fluorescence as plotted in Fig. 3 further effects the distribution for a single lifetime measurement. Measured are phase and modulation, but even if multiple measurements of the same lifetime result in a Gaussian distribution in phase and modulation, the corresponding lifetime distribution is strongly affected for long lifetime components ($\omega\tau_s$>>1). Such effect is displayed in Fig. 5. In imaging applications, where many pixels of identical lifetime compositions are analyzed (each pixel is a separate lifetime measurement), histogram analysis of pixels therefore gives direct access to the distributions of the measurement. Tails in the distribution as shown in Fig. 5 are a direct characteristic of very long lifetimes.

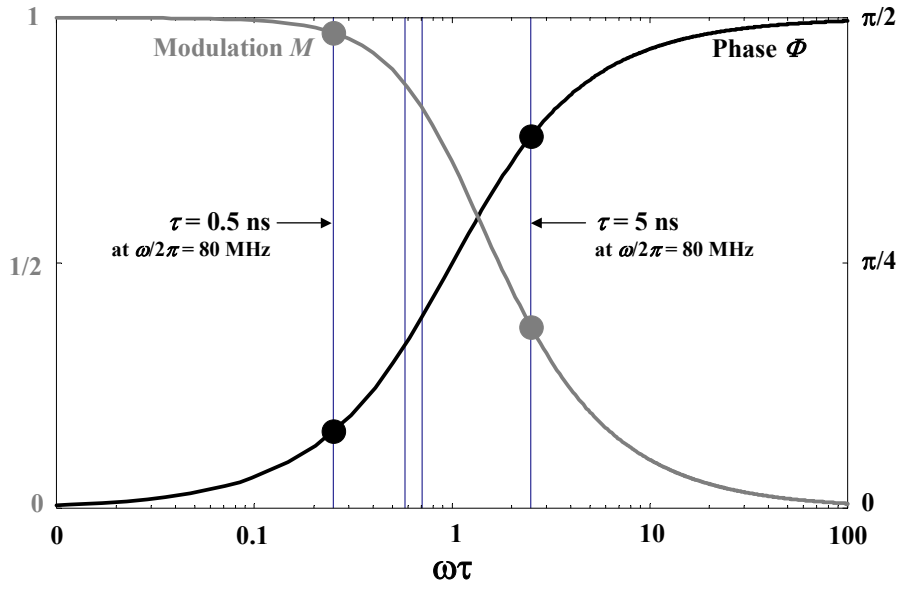

Fig. 3: Phase shift Φ (black) and modulation M (grey) as a function of the frequency of the light modulation ω for the case of a single lifetime component
The modulation frequency ω is given dimensionless in units of $\omega\tau$. The positions for the two lifetimes 0.5 and 5 ns are marked with filled dots for the case of a modulation frequency $\omega = 2\pi$ 80 MHz. Further the inflection point of the first derivative of the phase $\omega\tau = 1/\sqrt{3}$ and the point of highest sensitivity for modulation changes (the inflection point of the modulation) $\omega\tau = 1/\sqrt{2}$ are marked.

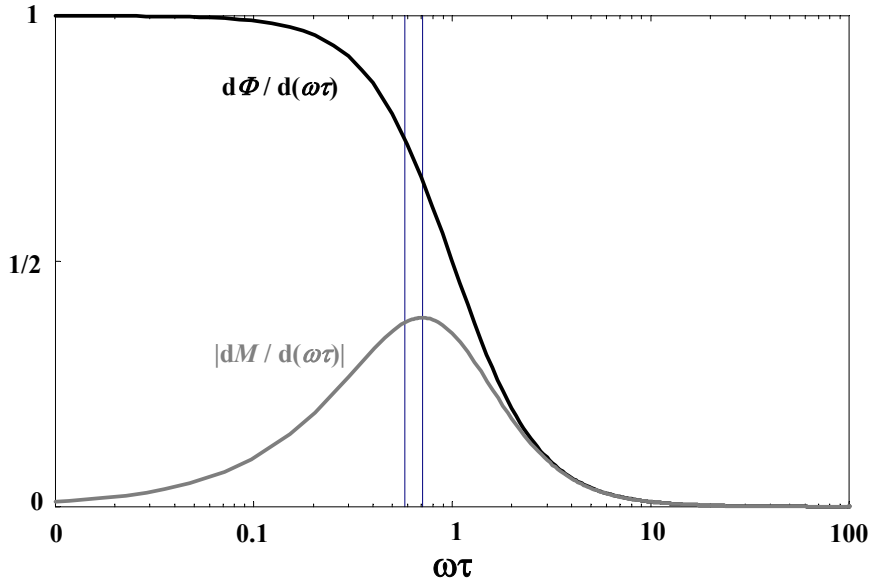

Fig. 4: First derivatives of phase Φ (black) and modulation M (grey) as a function of the frequency of the light modulation ω for the case of a single lifetime component
The modulation frequency ω is given dimensionless in units of $\omega\tau$. For the modulation the absolute values of the derivative are plotted. Further the inflection point of the first derivative of the phase $\omega\tau = 1/\sqrt{3}$ and the point of highest sensitivity for modulation changes (the inflection point of the modulation) $\omega\tau = 1/\sqrt{2}$ are marked.

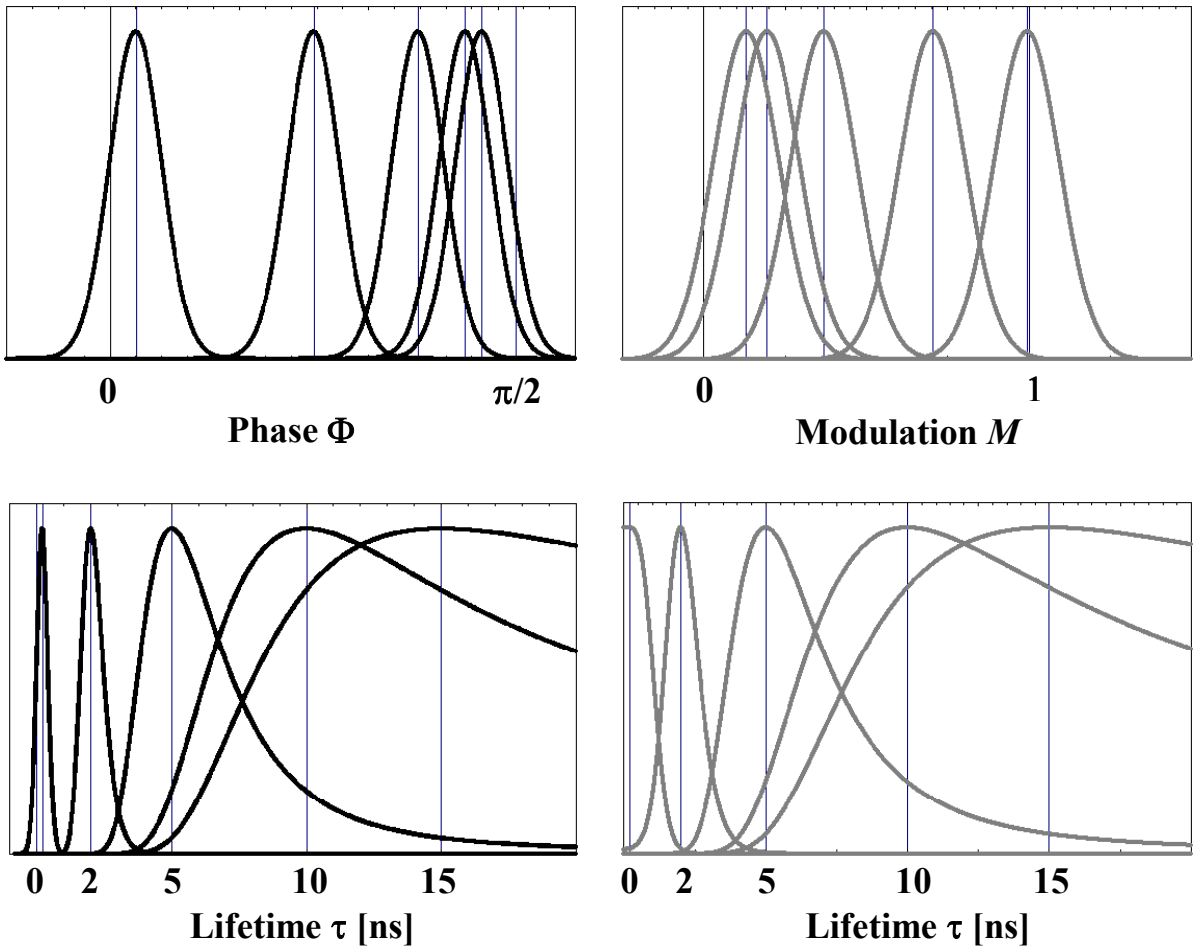

Fig. 5: Distribution transformation by lifetime calculation from phase Φ (black) and modulation M (grey)
Five identical Gaussian distributions ($\sigma = 0.1$) of phase and modulation values, whose centers correspond to lifetimes of 0.2, 2, 5, 10 and 15 ns are transformed according to the lifetime calculation for a single lifetime component at a radial modulation frequency $\omega = 2\pi\, 80$ MHz. The histograms of long lifetime components obtain a significant tail at the long lifetime side.

2.1.7 Frequency domain theory: Homodyne and heterodyne detection

Phase and modulation need to be determined from the fluorescence emission [as given in (2.19)] for a lifetime measurement. But the direct detection of optical signals, which are modulated at high frequencies between 10 and 100 MHz, requires sophisticated opto-electronical equipment. Especially for imaging applications with 10^4-10^6 simultaneous pixel measurements, direct detection is not possible. Therefore the high frequency signal is transformed to a series of DC signals (homodyning) or to an alternating signal of low frequency (heterodyning), which in both cases allows easy phase measurements at high precision.

Experimentally this is achieved by the use of a detection device, which is also modulated at high frequencies. This can be a modulated image intensifier, which is set before the camera or a modulated photomultiplier for non-imaging applications (see the following sections for a

description of the instrumental setup). In both cases the usual temporally constant gain G of the detection device becomes modulated at high frequencies and accordingly amplifies the fluorescence emission signal $F(t)$, which is impinging on the cathode of the detection device. As for the excitation, any kind of repetitive signal can be used for the gain modulation, but the case of sinusoidal modulation is of special interest:

$$\begin{aligned} G(t) &= G_0 + G_t \, 2\cos(\omega' t + \phi^G) \\ &= G_0 \, [\, 1 + M_G \, 2\cos(\omega' t + \phi^G)] \end{aligned} \tag{2.26}$$

In analogy to (2.18) the modulation depth of the gain modulation $M_G = G_t/G_0$ has been defined and ϕ^G is an arbitrary phase of the modulated detection device. The frequency of the gain modulation ω' in the general case of heterodyning is different from the modulation of the excitation light ω. Only in the special case of homodyning $\omega' = \omega$.

The detected fluorescence signal is then the product of the emitted fluorescence light $F(t)$ and the gain modulation $G(t)$. This product contains terms, which change with ω and 2ω. For typical frequencies in the range of tens of MHz such high frequency components average to zero during the data acquisition after integration for a few μs (typical integration times are tens of ms). The instrumentation described in this work uses a micro-channel plate (MCP) image intensifier in combination with a CCD-camera. The electron accumulation in the CCD functions effectively as a low-pass filtering operation. But the image intensifier displays the amplified image on a phosphore screen. The phosphore has decay times of 200-400 ns and therefore by itself is already functioning as a low-pass filter. For non-imaging applications the output voltage of the modulated photomultiplier is electronically low-pass filtered.

With $\omega' = \omega + \Delta\omega$ the low-pass filtered signal can be written

$$\left\{F(t)\,G(t)\right\}_{LP} = E_0\,G_0\sum_{s=1}^{S} a_s\,\tau_s + E_t\,G_t\,(\sum_{s=1}^{S} a_s\,\tau_s)\;M\;2\cos(\Delta\omega\,t + \phi^E - \phi^G - \Phi) \tag{2.27}$$

In the heterodyning case ($\Delta\omega \neq 0$) the frequency difference $\Delta\omega$ between light and gain modulation is usually chosen small ($\Delta\omega << \omega$), so that the low-pass filtered signal, which is recorded by the detector, is changing in time with the low frequency $\Delta\omega$ (the cross-correlation frequency).

In the homodyning case on the other hand $\Delta\omega = 0$, which means that the measured signal at the detector $S\left(\Phi, \Delta\phi^{E-G}\right)$ is temporally constant, but dependent on the phase difference $\Delta\phi^{E-G} = \phi^E - \phi^G$ between excitation light and gain modulation:

$$
\begin{aligned}
S\left(\Phi,\Delta\phi^{E-G}\right) &= Q\left\{F(t)\,G(t)\right\}_{LP}^{homodyne} \\
&= Q\left(\sum_{s=1}^{S} a_s\,\tau_s\right)\left[E_0\,G_0 + E_t\,G_t\,M\,2\cos\left(\Delta\phi^{E-G}-\Phi\right)\right] \\
&= Q\left(\sum_{s=1}^{S} a_s\,\tau_s\right)\left[1 + M_0\,M\,2\cos\left(\Delta\phi^{E-G}-\Phi\right)\right]
\end{aligned}
\tag{2.28}
$$

The proportionality factor Q accounts for all instrumentation effects. M_0 has been defined

$$M_0 = M_E\,M_G = \frac{E_t\,G_t}{E_0\,G_0} \tag{2.29}$$

as the maximal measured modulation, which one would obtain for lifetimes, which are very short against the period of the used modulation ($\Rightarrow$ M=1). M_0 can be determined experimentally for example by the measurement of reflected excitation light[14] or from the measurement of a sample with known lifetimes.

Controlled changes in the phase difference $\Delta\phi^{E-G}$ are possible, by changing either the phase of the excitation light or the phase of the gain modulation. Step by step shifts of $\Delta\phi^{E-G}$ and subsequent measurement of the steady-state signal (image), result in a sequence of measurement points, which reconstruct one high frequency period. This sequence is identical to the one obtained by the time-dependent signal in the heterodyning approach. Both methods are theoretically equivalent, but differ in their experimental realization. For imaging, homodyning has certain “advantages”, while the heterodyning technique is especially useful for non-imaging applications, as discussed in more detail in the Appendix 5.4.

The description of the phase and modulation method given in this section has been formulated for the case of a single lifetime measurement. As has been pointed out, such lifetime measurement is performed for each single pixel of the image. Therefore all the given parameters $E(t)$, E_0, E_t, M_E, ϕ^E, $F(t)$, F_0, F_t, Φ, M, S, a_s, τ_s, M_F, $G(t)$, G_0, G_t, ϕ^G, M_G, M_0, Q, $\Delta\phi^{E-G}$ and $S\left(\Phi,\Delta\phi^{E-G}\right)$ can differ in each single pixel.[15]

2.1.8 Data analysis

Equation (2.27) describes the actual pixel measurement signal, of which one acquires K measurement points (images). For most analysis procedures these K images are equidistant distributed over exactly one period. In the heterodyne case, in which the time t constitutes the variable parameter, the variable phase is defined by the product $\Delta\omega t$, running from 0 to 2π. In the homodyne case [equation (2.28)] the phase difference $\Delta\phi^{E-G}$ is varied in steps of $2\pi/K$. The measurement process in both cases is displayed in Fig. 6:

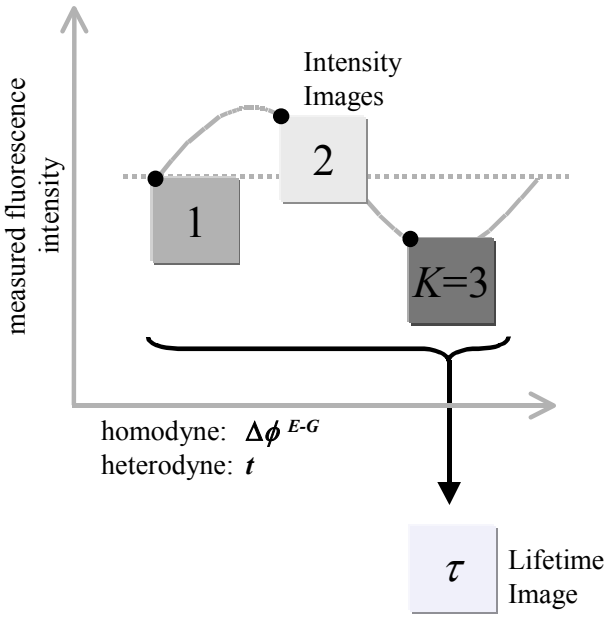

Fig. 6: Schematic of the measurement process for a fluorescence lifetime image in the frequency domain
In principle the homodyne and heterodyne method are equivalent (see Appendix 5.4). In the heterodyne case the time *t* is the variable parameter, in the homodyne case the phase shift $\Delta\phi^{E\text{-}G}$. The schematic demonstrates the time/phase dependence of the image intensity. The acquired intensity images are used for pixel by pixel analysis, resulting in a lifetime image.

The signals, acquired this way by homodyning or heterodyning, can for example be analyzed by Fourier analysis for total phase $\left(\Delta\phi^{E-G} - \Phi\right)$ and total modulation depth M_0 M in each pixel. The instrumental parameters $\Delta\phi^{E-G}$ and M_0 are not known a priori, but are determined in a comparative measurement (the instrument calibration), which determines phase and modulation for example of the fluorescence signal of a known lifetime standard or reflected excitation light. Depending on the spectral properties of the fluorophores under observation the calibration can be a difficult task. Further the calibration, together with the phase stability of the instrument are of greatest importance for the quality of a lifetime measurement. Therefore a more detailed discussion of the calibration procedure and the methodology developed for the special application presented in this work can be found in section 3.2.1.2. From the obtained instrumental parameters $\Delta\phi^{E-G}$ and M_0 , by subtraction/division one can determine directly the required phase shift Φ and modulation M.

The detailed signal analysis at homodyne detection[16] shall be given in the following section:
For the calculation of the fundamental Fourier components (the calculation of one lifetime image), at least three intensity images taken at different phase settings must be acquired. Due to this requirement, in the past this mode of analysis has been reserved for precision measurements rather than for really fast applications, for which other methods can be used (see Schneider and Clegg 1997). In section 3.1.2.2.1 it is demonstrated, that the requirement

of three intensity images per lifetime image is no obstacle for lifetime measurements even at video rate. The method therefore can be applied for both, fast and high precision measurements, depending on the fluorescence signal from the sample under observation.

K intensity images with the homodyned pixel signals $S\left(\Phi, \Delta\phi^{E-G}\right)$, defined in equation (2.28) , are acquired whereby $\Delta\phi^{E-G}$ is shifted by 2π /K between two successive images. From these K images the following values can be calculated for every pixel:

$$\tilde{F}_0 = \frac{1}{K}\sum_{k=0}^{K-1} S\left(\Phi, \Delta\phi^{E-G} + k\frac{2\pi}{K}\right) \tag{2.30}$$

$$\tilde{F}_{\sin} = \frac{1}{K}\sum_{k=0}^{K-1} \sin\left(k\frac{2\pi}{K}\right) S\left(\Phi, \Delta\phi^{E-G} + k\frac{2\pi}{K}\right) \tag{2.31}$$

$$\tilde{F}_{\cos} = \frac{1}{K}\sum_{k=0}^{K-1} \cos\left(k\frac{2\pi}{K}\right) S\left(\Phi, \Delta\phi^{E-G} + k\frac{2\pi}{K}\right) \tag{2.32}$$

These three calculated images represent the zeroth, time independent [Eq. (2.30)] component, and the sine [Eq. (2.31)] and cosine [Eq. (2.32)] time-dependent components for the fundamental frequency of the Fourier expansion at one pixel of the series of the K intensity images. These values can be further processed to yield the total phase $\left(\Delta\phi^{E-G} - \Phi\right)$ and total modulation depth M_0 M in each pixel:

$$\Delta\phi^{E-G} - \Phi = \arctan\frac{\tilde{F}_{\sin}}{\tilde{F}_{\cos}} \tag{2.33}$$

$$M_0\ M = \frac{1}{\tilde{F}_0}\sqrt{\tilde{F}_{\sin}^2 + \tilde{F}_{\cos}^2} \tag{2.34}$$

A reference experiment (instrument calibration) yields the measured phase ϕ_{meas} and modulation M_{meas} for a lifetime reference with known ϕ_{ref} and M_{ref} and therefore one obtains $\Delta\phi^{E-G} = \phi_{meas} - \phi_{ref}$ and $M_0 = M_{\text{meas}} / M_{\text{ref}}$.

By comparison with the measured $\Delta\phi^{E-G}$ and M_0 from the instrument calibration, the phase shift Φ and modulation M that are related to the fluorescence lifetimes can be obtained from equations (2.33) and (2.34). The actual composition of the lifetime components can then be calculated according to equations (2.21) and (2.22) if, in addition to the two measured parameters Φ and M, a sufficient number of parameters is known in order to solve the equation system. How this is done for the analysis of a specific single frequency measurement for a two lifetime component system is shown in the Appendix. But in general in imaging

applications the necessary number of additional parameters is not at hand. Therefore one calculates the apparent single lifetimes τ_{phase} and τ_{mod} from phase Φ and modulation M:

$$\tau_{phase} = \frac{\tan \Phi}{\omega} \tag{2.35}$$

$$\tau_{mod} = \frac{\sqrt{M^{-2} - 1}}{\omega} \tag{2.36}$$

In the case of a mono-exponential decay (a single lifetime component) these values correspond to the true values [compare Eq. (2.23) and (2.24)] and $\tau_{phase} = \tau_{mod}$, but for more complex lifetime compositions $\tau_{phase} < \tau_{mod}$. Additional determination of phase and modulation of the same object at different frequencies in principle allows to resolve complex compositions of multiple lifetime components (Gratton and Limkeman 1983; Jameson *et al.* 1984; Lakowicz 1999). This is a common method for non-imaging fluorescence lifetime measurements in a cuvette. If excitation and detection are chosen not purely sinusoidal, the analysis of higher frequency components can also be used for this purpose (see e.g. Clegg and Schneider 1996; Gadella Jr. 1999). The high precision multi-lifetime-component imaging measurements utilizing the time domain (as for example the simultaneous time- and space-correlated single photon counting) have already been mentioned in section 2.1.4.

Although the analysis of complex lifetime compositions in every pixel of an image without doubt can be extremely useful for certain applications, it involves drawbacks in measurement and analysis time. But as pointed out before, for many biological imaging applications the rapidity of the measurements is of importance due to photobleaching, sample movement or kinetic processes. In many cases a complete lifetime component analysis in every pixel is not necessary. Often one is only interested to visualize spatial domains of different lifetime-compositions in an image (e.g. for fluorescence diagnostic applications) or a number of parameters of a system are known or can be estimated, so that the two lifetime images [calculated by Eq. (2.35) and (2.36)] are sufficient to answer certain biological questions (compare e.g. the lifetime compositions in photosynthetic algae as analyzed in section 3.2 and the Appendix 5.5/5.6).

Data acquisition and analysis have to be selected in consideration of the questions that shall be answered by an investigation. The speed of the measurement has been one of the main objectives for the instrument developed in this work. Additional points of interest for rapid measurements should be mentioned:

$\Delta\phi^{E-G}$ need not be the same at all pixels to determine a lifetime image. Any distortion due to an iris effect (compare 3.1.1.5) is corrected for by comparison to a reference measurement.

However, if $\Delta\phi^{E-G}$ is constant over the whole image as it is true in our case (Schneider and Clegg 1997), one can compare the phase and modulation images with scalar reference values rather than with reference images, which again saves precious calculation time.
Further if $\Delta\phi^{E-G}$ is set to zero by the calibration procedure described above (and in section 3.2.1.2) the lifetime can be calculated directly by the following relation [compare (2.33) and (2.35)]:

$$\tau_{phase} = -\frac{\tilde{F}_{\sin}}{\tilde{F}_{\cos}\,\omega} \tag{2.37}$$

This saves the time for comparing the measurement to a reference value ($\Delta\phi^{E-G}$) and for calculating the arctangent (2.33) and tangent (2.35). This procedure has been fully integrated in the FlimFast program for imaging at video rate (compare 3.1.2.2).

For precision measurements, the single intensity images at every phase setting $\Delta\phi^{E-G}$ are recorded. This allows later analysis for example of the average lifetime of a spatial image region on the unprocessed raw data. The intensity signals from all pixels in the region are added and a single Fourier analysis can be performed for reduction of the measurement error. But for fast screening the intensity images do not need to be recorded. In this case the pixel signals $S\left(\Phi, \Delta\phi^{E-G}\right)$ are added according to equations (2.30)-(2.32) on the fly in the computer memory after every image acquisition, which saves additional time for the final calculation of the lifetime image after three (or more) intensity images at different phase settings.

Before a measurement is started a dark image with closed shutter is taken to determine the background light of the sample. Under general measurement conditions (if the room light is turned off) this image corresponds to a real dark image of the camera, which has been found to be sufficiently homogeneous over the whole image and constant. Therefore also in this case a scalar value can be used for the background subtraction rather than a background image. Nevertheless, every time before the shutter opens and the measurement is started the background value used for subtraction is measured. This assures correct measurements even under unfavorable conditions (e.g. scattered room light).

2.1.9 Visualization of fluorescence lifetime image information

The amount of information generated during continuous fluorescence lifetime image acquisition and analysis is enormous. The FLI instrument presented in section 3.1 is capable to acquire phase shifted fluorescence intensity images of about 74800 pixels at rates up to 26

fps. For single frequency measurements the per pixel Fourier analysis of three or more of those images yields to at least three meaningful scalar images respectively three real number (floating point) parameters per pixel: the mean fluorescence intensity $\tilde{F}_0$ [equation (2.30)] and the apparent single fluorescence lifetimes calculated from phase shift τ_{phase} [equation (2.35)] and demodulation τ_{mod} [equation (2.36)]. The aim of visualizing this multi-parameter image information is to provide a high-level description of the data that enables the user to emphasize and understand selected aspects of the measurement and easily survey the different parameters on a global scale, as well as identify their correlations with each other. It is apparent that the kind of visualization has to be selectively adjusted to the aims of the measurement.

The aims of fluorescence lifetime imaging are manifold. In addition to the quantification of fluorescence lifetimes at certain pixels, the qualitative distinction of spatial regions of different fluorescence lifetimes or intensities, the correlations of those parameters with structural, biological information, and the correlation of the parameters themselves neglecting spatial information, are of particular interest. Regions of different properties within an image can be distinguished using visualization in the form of color-coded bitmaps, iso-contour plots, height plots, or any combination respectively overlay of these. The combination of these displays is not limited to a single parameter but can be extended to displays generated from different parameters, thereby allowing for spatial correlation of several image parameters. Moreover, color-coding can be extended to include two or three pixel parameters by using multi-dimensional color lookup functions. Correlation of parameters neglecting the spatial position of pixels can be visualized in form of multi-dimensional scatter plots or histograms.

2.1.9.1 Color-coded lifetime images

Scalar images are most commonly visualized in form of color-coded images, often called false color or pseudo color images since there is no correspondence of the color code with the physical color in the image. The scalar at each pixel of an image is replaced by a color according to its value such that regions of the same scalar value have the same color and regions of different properties within an image can be distinguished by different colors. Using the same color code, fluorescence lifetime images from different measurements or calculated from phase shift and demodulation can be compared when displayed side by side.

Color-coding is commonly implemented by looking up (indexing) a predefined color array with 256 entries (8 bit), which is also referred to as a color palette or color look-up table (CLUT). This involves the normalization and clamping of the scalar parameter to a region of

interest given by minimum and maximum values, which are often chosen to yield a maximum of dynamic range, prior to the final lookup into the palette. The choice of a suitable palette and scale is often an artistic task that involves interactive adjustments. Intensity images are regularly coded using a linear grey-scale palette. Nonlinear palettes, such as the ubiquitous 'rainbow' palette, are chosen to visually enhance contrast.

The main advantages of this technique are its fast and straightforward realization and the availability of bitmap display routines that basically copy the final color bitmap from the computer main memory into the display buffer on the graphics card (bit blitting). These display routines are available on all computer systems and are generally highly optimized for speed, which makes them the preferred choice for display of color coded images at video rate.

Besides the appearance of possible aliasing artifacts in the color coded bitmaps that can originate from using nonlinear or low resolution color palettes, there are two main disadvantages specific to the visualizing fluorescence lifetime images by means of color coding. Both are related to the fact that fluorescence lifetimes are mostly independent of the fluorescence intensity. For one, by only taking into consideration the lifetime values obtained by Fourier analysis according to equations (2.35) and (2.36), any information about the quality of the data is omitted. Every pixel in the image is analyzed in the same way and given a lifetime value regardless whether its corresponding fluorescence intensity signal is actually sufficient for analysis. There is a need to weight the lifetime value of every pixel by its fluorescence intensity, which is fortunately also accrued during Fourier data analysis [equation (2.30)]. A simple way to achieve this is to mask (usually blacken) out those areas of the color-coded fluorescence lifetime image where the fluorescence intensity is below an arbitrary intensity threshold that is considered sufficient for accurate Fourier analysis.

A second disadvantage is that fluorescence lifetime images themselves often do not provide sufficient structural information in order to correlate the spatial distribution of fluorescence lifetimes with (for example) the location of biological structures such as a cell or cell nucleus. Except for cases of homogenous fluorescence or obvious spatial structure (e.g. micro titer plates, or micro capillaries), the mean fluorescence intensity image is a much better source of structural information. By displaying color-coded fluorescence lifetime and intensity images side by side, both images can be visually correlated by a human viewer. However, this can be a demanding, imprecise and tiring task, especially in cases of continuously and fast changing images. Multi-parameter image visualization techniques that integrate the information of both images into one single view can facilitate that task.

2.1.9.2 Multi-parameter displays: color-coded height plots and image overlays

Several visualization techniques can be used to assist the operator in structurally correlating and weighting fluorescence lifetime images with their corresponding fluorescence intensity images. Typically the intensity image is displayed in form of a height plot, iso-contour plot, or color-coded image and combined respectively overlaid with its corresponding color-coded fluorescence lifetime image.

Height plots, such as bar charts and surface renderings, make use of the third dimension to include the weighting and structural information of the fluorescence intensity image. The spatial dimensions of the image are represented in the x-y plane while the fluorescence intensity $\tilde{F}_0$ is plotted in the z dimension. **Color coded surface renderings** respectively relief plots have been found particularly useful for visualizing fluorescence lifetime images of biological cells (Holub and Schneider 1997; Schneider 1997). For each pixel in the image the coordinates (x, y, $\tilde{F}_0$) are used as control points, through which a bi-linearly interpolated solid surface is rendered. The color at each control point is given by its corresponding lifetime color code and is also interpolated among the surface. The z-coordinate and color-coding can of course be assigned to any arbitrary image parameters. Color-coded surface renderings tend to be relatively easy to comprehend, partially because they are so reminiscent of geological terrains. Discontinuous changes in the z-parameter (e.g. noise) can easily be detected visually as peaks whereas they might remain unnoticed in a color coded image. The method goes along with an elaborate implementation and often long rendering times compared to the simple display of color-coded bitmaps. Therefore historically it has been applied to non real-time, offline data visualization only. However, as will be presented in section 3.1.2.2.2, hardware accelerated polygon based rendering in conjunction with multi-texture mapping can be used for implementing real-time color-coded shaded surface renderings. There are two principle drawbacks to height plots due to their three-dimensional nature. Although height plots are three-dimensional, they are viewed from a certain angle and projected onto a two-dimensional plane in order to display them on a monitor. Depending on the viewing angle, parts of the plot might be hidden by other parts. Moreover, the visual perception of depth in a two-dimensional projection of a three-dimensional object is often problematic. Techniques to enhance the depth perception by making the rendering look more ‘realistic’ (although there is no corresponding object in the real world) such as perspective projection, shading using one or more light sources, or depth cueing often complicate the understanding of the actual image data and can even lead to false interpretations (e.g. shading and depth cueing change the perception of surface color). Stereo rendering and the ability of the viewer to interactively

change the viewing angle in real time greatly helps to moderate the problems of hidden data and perception of depth.

An alternative to surface renderings are **iso-contour plots,** which are frequently used for visualizing geological terrains, too. Again, the image is interpreted as a height field that spans a surface, but only the intersections of the surface with x-y planes at certain heights (iso-values) are drawn, in the x-y dimension. The iso-values are commonly chosen to be evenly spaced such that a high density of iso-contours indicates a steep change of the scalar field. Iso-contours can provide good outlines of large and distinct structures (such as a cell or nucleus in a microscope image), but they easily become un-interpretable for noisy data or structures with small differences in the z-dimension. Practically iso-contours are obtained either by tracing the scalar image for each iso-value and drawing lines along the traces (iso-contour lines) or by coloring small intervals (in scalar space) around each iso-value. While the first method is slow, the second requires interpolative rendering routines with sub-pixel precision to yield plausible results**.** The iso-contours obtained from the fluorescence intensity image can be overlaid onto a color-coded lifetime bitmap. This overlay plot is not so much useful for weighting the data of individual pixels, but for correlating the spatial distribution of fluorescence lifetimes with the distinct structures provided by the intensity image.

A multi-parameter visualization method that is often used in fluorescence imaging is the overlay respectively combination of two (or more) color-coded bitmaps into one bitmap by simply adding or averaging their RGB channels. To prevent ambiguities regarding the resulting colors, the single images are typically color-coded using different color channels, e.g. one image is encoded using a linear red scale palette while the other uses only the blue channel. A more elegant and less ambiguous way to combine the information of two or more (multiple) images is to directly color code them into a single bitmap by using **multi-parameter color coding**: for each pixel the multiple image parameters are normalized and clamped to certain regions and used to independently index the different dimensions of a multi-dimensional color lookup table (palette). While these image overlay methods are straightforward to implement and can revert to fast bitmap display routines, they often require extended manual adjustments to the color code and tend to be unintuitive except for simple cases where distinct and mostly non-overlapping structures are visible in the single images. This makes them unsuitable for real-time visualization of constantly changing data.

2.1.9.3 Two-dimensional fluorescence lifetime histogram and scatter plots

Multi-parameter image displays can also be used to correlate and compare the apparent single fluorescence lifetime images obtained from the phase shift and demodulation. As discussed in section 2.1.8 these two parameters only coincide when only a single lifetime component is present in a pixel, while they differ to certain degrees in case of multiple lifetime components. A comparison of both parameters based on side-by-side displays of the color coded images or a multi-parameter display leaves valuable information undetected. A **two-dimensional per pixel scatter plot of τ_{mod} vs. τ_{phase}**, which discards spatial information, has been found particularly useful for the interpretation of single frequency FLI measurements (Holub and Schneider 1997; Schneider 1997; Gadella Jr. *et al.* 1994). Pixels with single lifetime components are located on the $\tau_{phase} = \tau_{mod}$ diagonal of the plot, while those with multiple lifetime components fall within the $\tau_{phase} < \tau_{mod}$ area. In case of systematic measurement errors (e.g. wrong calibration) or bleaching (for which the digital Fourier analysis of equations (2.30)-(2.32) does not account), pixels can fall in the $\tau_{phase} > \tau_{mod}$ area. A **two-dimensional image histogram of τ_{mod} vs. τ_{phase}**, henceforth called the 2D lifetime histogram, provides an even more content rich view of the data since it can also reveal statistical information such as a center, spread and skewness of the data in addition to the presence of outliners or multiple modes. A two-dimensional image histogram is obtained from the data of two images by splitting the two-dimensional range of data into equally sized square bins. The number of pixels that falls into each bin is counted. As any two-dimensional scalar field, two-dimensional histograms can be visualized as color coded bitmaps or surface plots.

The two-dimensional per pixel scatter plots and image histograms can easily be extended by one dimension to include the mean fluorescence intensity as a weighting parameter. However, the visualization of a three-dimensional histogram (e.g. by iso-surface or volume rendering) is such a demanding task in terms of both computational power and interactive adjustments required by the viewer, that it can currently not be considered practicable for real-time imaging. A simple three-dimensional per pixel scatter plot of τ_{mod} vs. τ_{phase} vs. $\tilde{F}_0$ provides almost the same information. Measurement artifacts and anomalies, such as off-scale intensities, bit-noise or bleaching, can easily be detected visually, as can the independence of lifetimes from the intensity.

2.2 Photoprotection during photosynthesis

Plants and algae have the ability to adapt to environmental conditions in numerous ways in order to optimize their photosynthetic activity. While developmental responses govern the long time scale, plants can respond in seconds to changes in light intensity. Such rapid regulation is necessary not only to maintain optimal photosynthetic activity, but also to hold the production of damaging reactive species at a minimum during photosynthesis. During times of excessive light intensity, plants dissipate the potentially harmful energy that is not used for photosynthesis as heat. Photoprotection of this kind can be monitored by non-photochemical quenching (NPQ) of the chlorophyll (Chl) *a* fluorescence produced in photosystem (PS) II (for reviews, see Renger *et al.* 1995; Gilmore and Govindjee 1999; Horton *et al.* 1999; Demmig-Adams and Adams III 2000; Müller *et al.* 2001; Govindjee 2002).

Light is absorbed by Chls and carotenoids located in pigment-protein complexes, the light-harvesting-complexes (LHCs) of the two photosystems PSI and PSII in the thylakoid

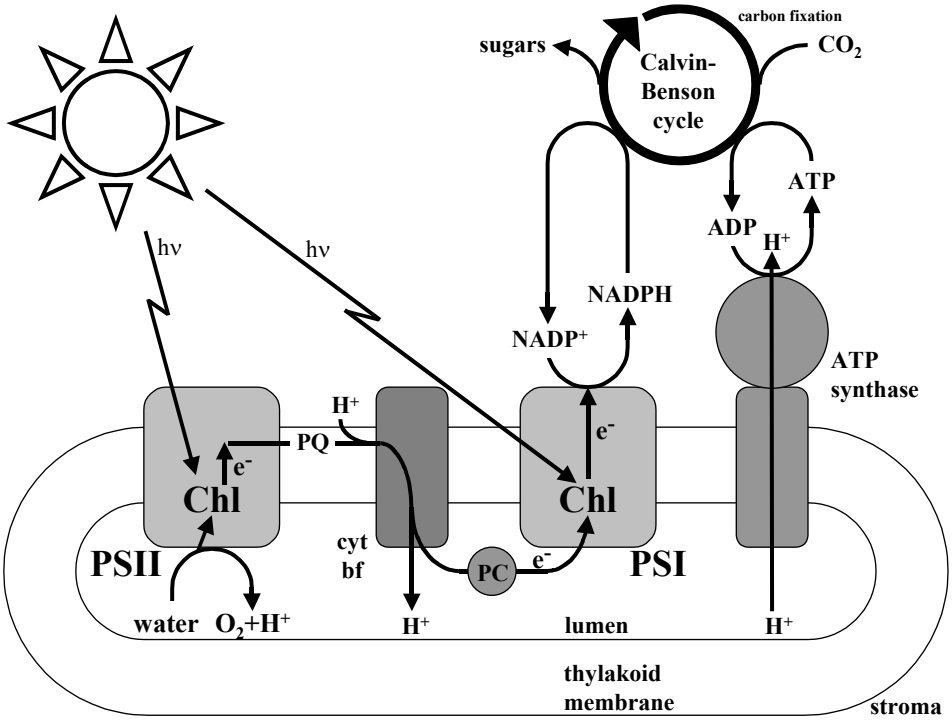

Fig. 7: Overview of photosynthetic processes as they occur in plants and algae
Schematic representation of the electron transport chain along the thylakoid membrane of a chloroplast. Diffusion of the two electron carriers plastoquinol (PQ) and plastocyanin (PC) constitutes the connection between three protein complexes – the two photosystems (PS) I and II and the cytochrome b_6f complex (cyt bf). Light absorption or exciton transfer to chlorophyll (Chl) *a* in the PSI and II reaction centers drives the electrons from H_2O to $NADP^+$ forming NADPH and consequently transports protons from the stroma into the thylakoid lumen. H_2O molecules are oxidized by the oxygen-evolving complex of PSII, yielding O_2. The resulting proton gradient (formed during water and plastoquinol oxidation) powers the synthesis of ATP by ATP synthase. The energy in form of NADPH and ATP is used for carbon fixation.

membranes of the chloroplasts (see Fig. 7 for an overview of basic photosynthetic processes).

Absorption results in singlet-state excitation of Chl molecules with a subsequent return to the ground state via several different competitive pathways (which have been discussed in more detail in the general context of Fig. 1):

(a) Förster energy transfer between Chl molecules as part of an energy migration by which the energy is channeled to the reaction center where it is used to drive photochemistry.[17]

The energy of the excited molecules is quenched by being transferred to other non-emitting molecules, which can be thermal dissipation by collisional transfer

(b) to water molecules (internal conversion) or

(c) to different molecules by formation of a collisional complex (dynamic quenching).

(d) Transition from the excited Chl singlet-state (^{1}Chl*) to the Chl triplet-state (^{3}Chl*) by intersystem crossing, which in turn can transfer energy to the ground-state of oxygen (a triplet: $^3O_2$), generating singlet-state oxygen ($^1O_2$*) as well as superoxide anions ($^{\bullet}O_2^-$) and other radicals. All of these are highly damaging photoreactive species, which can attack, oxidize and decompose pigments, lipids and proteins.

(e) Light can be emitted as fluorescence.

Due to the competitive pathways for de-exiting the excited state, the Chl fluorescence (intensity and lifetime), which at room temperature originates mainly from PSII, contains information about all the other non-fluorescence pathways of de-excitation. The deactivation pathways that involve photochemical reactions are quenching the fluorescence and are defined as photochemical quenching, qP. Additionally all other deactivation pathways quench the fluorescence and are called collectively non-photochemical quenching, NPQ.

In case of constant NPQ and non-changing rate constant for fluorescence k_F, changes in the fluorescence emission directly reflect qP and thereby allow to monitor the reactions of PSII (see Fig. 8).

The photochemical reactions of PSII involve charge separation at the reaction center P680 (the primary electron donor; a special arrangement of four Chl molecules). Excited P680 can transfer an electron to pheophytin (Pheo), creating the charge-separated state $P680^+/Pheo^-$. Subsequent fast electron transfer steps prevent this primary photochemical reaction from recombining by transferring the electron from $Pheo^-$ to the primary quinone acceptor Q_A (a bound plastoquinone (PQ) molecule). From Q_A^- the electron is transferred to another plastoquinone molecule Q_B, that is bound to a special pocket of PSII (the Q_B site).

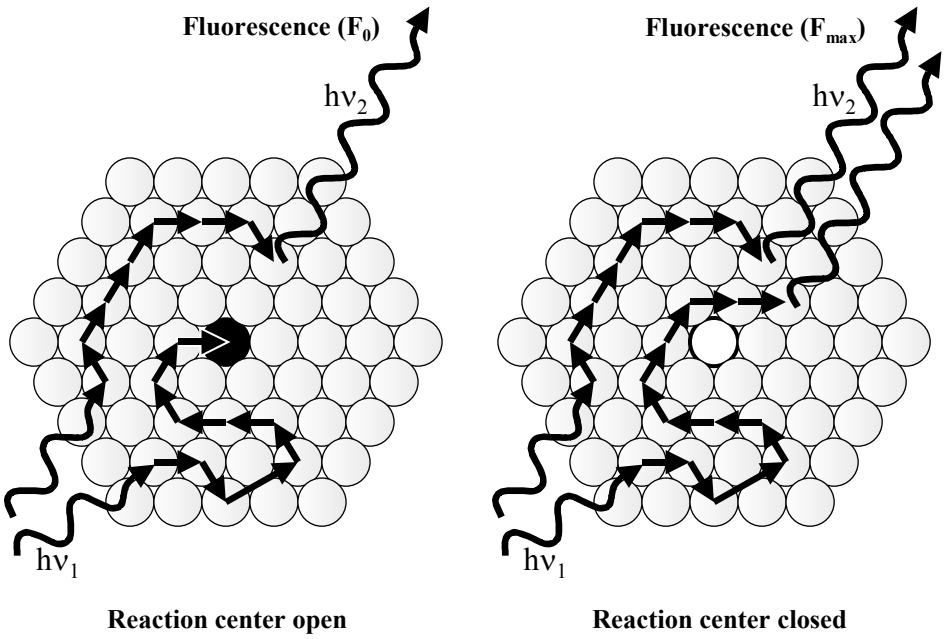

Fig. 8: Chl *a* fluorescence allows to monitor and probe the photochemical reactions of PSII
Antenna Chl (grey circle) excitation and consecutive Förster fluorescence resonance energy transfer allows energy migration to an open reaction center (black circle). The fate of two absorbed photons is displayed. A closed reaction center (white circle) leads to an increase in fluorescence intensity and lifetime.

After two photochemical turnovers (successive absorption of two photons by P680) Q_B becomes fully reduced to plastoquinol (PQH_2), after which it is replaced by another PQ molecule from the PQ pool and released into the thylakoid membrane.

The water–oxidizing complex of PSII, which includes a $(Mn)_4$ cluster, provides the electrons for the reduction of a tyrosine residue (labeled as Yz) on one of the two PSII core proteins D1, which itself transfers the electron to $P680^+$ (see Renger 2001 for a review; for an introduction to PSII see, Whitmarsh and Govindjee 2001; compare also with the three-dimensional structure of PSII as determined to 3.8-Å resolution by Zouni *et al.* 2001).

The photochemical reactions of PSII as described above strongly affect the Chl fluorescence. When Q_A is oxidized, the reaction center is able to utilize the light energy harvested by the antenna system for charge separation and the fraction of excitation lost to fluorescence is low, giving rise to low fluorescence yields (compare Fig. 8). But in contrast, when Q_A is reduced, the reaction center is unable to undergo stable charge separation and the fraction of excitation lost to fluorescence is high, giving rise to the maximum fluorescence yield. Such changes in fluorescence intensity have been first discovered by Kautsky and Hirsch (1931). They found that fluorescence intensity undergoes large changes with time, when dark-adapted leaves are brought from darkness to constant irradiation. This effect has been named Kautsky effect, which is also usually referred to as the "fluorescence induction" or the "fluorescence transient". The characteristics of this transient are identified by the acronym OJIPSMT, where

O refers to the "constant" minimum fluorescence, J and I refer to the intermediate inflections before the fluorescence reaches its maximum P, S signifies a semi-steady state, M stands for another peak (or maximum), and T is the terminal steady state (for reviews see, Govindjee 1995; Lazar 1999). As stated before, the transient reflects mainly the kinetics of electron transfer in PSII, but it is influenced by protonation events, by PSI activities, and by changes in the absorption cross-section. At high light intensities, changes in non-photochemical quenching also strongly influence the transient on a time scale of seconds (that is mainly after the P-level has been reached, therefore during the P-to-S decline).

Fig. 9 shows a transient and the effect of the variable contribution of NPQ. As displayed in this figure, NPQ is often further divided into categories according to their relaxation times:
(a) Energy-dependent quenching (qE) requires the build up of a proton gradient and relaxes in seconds to minutes. qE will be discussed in more detail below;

(b) State-transition quenching (qT) requires tens of minutes. Under "state transitions" (Allen and Forsberg 2001) one understands the phenomenon that a portion of LHCIIs, a mobile LHC, can separate from the strongly fluorescent PSII, thereby reducing the antenna size, and move to the weakly fluorescent PSI. Plastoquinol accumulation at excess light (of a wavelength, which is absorbed predominantly by PSII) may stimulate, through a series of biochemical events, the phosphorylation of LHCIIb polypeptides, which then can move physically from the PSII region to the PSI region of the thylakoid membrane. This reorganization, which leads to a state referred to as state II, causes a decrease in the fluorescence intensity, but not in the fluorescence lifetime. If plants are exposed to light absorbed predominantly by PSI, the process is reversed to state I, which is characterized by higher fluorescence intensity (but unchanged fluorescence lifetime).
At this point it further should be mentioned that, if LHCII only separates from PSII and becomes free, its lifetime of fluorescence will increase, not decrease; but if it moves to PSI, the yield will decrease. Further the yield could decrease if the free LHCIIs aggregate;

(c) Photoinhibitory quenching (qI) is often very slow, sometimes lasting in the range of hours.

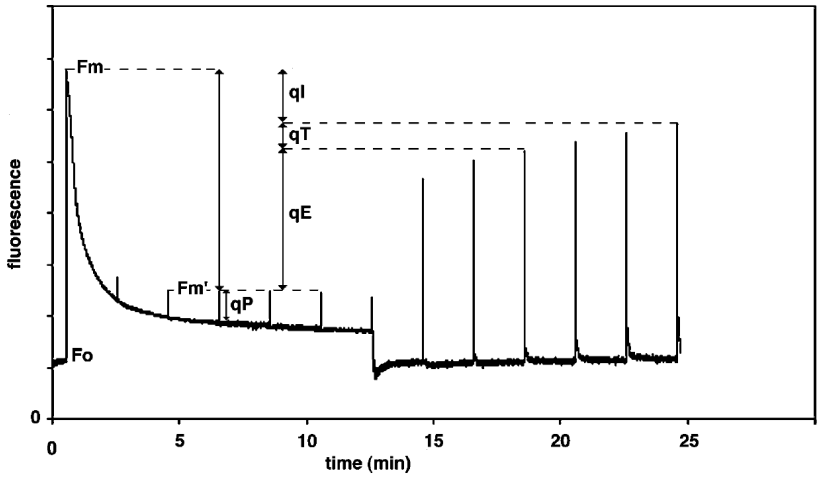

Fig. 9: Quenching during the fluorescence transient. Chl *a* fluorescence measurement from an *Arabidopsis* leaf

In the presence of only weak measuring light the minimal fluorescence (F_0) is recorded. When a saturating light pulse is given, the photosynthetic light reactions are saturated and fluorescence reaches a maximum level (F_m'). Upon continuous illumination with moderately excess light (750 μmol photons m^{-2} s^{-1}; growth light was 130 μmol photons m^{-2} s^{-1}), a combination of qP and NPQ lowers the fluorescence yield. NPQ (qE + qT + qI) can be seen as the difference between F_m and the measured maximal fluorescence after a saturating light pulse during illumination (F_m'). After switching off the light, recovery of F_m' within a few minutes reflects relaxation of the qE component of NPQ.
Reproduced from (Müller *et al.* 2001). The described method has been introduced by Bilger and Schreiber (1986).

The qE is correlated with the activation of the so-called xanthophyll cycle (Demmig *et al.* 1988; Demmig-Adams *et al.* 1996), see Fig. 10.

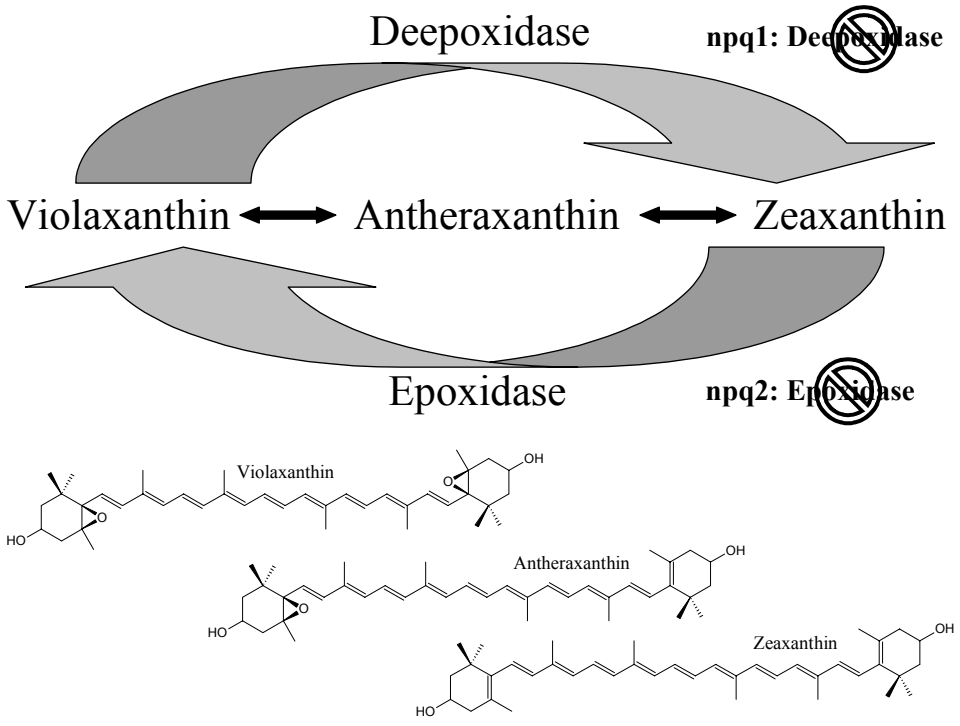

Fig. 10: Xanthophyll cycle (Yamamoto *et al.* 1962; Yamamoto *et al.* 1999)

The cycle consists of the de-epoxidation of the xanthophyll violaxanthin in high light to first antheraxanthin and then zeaxanthin, catalysed by violaxanthin de-epoxidase (VDE), an enzyme, which is activated at low pH. Zeaxantin epoxidase (ZE) catalyses the reverse epoxidaton reactions that complete the violaxanthin cycle. The two mutants npq1/npq2 used in this work are deficient in VDE and ZE, respectively, and accordingly accumulate violaxanthin (npq1) or zeaxanthin (npq2).

The current model of qE can be summarized in Fig. 11.

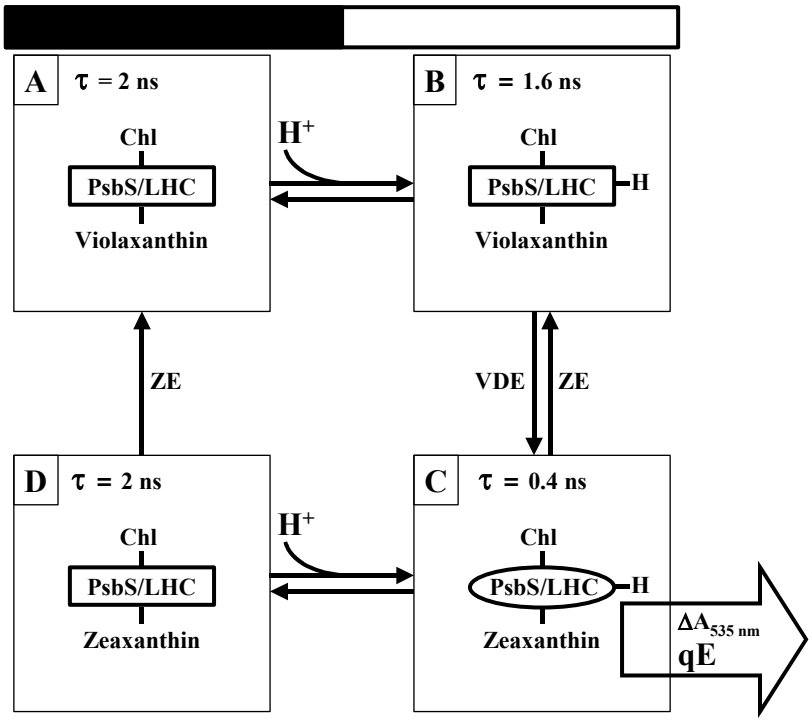

Fig. 11: Summary model for energy-dependent Chl fluorescence quenching (qE)
A) In limiting light or darkness (black bar on top) no quenching occurs.
B) In high light (white bar) PsbS and LHCII proteins become protonated, causing a shift in Chl fluorescence lifetime to 1.6 ns.
C) A quenching complex with a different conformation (measurable as absorption change $\Delta A_{535\ nm}$) is formed when zeaxanthin and protons are bound, reducing the fluorescence lifetime to 0.4 ns. Conversion of violaxanthin to zeaxanthin by violaxanthin de-epoxidase (VDE) occurs more slowly than protonation. Zeaxanthin might bind to the same site as violaxanthin or a different one.
D) When the light stress has ended, the PSII proteins are de-protonated rapidly, whereas the epoxidation of zeaxanthin to violaxanthin by zeaxantin epoxidase (ZE) is slower. In the dark, formation of complex D from complex A is not possible in vivo, but can artificially be induced by decreasing the pH in the thylakoid lumen.
Reproduced from (Müller *et al.* 2001). Note, however, that the inclusion of information on lifetime of fluorescence is based on the work and the model of Gilmore *et al.* (1995; 1998).

Under intense irradiation that exceeds a plant's capacity for CO_2 fixation, lumen acidification leads to the enzymatic conversion of violaxanthin to zeaxanthin *via* antheraxanthin. In addition, the buildup of the thylakoid ΔpH (Krause 1973; Briantais *et al.* 1980) leads to protonation of and conformational changes in the LHCIIs, which might favor the binding of zeaxanthin. The combination of these two events leads to a quenched state of PSII with lowered Chl fluorescence intensity and lifetime (Gilmore *et al.* 1995; Gilmore *et al.* 1998).

Conformational changes in the thylakoid membrane could be inferred from the lifetime measurements of Gilmore *et al.* (as cited before) and from absorbance changes ($\Delta A_{535\ nm}$) measured at 535 nm (Krause 1973; Bilger and Björkman 1994).

There is a debate about the exact site (or sites) of the thermal energy dissipation in PSII - the location[18], at which the conformational change occurs. Two problems have to be clarified.

First, in which pigment-protein complex is the quenching state formed and second, which particular pigments in the complex are involved in the quenching. Nothing so far is known about the second point, but three sites have been suggested for the pigment-protein complexes involved: The minor antenna Chl-protein complexes CP26 and CP29 (LHCII monomers), the major peripheral antenna light-harvesting complexes LHCIIb (LHCII trimers) and the 22 kD PSII protein *PsbS*, which belongs to the LHC protein superfamily.

Bassi *et al.* (1993; 1997) suggested the involvement of CP26 and CP29 in NPQ due to preferential binding of xanthophylls to these proteins. Further, Frank *et al.* (2001) and Crimi *et al.* (2001) showed that the binding of zeaxanthin leads to a shorter lifetime for the Chl fluorescence component *in vitro* in CP26 and CP29. See also Crofts and Yerkes (1994) for a description of such a quenching mechanism *via* the internal minor antenna. On the other hand, Andersson *et al.* (2001) investigated antisense *Arabidopsis* plants that lacked CP26 or CP29 and could show that the loss of the minor antenna complexes did not alter NPQ.

The major antenna had been excluded by Gilmore *et al.* (1996) as the location for the quenching, because they did not observe changes in NPQ in a mutant, which had reduced levels of trimeric LHC. Chow *et al.* (2000) on the other hand found a correlation between different levels of major LHC and NPQ. Elrad *et al.* (Elrad *et al.* 2002) could establish a clear relationship between NPQ and a trimeric LHCIIb, by investigation of a mutant of *Chlamydomonas reinhardtii* called npq5, which lacks a major light-harvesting polypeptide (*Lhcbm1*). This mutant is defective in qE, but transformation of the mutant strain with the *Lhcbm1* gene led to restoration of normal NPQ.

Finally the protein *PsbS* has been found to be essential for qE (Li *et al.* 2000). An *Arabidopsis* mutant npq4-1, which lacks the *PsbS* protein, is also deficient in qE. This mutant further lacks the conformational change monitored by $\Delta A_{535\ nm}$, but has normal levels of xanthophylls and of the other LHCII proteins and is not impaired in light harvesting.

Multiple environmental and molecular interactions that affect the qE have been investigated. Isolated thylakoids exhibit qE in the absence of zeaxanthin, but only at lumen pH values lower than normally occurring *in vivo* (Rees *et al.* 1992). Wentworth et al. (2000) found that in isolated LHCs of PSII quenching is induced by zeaxanthin alone, without ΔpH. Inhibition of qE could be observed when the zeaxanthin synthesis was blocked *in vivo* (Horton *et al.* 1994). Antheraxanthin also plays a role in qE (Gilmore and Yamamoto 1993; Gilmore *et al.* 1998) and can partially replace the role of zeaxanthin in certain algae (Goss *et al.* 1998). Another xanthophyll, lutein, seems also to be involved (Niyogi *et al.* 1997; Niyogi *et al.* 2001).

In general the quenching of Chl fluorescence correlates with the amount of zeaxanthin produced (Demmig-Adams 1990). The exact mechanism of the Chl de-excitation by xanthophylls is not known. The role of the xanthophylls could be indirect, affecting the structural antenna rearrangement by inducing conformational changes in the antenna complexes and disrupting energy transfer pathways along the Chls, thereby allowing Chl molecules to act as the quencher. This would correspond to an overall increase in the rate constant of internal conversion, in combination with a decrease in the rate constant for Förster transfer. Xantholhylls could also act directly and dynamically in the deactivation process
(1) if, by close association of Chl and xanthophylls (which is known to exist in certain cases), nevertheless exciplex formation (that is pure dynamic quenching) or a combination of dynamic and static quenching cannot be excluded and/or
(2) if the xanthophyll molecules act as acceptors in an energy transfer process from Chl molecules. Such hetero-energy transfer (Förster transfer) is in principle possible, because the lowest singlet excited state S_1 of Chl *a* is higher than the S_1 states of the xanthophylls (Polívka *et al.* 1999; Frank *et al.* 2000; Polívka *et al.* 2002). The question remains if transfer to zeaxanthin is more feasible than to violaxanthin. This depends not only on the energy levels, but also on the distance and the orientations, about which nothing is known yet.

The isolation of NPQ mutants opened new possibilities for *in vivo* studies of this process (for review, see Niyogi 1999). Two of these mutants are investigated in this work.
The mutant npq1 is deficient in violaxanthin de-epoxidase and therefore unable to convert violaxanthin to antheraxanthin and zeaxanthin (Niyogi *et al.* 1997). The mutant accumulates violaxanthin and lacks zeaxanthin/antheraxanthin.
The mutant npq2 is deficient in zeaxanthin epoxidase; therefore, it is unable to convert zeaxanthin to antheraxanthin and violaxanthin. This mutant accumulates zeaxanthin and lacks violaxanthin /antheraxanthin.
The characterization of the mutants npq1 and npq2, provided by Niyogi *et al.* (1997), has been extended by Govindjee and Seufferheld (2002). At high excitation light intensities they found lower rates of oxygen evolution for the violaxanthin-accumulating npq1 in comparison to wild type (WT)/npq2, which showed similar rates. This might be an indication for antioxidant action of zeaxanthin in addition to its direct quenching properties. The lack of zeaxanthin in npq1 would then result in less photoprotection.
The zeaxanthin-accumulating npq2 mutant shows a strong fluorescence quenching (as measured with a Pulse Amplitude Modulation instrument) not only for initial quenching of dark-adapted cells, but apparently also for the ΔpH requiring NPQ and even in the presence of

an inhibitor of the electron transport, DCMU (3-(3,4-dichlorophenyl)-1,1-dimethylurea). npq1 on the other hand still shows a significant steady state level of NPQ (similar to that in WT cells). This might be additional indication for the involvement of other species (most likely another carotenoid) in the mechanism of energy dissipation, as cited above. Also it was found that the xanthophyll cycle mutations do not affect either the "two-electron gate" (i.e., the acceptor side of PSII), or the back reactions from both Q_B^- and Q_A^- to the S_2 state of the

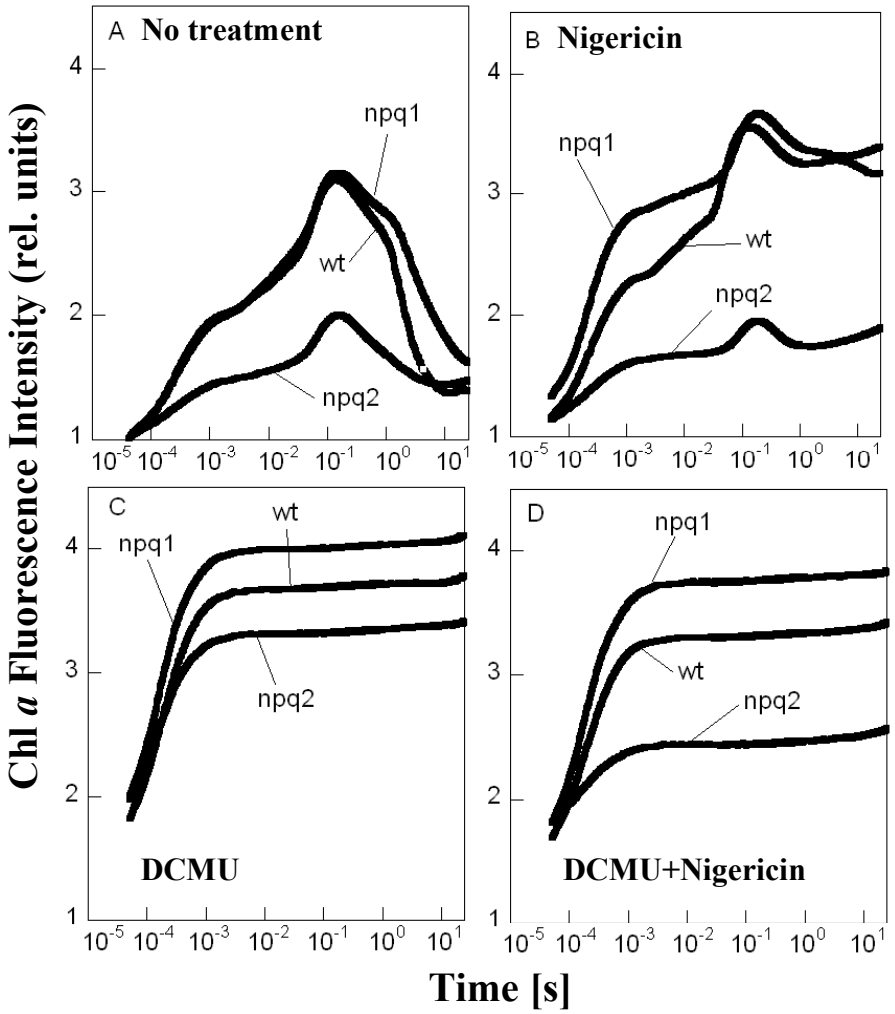

Fig. 12: Chlorophyll *a* fluorescence transients of cell suspensions of wild type (WT) and npq1 and npq2 mutants of *Chlamydomonas reinhardtii,*
measured with a Plant Efficiency Analyser (PEA) fluorimeter (Hansatech Instruments Ltd., Norfolk, UK). Cells were grown at 100 μmol photons m^{-2} s^{-1} in Tris-Acetate Phosphate (TAP) medium. Cells, which were harvested at late log growth phase, were exposed to light (650 nm; 2200 μmol photons m^{-2} s^{-1}) after the samples were dark-adapted for 5 minutes. All traces were normalized by dividing the measured values by the value for the data point at 40 μs of the untreated WT, which was taken as F_0. In all cases, the cell suspensions were gently centrifuged and the pellet re-suspended in fresh High Salt (HS) medium prior to the measurements. Cell suspensions were adjusted to 15 μg of Chl per ml. Panel **A**: Cells without treatment. Panel **B**: Cells were incubated with 10 μM nigericin in dark for 5 min. Panel **C**: Cells were dark adapted for 5 min and then treated with 10 μM DCMU (final concentration) and incubated for additional 5 min in the dark. Panel **D**: Cells were treated as in panel C except that nigericin was added to a final concentration of 10 μM. Reproduced from (Govindjee and Seufferheld 2002).

oxygen evolving complex. Thus, photoprotection may not involve cyclic reactions in PSII.

The quenching can also directly be seen in the fluorescence transients. Fig. 12 displays the transients for the xanthophyll cycle mutants npq1, npq2 and the WT (without cell walls) as given in Govindjee and Seufferheld (2002).

Significantly reduced fluorescence intensity (about 25-35% at P-level for the unnormalized data) has been detected for the npq2 mutant in comparison to WT and npq1 mutant (both of which showed about similar levels) even in the presence of the inhibitor DCMU and the uncoupler nigericin.

These studies cannot be interpreted unambiguously. The npq2 cells have a higher level of the measured initial fluorescence, F_{0meas}, in comparison to the WT/ npq1 cells, in spite of the higher level of NPQ. The operational definition of the extent of NPQ depends on the normalization with F_0 when one is measuring only fluorescence intensities. Therefore we have made direct measurements of the lifetime of fluorescence to clarify these ambiguities.[19]

In addition, changes in the absorption cross-section of the PSII antenna cannot be distinguished from true differences in the quantum yield of fluorescence when only fluorescence intensities are compared. Especially "state changes" (Delosme *et al.* 1996), as has been explained in more detail above, might change the fluorescence intensities and therefore might give rise to erroneous interpretations, if such processes are not taken into account. Additional determination of the quantum yield, as provided in this work, resolves these ambiguities and should lead to a better understanding of the NPQ mechanism.

For this investigation we have employed some novel measurement techniques and methods:

a) We have built an instrument for "Fast Fluorescence Lifetime-resolved Imaging (FLI)" and have used it to compare the ensemble lifetime characteristics of the two xanthophyll cycle mutants and the wild type (WT) in a single image measurement. These measurements also have been carried out in the presence of treatments with chemicals that interfere with certain steps in the photosynthetic cycle: DCMU inhibits the electron transport between PSII and PSI; nigericin dissipates the thylakoid proton gradient; and methyl viologen (MV) accepts electrons highly efficiently from PSI.

b) We have carried out ensemble lifetime measurements in micro-capillaries using FLI in order to observe the algae under swimming and resting (geotaxis physiological) conditions. Comparative measurements with micro-capillaries of both mutants and the WT in a single image have been acquired.

c) Measurements of the “Fluorescence Lifetime Transient”: For the first time, the temporal development of the fluorescence lifetimes during the fluorescence transient, which is present during constant illumination, have been recorded.

d) Our Fast FLI method has been applied to measure lifetime images of single cells and to follow their changes over time.

3 Experimental part

This work involved the construction of an instrument for Fluorescence Lifetime Imaging (FLI) with real-time capability[20] for data acquisition, analysis and visualization. Such instrumentation is not commercially available. While the performance of the first real-time instruments, presented by Schneider and Clegg (1997), have been limited by the computational power available at that time, the instrumentation presented in this work could be accelerated to its hardware dictated limitations. This has been made possible by a combination of new and conceptually different hardware and software design. The constructed system allows the continuous acquisition, analysis and visualization (e.g. surface-rendering) of fluorescence intensity and lifetime images at video-rate.[21] Rates up to 26 fps have been achieved for 320 x 240 pixel images. A partial description of the instrument can also be found in (Holub *et al.* 2000).

The second part of this work concerns the question how photoprotection during photosynthesis is affected if the xanthophyll cycle, which is known to be involved in the mechanisms that protect plants during excess light levels, is rendered inoperative in one direction: What happens to photoprotection during photosynthesis if violaxanthin cannot be converted to zeaxanthin any more (or vice versa)? The rapid image acquisition capabilities provided by the constructed instrument could be utilized to provide answers to these questions and to introduce new methods for the study of the fluorescence of photosynthetic samples.

3.1 Instrument for fast Fluorescence Lifetime Imaging (FLI)

The description of the FLI instrument is divided into two parts: In 3.1.1 all instrumental hardware components are presented and discussed in their functional context and in 3.1.2 it follows the description of the custom designed software.

3.1.1 Instrumentational design and construction

3.1.1.1 Instrument overview

Figure 13 shows a scheme of the optical and electronically setup and Fig. 14 a photograph of the FLI instrument. The single components shall be discussed in detail in the following parts.

The instrument operates in the frequency domain at a single frequency with sinusoidally modulated light for the excitation of the fluorescent object, and employs a full-field, homodyne detection of the phase-shifted and amplitude-demodulated fluorescence emission signal. Refer to the schematic drawing given in Fig. 13.

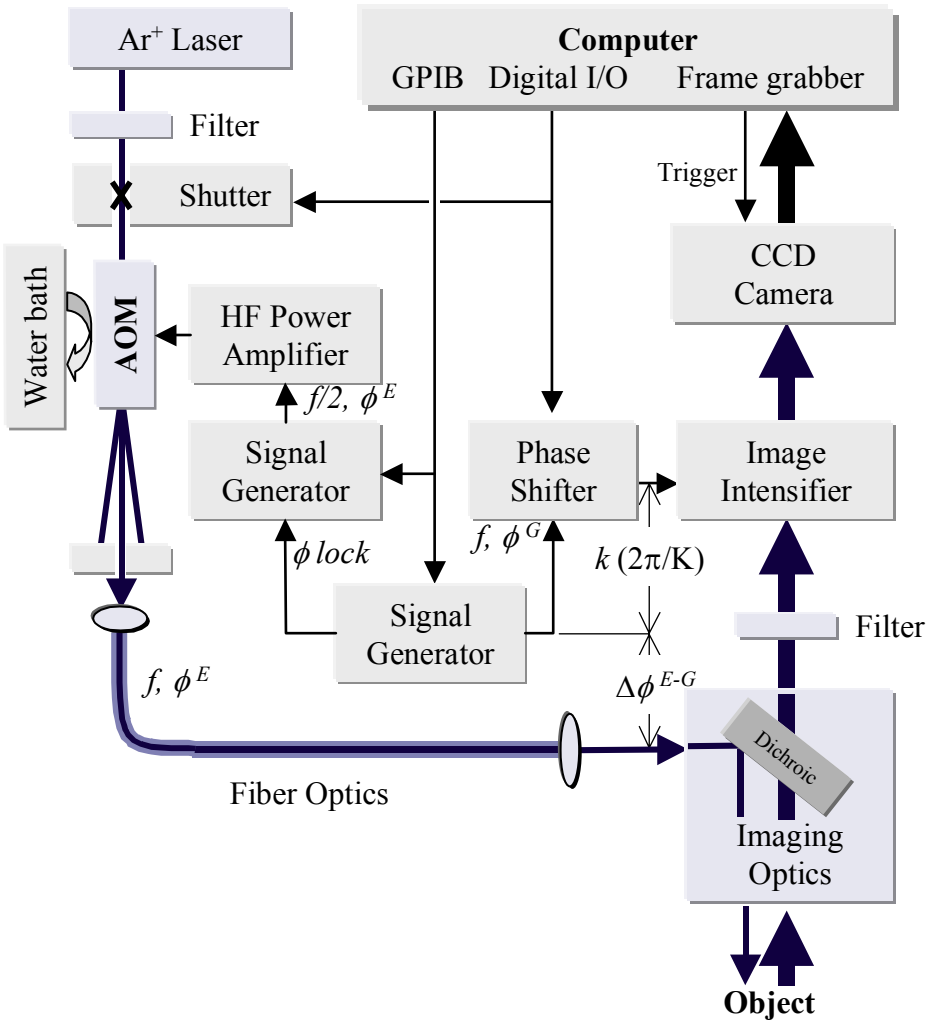

Fig. 13: Scheme of the frequency domain FLI-instrument
Light from a continuous wave argon-ion laser is sinusoidally modulated at high frequency (HF) with a standing wave acousto-optical modulator (AOM). Objectives of a Zeiss Axiovert 135 microscope (optical setup 1) or long working-distance objectives (optical setup 2) with magnifications of 5 to 100 times are used for irradiating the sample with the modulated light. The sample is placed on the microscope stage (setup 1) or a temperature controlled xyz-scanning stage (setup 2); the fluorescence image is projected onto an image intensifier. The cathode voltage of this microchannel plate (MCP) image intensifier is modulated with the identical frequency *f* of the modulated excitation light (this constitutes a homodyne mode of operation). The phase of the image intensifier modulation ϕ^G differs from the phase of the modulated excitation radiation ϕ^E by $\Delta\phi^{E-G}$, which is under computer control. $\Delta\phi^{E-G}$ is incrementally varied by $2\pi/K$ during the measurement of K intensity images. A fast charge coupled device (CCD) camera captures the separate images taken at several incrementally phase-delayed settings, and the acquired images are processed and displayed in real-time on a personal computer (PC).

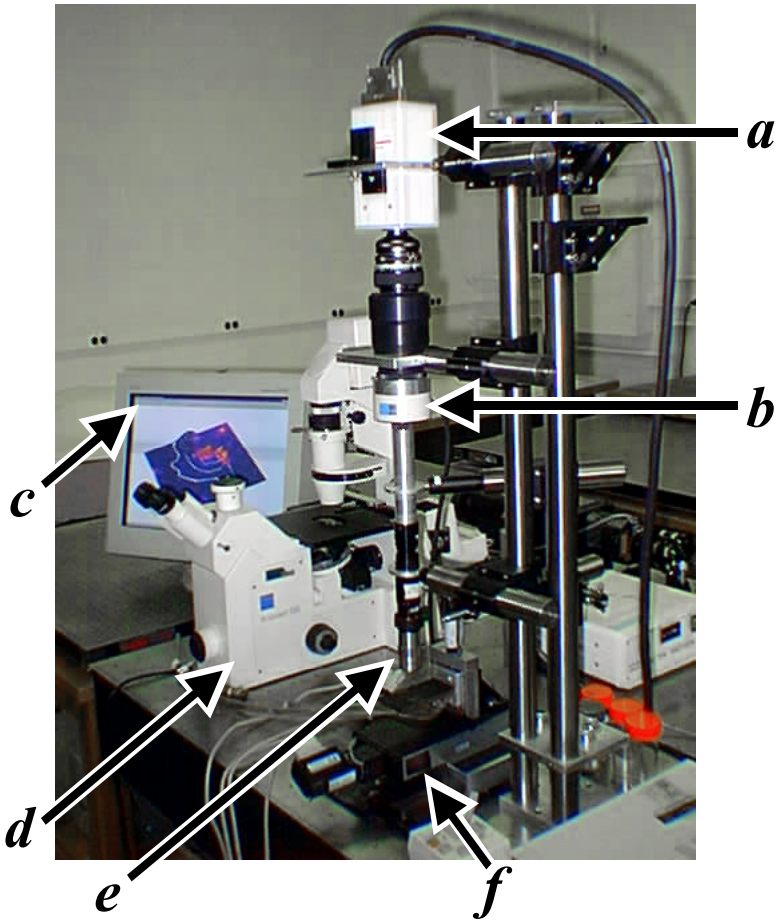

Fig. 14: Photograph of the instrument for fluorescence lifetime-resolved imaging (FLI)
The instrument is described in more detail in the legend of Fig. 13. Two different detection optics are shown. Setup 1 incorporates a complete microscope, while Setup 2 is a stage-scanning instrument, which uses long working distance objectives.
a: Fast readout charge coupled device (CCD)-camera. *b*: High frequency-modulated image intensifier. *c*: Real-time computer display. *d*: Setup 1: Zeiss Axiovert 135 microscope (gets attached to image intensifier). *e*: Setup 2: Long working distance objective. *f*: Setup 2: Temperature controlled xyz-positioning stage.

Light from an air-cooled multi-line argon-ion LASER is passed through a laser line filter (for the selection of a single wavelength: 457, 488 or 514 nm[22]) and a light shutter, is then modulated at a fixed high frequency (HF: 20 - 100 MHz) by means of an acousto-optical modulator (AOM), which is cooled by a water bath, and coupled into single mode fiber optics for guidance to a long working-distance stage-scanning imaging system or a microscope. The fluorescence emission of the object is passed through an emission filter, imaged onto the cathode of a HF-modulated image intensifier, detected by a fast chilled digital CCD camera, digitized with 10 bit precision, and transferred into computer memory by a digital frame grabber card. The signals of two phase locked frequency synthesizers are used to modulate the AOM and image intensifier. The signal applied to the AOM is first amplified by a RF power amplifier. A fast 9 bit digital delay line phase shifter shifts the phase of the HF signal, which modulates the image intensifier cathode, relative to the signal used for the excitation

light modulation. This allows homodyne detection of the high frequency fluorescence emission signal at any given phase shift. A personal computer system equipped with digital frame grabber, multifunctional data acquisition (DAQ) card, and general purpose interface bus (GPIB) PCI cards is used to acquire images from the camera, to control the phase shift and light shutter, as well as to synchronize those processes.

3.1.1.2 List of the instrumentation components

The following section lists the single components, which have been used for the construction of the FLI instrument, together with their manufacturer information:

- AOM (20, 40, 80 or 100 MHz light modulation): acousto-optic standing wave modulator *SWM-102AE1-1, SWM-202AE1-1, SWM-804*, acousto-optic mode locker *SFM-502F1-1* (all: *IntraAction*, Bellwood, IL, USA).
- CCD-camera (cooled fast scan multi-format with 10 bit fast scan mode): *C4880/81* (*Hamamatsu Photonics*, Hamamatsu City; Japan).
- Computer hardware and software: see section 3.1.1.9
- Digital delay line phase shifters (20, 40 or 80 MHz; 0.7º (9 bit) phase resolution): *DP-2-9-20-77*, *DP-2-9-40-77*, *DP-2-9-80-77* (*Lorch Microwave*, Salisbury, MD, USA).
- Filters and mirror: laser line filters *XL05* (457 nm), *XL06* (488 nm), *XL07* (515 nm) with blocker *B5/B6*, dichroic *XF27/550DCLPO2*, fluorescence emission *XF70/690DF40* (*Omega Optical*, Brattleboro, VT, USA).
- Image intensifier (HF-modulated): *C5825* (*Hamamatsu Photonics*, Hamamatsu City, Japan).
- Laser: air-cooled multi-line argon-ion *2213-150 MLYVW* (*Uniphase*, San Jose, CA, USA).
- Linear positioning stage (Setup 2): *PI-M 100* series (2x *M155.11;* 1x *M125.10*) (*Physik Instrumente*, Waldbronn, Germany).
- Microscope (Setup 1): *Axiovert 135* inverted microscope (*Carl Zeiss*, Jena, Germany) with 10x/100x objectives.
- Objectives (Setup 2; long working-distance): *Mitutoyo M Plan Apo 5*× (NA 0.14; WDist. 3.4 cm; DF 14 µm), 10× (NA 0.28; WDist. 3.35 cm; DF 3.5 µm), 50× (NA 0.55; WDist.

1.3 cm; DF 0.9 µm), 100× (NA 0.70; WDist. 0.6 cm; DF 0.6 µm) (*MTI*, Aurora, IL, USA).

- Radio frequency (RF)-power amplifier: *ENI 603L* (3 W linear) (Electronic Navigation Industries *ENI*, Rochester, NY, USA).
- Shutter: *Uniblitz LS2Z2* (*Vincent Associates*, Rochester, NY, USA).
- Signal generators: *HP-8657A* (*Hewlett Packard*, Palo Alto, CA, USA); *PTS 500* (*Programmed Test Sources PTS*, Littleton, MA, USA).
- Single mode fiber and couplers: *Kineflex-M* single mode fiber delivery system FDS-*D-P-1-S-458/514-0.65-FCP* with connectorised optics *FDS-OP/D-458/514-FC-0.65* and coupler *Kinematix-P* (all: *PointSource*, Winchester, Hampshire, England).
- Water bath: *RTE-140* (*Neslab Instruments*, Newington, NH, USA).

3.1.1.3 Modulated light source

Different techniques have been used to modulate light at high frequencies (for review, see e.g. Teale 1983). While modulations at a few MHz still can be obtained by mechanical chopper setups (turbine-driven sector discs), modulations at 100 MHz are reached by electro- and acousto-optical methods. First setups used the electro-optical Kerr-cell, which was then replaced by the acousto-optical Debye-Sears ultrasonic tank. New developments nowadays allow the use of directly modulatable diodes and HF pulsed diode lasers. But the electro-optical Pockels cell and the acousto-optical modulator (AOM) are probably still the methods employed in most cases, in which no expensive intrinsically modulated laser sources (such as mode-locked lasers) are used. In our FLI-instrument, monochromatic light, selected with laser line filters from the multiline output of a continuous-wave Ar^+-laser, is sinusoidally modulated by an acousto-optical modulator (AOM). The used AOM is a so-called standing wave or Raman-Nath-AOM[23] (Raman and Nagendra-Nath 1935, 1936). Piezoelectric ceramics produce an acoustic wave, which travels through a block of glass and which is reflected at the other side. If the traveled distance through the block corresponds to a multiple of half of the wavelength, then a standing wave can be formed in the crystal. The standing wave produces a density grating, which can be seen as a diffraction grating, on which the light hits perpendicular (parallel to the acoustic wavefronts). The density grating does not exist constantly in the crystal, but is formed and dissolves sinusoidally, following the sinusoidal driving signal (from a signal generator and then amplified by a power amplifier). Two times per period of the driving signal (or the acoustic signal), no density grating is build

up. The light is passing undiffracted through the homogenous crystal (maximal 0^{th} diffractive order). When the grating is maximal on the other hand, the higher diffractive orders obtain their highest signal. If one is picking only one of the diffractive orders by letting it pass trough an iris and thereby blending out all other diffractive orders, one obtains a sinusoidal light modulation of the laser beam with double of the frequency of the signal driving the crystal. Usually one will pick either the 0^{th} or the 1^{st} diffractive order beam due to the low light intensity of the higher orders. Usage of the 0^{th} order is especially useful if the laser beam is passing through multiple AOM's to allow for a fast switching of the modulation frequencies (see e.g., Schneider and Clegg 1997). For the instrument described in this work, the 1^{st} order has been chosen due to its cleaner sinusoidal modulation.[24] The modulation of the laser beam could be checked directly by the use of a fast photo diode (High speed photo detector DET110; Thorlabs Inc., Newton, NJ, USA) connected to a sufficiently fast oscilloscope. Standing wave AOM's typically can be driven with frequencies around 10-50 MHz, which allows sinusoidal light modulations between 20-100 MHz. A quasicontinuous distribution of modulation frequencies from DC to 320 MHz has been reported for a system, which employs two AOM's in series (Piston *et al.* 1989). The driving frequencies for an AOM cannot be chosen absolutely freely due to the resonance conditions for the formation of a standing wave in the crystal. But the frequencies can be selected in steps of about 200 kHz.[25] For a chosen frequency one will look for optimal resonance conditions, that is one has to check adjacent resonances for the resonance frequency with the greatest modulation depth. This can be done in an automated procedure (Schneider and Clegg 1997), which is of help if one is changing the frequencies often, or manually. At the greatest modulation depth the average light intensity of the 0^{th} order beam has its local minimum and accordingly the 1^{st} order beam its maximum (optimal diffraction in the higher orders). The resonance frequencies and with it the phase of the light modulation are strongly temperature dependent, which makes it necessary to keep the AOM at a constant temperature (20º C) with a water bath. Under these conditions the optimal resonance frequency has been found to be stable and did not need to be adjusted before every measurement.

The phase stability of the light modulation during the measurement is of absolute importance for the quality of the lifetime measurement. Therefore the instrumental calibration has always been checked before and after a measurement. Small temperature changes at the AOM can directly be followed as drifts in the phase of the modulation. The importance of temperature stabilization therefore cannot be overemphasized.

Before the diffraction pattern can be clearly distinguished and the first order beam be selected with the iris, a longer light path is necessary.[26]

The light shutter, which is under computer control, has been inserted after the AOM, directly before the coupling into the single mode fiber (see following section). This position is of importance. The shutter had been inserted previously directly after the laser and before the laser line filters. In this case a kinetics in the excitation light intensity could be detected after each opening of the shutter, probably caused by heating up the laser line filters, which induces a slight tilt in the filter surface and thereby changes the position of the laser beam and therefore the coupling into the fiber. Positioning the shutter directly before the fiber coupling, which ensures that the laser line filters and the AOM are under constant laser illumination, removed this kinetics.

3.1.1.4 Illumination and imaging optics

3.1.1.4.1 Single mode fiber optics

The sinusoidally modulated light (after selection of the 1st order beam of the AOM) is coupled into a single mode optical fiber. The *PointSource Kinematix-P* coupler offers a relatively inexpensive system, which is easy to handle and which provides the necessary stability for the difficult task of coupling the laser beam into the single mode fiber with its 5 µm core diameter. An optical system consisting of a single lens in a metal cylinder is permanently connected[27] with a single mode fiber (5 µm core diameter; 125 µm cladding; 245 µm coating). The system is optimized for the 458-514 nm wavelength range and 0.65 mm input laser beam diameter. The output side is connectorized with a Franck-Condon (FC) connector, which allows the connection with optics similar to the input system. The *Kinematix-P* coupler offers a four axis adjustment of the coupling optics relative to the laser beam.

Single mode fibers have been chosen instead of multi-mode fibers for different reasons. A big advantage of the single mode fiber is that it does not produce a speckle pattern. In the multimode fiber, the fiber diameter is large compared to the wavelength of the light and the light propagates by total reflection at the core-cladding-border. This results in different pathlengths for the different modes of the coupled beam, depending on the coupling angle and the bending of the fiber. Therefore interferences occur in the illuminated plane, which produce a grainy speckle pattern that is very sensitive to movements of the fiber. Such a spatially and temporally changing illumination pattern would not be acceptable for our purposes. Especially for photosynthetic samples a constant illumination intensity is of importance for the lifetime measurement, because the lifetimes in this special case depend on the illumination intensity. In general the fluorescence lifetime of a fluorophore is independent of the illumination light intensity. But even in this case, temporally changing intensities will

distort the lifetime analysis, since the method uses sequences of intensity images. Light-scrambling devices (see e.g. Gadella Jr. 1999) or fiber shakers have to be applied to average out these effects during the measurement. These procedures will fail if fast image acquisition rates are required.

The single mode fiber on the other hand has a very small core diameter, which allows only the TEM_{00}-mode to propagate. The single mode prevents the interferences of different modes and therefore does not produce a speckle pattern, but a temporally constant Gaussian illumination profile. While the instrument of Schneider and Clegg (1997) already incorporated a normal single mode fiber, a polarization-maintaining single mode fiber has been chosen for our lifetime instrument. In this fiber type the fiber core lies between two stress applying sectors, which induce birefringence, i.e. a different refractive index for the two orthogonal polarization modes of propagation. In normal single mode fibers the birefringence can be induced by bending. Therefore the polarization-maintaining fiber offers the highest signal stability, even in the case of fiber movement. Additionally this fiber is about a factor of 1000 more insensitive to temperature changes than a normal single mode fiber. The *PointSource Kinematix-P* coupler allows simple polarization optimization and locking of the polarization state.

The disadvantages of single mode fibers are its lower throughput efficiencies of about 70 % (although this should still be acceptable for most applications) and the requirement of precision coupling. This can be handled with the mentioned optics, but sensitive coupling also requires a good laser pointing stability[28]. This is given with most modern laser systems. Another disadvantage of single mode fibers is that they are only optimized for a small wavelength range. Longer wavelengths are strongly attenuated and for shorter wavelengths the fiber becomes a multimode fiber. In our case this does not constitute a problem due to the use of an argon-ion laser.

The general utilization of fiber optics allows a modular construction of the instrumentation. Although also common camera optics for the detection of larger areas has been used, the modular design has especially been applied for two optical setups, a fluorescence microscope and a long working-distance stage-scanning microscope, which shall be described in the following sections.

3.1.1.4.2 Fluorescence microscope

For microscopic measurements, the modulated laser light, guided to the microscope by a single mode optical fiber, is coupled into the epi-fluorescence illumination port of a Zeiss Axiovert 135 inverted fluorescence microscope. The light coming out of the single mode fiber

acts like a point light source and could be widened to a parallel beam (of 1.5 cm diameter) by a single lens. This beam is coupled into the microscope *via* the epi-luminescence port, where it replaces the usual mercury lamp. Zeiss also offers a lamp housing for two illuminators with a rotatable mirror (Cat.# 447230 9901), which can be moved in two fixed positions and thereby allows easy switching between lamp and modulated laser light.

Directly before the widened beam enters the epi-luminescence port of the microscope it passes through two neutral density filters. A selection of neutral density filters with different optical density is installed in a manually rotatable double filter wheel (New Focus, Santa Clara, CA, USA). The light always passes through two filters, which can be combined to achieve the desired level of intensity reduction. The filters have identical thickness (and similar refractive index) to keep the light pass unchanged and not to introduce unwanted phase differences (compare 3.2.1.2). It is of importance not to position the neutral density filters in the light pass before the coupling into the fiber, because there a filter change will deflect the (unwidened) laser beam slightly different to the coupling optics and result in unfavorable coupling. The widened beam, which enters the microscope, is insensitive to such small tilts of the filter surface.

In the microscope the modulated laser light is reflected at a dichroic mirror. A dichroic mirror is an interference filter, which allows longer wavelengths (fluorescence emission) to pass through, but which reflects the shorter wavelengths (the excitation light). The reflected excitation light passes through the microscope objective and illuminates the sample. The incoming excitation light is focused in the back focal plane of the microscope objective. This way one obtains an illumination of the sample with a parallel beam, which shows a Gaussian intensity profile due to the use of the single mode fiber.

On the sample the illumination excites the fluorescence emission, which is imaged from the objective in the primary image plane. The fluorescence passes through the same dichroic mirror and an additional emission filter, which defines the spectral window of observation and suppresses stray light. The spectral properties of the dichroic mirror and filter have to be selected for the application under investigation. Below the emission filter the fluorescence passes through an exchangeable lens mounted on a rotatable wheel in the Axiovert. This offers different magnifications of the fluorescence image. Depending on the selected zoom, the illumination intensity differences, dictated by the Gaussian profile, in the observed image can be reduced to very acceptable (nearly homogeneous) sample illuminations[29]. One is thereby zooming into the Gaussian illumination profile. The filtered fluorescence image either can be observed directly with two oculars or put on the camera port of the trinocular head of the microscope, where the image intensifier (see later description) is mounted. In this way the

microscope optics is integrated into the instrumental setup and provides all components and functions necessary for microscopic cell work.

The dichroic mirror and the emission filter are mounted in one of three filter cubes fixed in a three position fluorescence filter slider of the Axiovert 135. For the lifetime measurements it has been found of importance to position the emission filter in the slider in a way to prevent backreflections[30], which were only visible in the lifetime images as spots of longer lifetime. These reflections result from fluorescence light passing through the dichroic mirror but being reflected at the emission filter, because the wavelengths of the light lie outside the spectral window of the filter. These reflections can reach the sample again and excite fluorescence for a second time due to spectral overlap between excitation and emission spectrum. The longer light path, which these reflections have to travel, shows up as a longer lifetime.

All measurements presented in this work have been performed with the fluorescence microscope as described in this section.

3.1.1.4.3 Long working-distance stage-scanning microscope

A second optical setup has been found useful (see also photograph in Fig. 14) for fast scanning of larger samples or many microscopic samples on larger areas. The magnification optics in this case is a compact microscope optics. A dichroic mirror and emission filter have been integrated into a zoom-optics setup from *Micos* (Zoom 70; Micos, Hamburg, Germany). The FC connector of the single mode fiber screws in an end holder, which is attached to a small optical rail. A lens guides the widened beam onto the dichroic mirror and through the objective. The fluorescence passes objective, dichroic mirror, emission filter and zoom optics, before it reaches the image intensifier. This instrument allows the use of long working-distance air objectives from *Mitutoyo* (5x to 100x magnification; see the instrumentation component list for the technical data of the objectives). While the previously described setup, which incorporates a Zeiss microscope, allows the use of high resolution oil immersion objectives with high magnifications (100x), the stage-scanning instrument offers the same magnification at a still acceptable resolution (NA 0.70) with an air objective. With the enormous working distance of 0.6 cm of this non-immersion objective, the fluorescence lifetimes of large samples can be easily scanned even at high magnifications. For this purpose the instrument is equipped with a xyz-positioning stage. Because the fluorescence lifetime of many fluorophores is strongly temperature dependent, the platform of this stage is connected to a water bath, which offers precise temperature control of the sample. All three spatial directions of the stage can be manually controlled with a joystick or computer controlled *via* general purpose interface bus (GPIB) or serial port (RS 232).

All applications presented in (Holub *et al.* 2000) have been investigated with this stage-scanning instrument.

3.1.1.5 Modulated image intensifier

All optical setups described in the previous section project a fluorescence image on the cathode of the HF-modulatable microchannel plate (MCP) image intensifier C5825 from *Hamamatsu*. Photoelectrons are freed at the cathode and then accelerated to the MCP in an electrical field. The spectral characteristics of the cathode depend on the material used. The image intensifier of our instrument is equipped with a S20 material, which shows highest sensitivity for light between 400 and 500 nm and good noise characteristics. Test measurements with S25 material, which has a higher sensitivity in the red spectral range, have been reported to give unsatisfactory noise characteristics (Schneider 1997).

A MCP is a secondary-electron multiplier, which detects and amplifies electrons in two dimensions. It is a plate, which consists out of 1.5 million hollow glass capillaries, which are 0.48 mm long and coated internally with a photoelectric material. The glass capillaries have an inner diameter of 12 μm, are arranged parallel to each other in the direction of the light path and are fused together. Approximately 900 V of high-tension lies across the plate parallel to the capillaries. Every element (capillary) of the MCP acts like a dynode-cascade of a miniaturized photomultiplier: The voltage applied across the input- and output-side electrodes of the MCP builds up a potential gradient along the channel direction. If an incident electron (generated at a place on the photocathode, which has been hit by a photon) strikes an inner wall on the input side, a number of secondary electrons are emitted. These secondary electrons are accelerated by the potential gradient and travel along a parabolic path, which is determined by their initial velocity. They then collide with the opposing wall surface, causing further secondary electrons to be emitted. In this manner, the electrons collide repeatedly within the channel as they pass towards the output side. The result is a large multiplication of the incident electron. Due to the multitude of the single elements the spatial resolution is retained for image details larger than the MCP element sizes. At the output of the MCP a spatial electron density distribution is obtained, which corresponds to the intensity distribution of the image, which has hit the cathode. This electron density distribution is accelerated by another electrical field onto a phosphor screen. Here the hitting accelerated electrons are transformed into photons. Therefore an image is formed on the phosphor screen, which is amplified in comparison to the original fluorescence image and which shows identical relative spatial intensity distribution. The color information of the original image is lost after passing the image intensifier, except a wavelength dependency of the sensitivity of

the cathode material. Also temporally changes cannot be transmitted, if they are not noticeably longer than the phosphorescence decay times of the image intensifier. Depending on the type of phosphor, these can lie between 80 ns up to multiple ms and can be composed out of several lifetime components. For the here described application, which requires short measurement times and high image repetition rates, a phosphor of type P43 with decay times of 200-400 ns has been chosen.

There are two ways to obtain the desired HF modulation from the image intensifier, either by modulating the voltage a) between cathode and MCP (possible in a wide frequency band from 100 kHz - 300 MHz) or b) across the MCP (only possible in small frequency band 35-40 MHz). The *Hamamatsu* C5825 uses the first method.

There are certain difficulties, which have been reported for such cathode-modulated image intensifiers:

1) Defocusing effect

   During the modulation at the cathode a defocusing effect is possible, if in the phases of low potential difference between cathode and MCP the focusing of the photoelectrons is not ensured any more and the electrons, instead of following a direct path between cathode and MCP, start to diverge with additional side components. As a result of such diverging electron clouds, the signals from the positions on the photocathode do not correspond any more with the input signals of a few microchannels of the MCP, but reach larger numbers of microchannels. The electrons from one cathode position then get distributed over larger areas on the MCP and a single microchannel of the MCP obtains electrons from the overlapping electron clouds, that is electrons freed at different cathode positions. Such defocusing cannot happen in MCP-modulated image intensifiers, because the spatial resolution is ensured as soon as the electrons have reached the MCP.

2) Iris effect

The iris effect is an inhomogeneous distribution of the phase of the modulated signal over the image. This effect is often seen at cathode-modulated image intensifiers due to the spatial and temporal inhomogeneities in the electrical potential over the surface of the cathode when the amplification of the cathode voltage is modulated at very high frequencies. The effect arises due to a time lag of the electrical potential in the middle of the cathode relative to the potential at the edges of the cathode, where the HF modulating voltage is applied. Because of its mostly circular appearance in the phase images this phenomenon is called iris effect.

Both effects do not appear with MCP-modulated image intensifiers, but here one would have to accept a very small frequency band and low modulation depths. The frequency of modulation has to be chosen according to the system under investigation, and therefore a restriction to frequencies between 35 and 40 MHz has to be understood as a limitation of the possible applications.

Fortunately *Hamamatsu* with the C5825 has managed to construct a cathode-modulated image intensifier with large modulation frequency bandwidth, for which the above-mentioned two effects do not constitute problems. They use a thicker photoelectric cathode material, which allows faster electrical charge distributions at the cathode. The iris effect has been measured for the C5825 in a precision measurement (Schneider 1997; Schneider and Clegg 1997) and be found so small in comparison to other noise characteristics that accompany rapid lifetime measurements, that it can be neglected for fast measurements.

A 2:1 relay lens system (*Hamamatsu* relay lens + Nikkor 50 mm f 1.4; *Nikon*, Tokyo, Japan) couples the output of the image intensifier (the image at the phosphor screen) to a fast charge-coupled device (CCD) camera for digital image acquisition.

The spatial resolution of the modulatable image intensifier is provided by the manufacturer in form of the spatial modulation transfer functions (MTFs) at different (temporally) modulation frequencies. The MTFs describes the detectable contrast of a periodic line pattern (the contrast between a black line and its white spacing) as a function of the spatial frequency. The MTF starts at 100% contrast and decays to zero, which is reached at the cutoff frequency. The cutoff frequency defines the resolution limit and is given for the temporally unmodulated (DC) use of the image intensifer at about 35 lines per millimeter, with 10 MHz modulation at 25 lines per millimeter and with 300 MHz at about 18 lines per millimeter. Control measurements of Schneider (1997) could support the data provided by the manufacturer.

The voltage between cathode and MCP of the image intensifier is sinusoidally modulated at a high frequency. The modulation is produced by a signal generator, which is phase-locked to the second frequency generator, which controls the AOM modulation. The modulation of the cathode-MCP voltage corresponds to the gain modulation of the image intensifier as given in equation (2.26). Depending on the measurement modus, its frequency is identical to the modulation frequency of the laser light (homodye case) or slightly different (heterodyne case). See Appendix 5.4 for a comparison of these two detection modes. The signal at every point of the phosphor screen therefore depends on the intensity of the fluorescence at the corresponding point in the observed object, but also on the phase difference between the fluorescence modulation and the modulation of the gain in the image intensifier [equation (2.27)]. In the heterodyne case the phase is automatically running through with the difference of the two modulation frequencies, but in the homodyne case the phase difference between every two images has to be changed stepwise. For this purpose our homodyne instrument uses a delay line phase shifter.

3.1.1.6 Digital phase shifter and signal generation

None of the chosen two signal generators (see component list above for details), which produce the HF signals for image intensifier and light modulation, is equipped with a phase shifter. The *PTS* signal generator can be equipped with it and several other companies (e.g. *Hewlett Packard* or *IFR*[31], *Instrument Flight Research*, Wichita, Kansas, USA) offer signal generators with build-in phase shifters, which are under computer control, mainly *via* GPIB (General Purpose Interface Bus). Instead fast external digital delay line phase shifters from *Lorch Microwave* have been used. Each phase shifter is optimized for a single frequency but with a sufficiently large bandwidth for many of the AOM resonance frequencies. It is equipped with nine delay lines, which are combined by fast GaAs switches. The switches have a switching time of maximally 100 ns and extremely low switching transients. For each of the delay lines the switches are digitally controlled. A TTL high voltage corresponds to zero phase shift, a low voltage to the phase shift of the corresponding line. The highest delay line can produce a phase shift of 180° and each of the eight following ones half of the preceding one. Therefore combination of the nine lines allows full period phase control with phase shifts of 0.7° phase resolution.

The phase shifter is inserted between signal generator and image intensifier and the phase is shifted about the selected step size before the acquisition of each homodyned and therefore temporally constant image.

The combination of an AOM, optimized for a single main resonance frequency, and a digital

delay line phase shifter for the same frequency offers relatively inexpensive modulation and phase control. Further these phase shifters allow a faster phase control than the usual hardware handshaking over GPIB.
Future developments, which use real digital phase shifters, as developed by Gratton (see Appendix 5 in Jameson *et al.* 1984), on microchip integrated circuits and perhaps in direct combination with chip internal signal generation, will provide really inexpensive, miniaturized and versatile phase shift control.

3.1.1.7 Fast Charge-Coupled Device (CCD) camera

The *Hamamatsu* C4880-81 (or C4880-80-12A) CCD camera, a new development in 1996 when it was purchased, was considered the best compromise with regards to resolution, dynamic range and speed at this time. The camera uses a 0 °C peltier-cooled progressive scan interline transfer chip with 659 (H) x 494 (V) pixel resolution of 9.9 x 9.9 μm^2. It can either operate in a fast scan mode with 10 MHz readout rate (28 Hz frame rate) and 10 bit precision per pixel (20 electrons readout noise level) or a 12 bit high precision, low noise scan mode (5 electrons readout noise) with a readout rate of 312 kHz (1 fps). The spectral response characteristics are optimized for light of wavelengths around 520 nm and therefore show optimal sensitivity for the light emission of the chosen P43 phosphor-screen of the *Hamamatsu* C5825 intensifier, which has a narrow maximum emission peak around 540 nm. Exposure times from a few µs to 10 s are possible. The camera is able to perform binning, where 2x2, 4x4, 8x8, 16x16, or 32x32 neighboring pixels of the CCD chip are merged into so called 'superpixels'. This allows for reduction of the integration time and hence faster frame rates, and it improves the signal to noise ratio because the electrons of the binned pixels are read out and digitized together. The camera supports sub-array scans, where only a selected region of interest (ROI) of the CCD array is read out at faster rate than reading out the full array. Frame rates of up to 529 fps can be achieved in 32 x 32 binning fast scan mode and minimum exposure time.

The electrical charges that were accumulated on the CCD chip during the frame integration time are read out by progressive scan interline transfer. The double number of pixel wells exists on the CCD chip and every second line is non-translucently masked. Electrons, which have been accumulated in the active pixels during the frame integration time, are shifted by one pixel into the masked region, from were they are read into a camera internal controller (with a readout rate of up to 10 MHz). During the readout of the image from the masked regions, a new image can already be integrated by the active pixels. This eliminates the need

for a mechanical shutter and increases overall acquisition speed. The analog data are digitized in the camera controller with 10 respectively 12 bit precision and transferred to a digital frame grabber card (section 3.1.1.9.3.1) via a RS-422 16 bit parallel interface and cable. The digital transfer circumvents possible interference of an analog transfer to a frame grabber with A/D converter.

A RS-232 interface is used to communicate with the host computer. Commands can be sent to control or readout the various camera states. A 50-ohm terminal input at TTL level is used when the camera is operated using external synchronization. A trigger is activated at the rising edge of the external signal.

Unless stated otherwise, throughout the experiments the camera is operated in a continuously monitoring/acquiring, externally triggered, fast scan mode, with 2x2 binning enabled and contrast enhancement disabled. The effective resolution of 328 x 247 pixels with 10 bit precision per pixel provided by this mode has proven to be a good compromise for fast fluorescence lifetime imaging with regards to overall resolution, precision and speed. Increased signal to noise ratios can be achieved by increasing the frame integration time on the camera at the expense of acquisition rate. Higher acquisition rates and increased signal to noise ratios are achieved by binning of pixels on the camera at the expense of spatial resolution.

By operating the camera in a 2x2 binning mode the resolution of the camera is reduced to 328 x 247 pixels. This increases the acquisition speed and reduces the computation time for per pixel analysis and image visualization (at a still acceptable resolution), which is important for real-time lifetime imaging at video-rate. Only a central region of interest of 320 x 240 pixels (or 300 x 220 pixels for compatibility reasons) is further processed by the software in order to eliminate readout artifacts occurring at the edges of the CCD chip and to comply with the QVGA video size standard (320 x 240).

In the fast scan mode the nominal precision is 10 bit. However, the true dynamic range of the digitized signal depends not only on the number of bits used for digitization, but also on the amount of a constant offset and readout noise. The dynamic range has been determined according to the following formula to be better than 8.9 bit:

$$D[Bit] = \frac{\ln\left(\frac{C-B}{N}\right)}{\ln 2}$$

Here *C* gives the maximal number of digital units (1024), *B* the constant offset due to the dark current (≈ 60) and *N* the readout noise (< 2).

When operating in monitor mode the camera continuously acquires data at the specified exposure time, scan mode, and scan speed until a stop command is received. A persistent readout rate of 52 fps is achieved in the case of fast scan mode with 2x2 binning and minimum frame integration time. However, performing fluorescence lifetime measurements with homodyne detection requires the image readouts from the camera to be synchronized with phase changes. It must be ensured that any frame, which is integrated while the phase has changed, is discarded. The synchronization is done by triggering the camera with an external TTL signal after every phase change. There is a loss of one camera frame regardless of the integration time. Hence the maximum image acquisition speed is limited to 26 fps in the mentioned mode.

3.1.1.8 Automated control

The minimum prerequisites in order for software to automatically acquire fluorescence lifetime images from the instrumentation are facilities to transfer images from the camera to the computer memory, to control the phase difference of the signals applied to AOM and image intensifier, and to synchronize these two processes. For convenience of use of the instrumentation and flexibility of software acquisition modes it is generally desirable to be able to control and read out by software, all functions and parameters of the external devices. Most desirable for frequency domain fluorescence lifetime imaging are the control of camera frame integration time, camera binning, camera ROI, the state of the light shutter, the gain of the image intensifier, the frequency of the modulation light, the amplitude of the laser light as well the focusing stage of the microscope. In addition to triggered image acquisition and phase shift control, we control by software the camera frame integration time, the light shutter, and the frequencies of the synthesizers.

3.1.1.9 Computer hardware and software

Historically, proprietary and expensive *Sun* and *SGI* workstations or *Apple* computer systems were the preferred choice over *Microsoft* Windows based personal computers (PC) systems for real-time scientific image acquisition and visualization applications such as fast fluorescence lifetime imaging (Holub and Schneider 1997; Schneider 1997). This preference is now largely reversed. The ubiquitous and comparatively inexpensive *Intel* Pentium (III and IV) and *AMD* Athlon processor based PC systems provide sufficient floating point processing power and I/O (input/output) speed (with regards to memory, hard disk, graphics and

peripheral components) for those tasks. Driven by the mass market of computer games and multimedia software, graphics cards containing extremely powerful processors dedicated to the acceleration of video processing and 3D rendering are available at low cost. Mainboards are available with dual processor support. A large number of bus master compatible peripheral component interconnect (PCI) cards for video frame grabbing, data acquisition and acquisition control are available. In comparison to Windows 98, the *Microsoft* Windows NT line of operating systems (including Windows 2000 and XP) is robust, has a sufficiently good architecture for soft real-time imaging applications and support for multiple processors. It also provides the user and programmer with a common, user-friendly operating environment. Integrated software development environments and speed optimizing compilers are available for Windows.

However, effectively utilizing the power of this PC hardware and software for real-time imaging acquisition and visualization requires a great deal of low-level understanding of the hardware and low-level programming.

3.1.1.9.1 Computer systems

Two desktop personal computer systems were used alternatively for software development, data acquisition and analysis. The systems were custom built from widely available commercial components, which were selected for stability, low cost, speed, as well as ease of upgradeability and programmability. The computers are integrated into a LAN network via a *3COM* 3C905B 10/100 Mbps network interface PCI card (*3COM*, Santa Clara, CA, USA). A 21” cathode ray tube monitor (Multiscan 500 PS, *Sony* Corp., Tokyo, Japan) was the preferred choice for display over a high resolution LCD monitor because of the lower price, greater color accuracy and faster response times at the time of development. Both of the latter reasons are important for video-rate imaging. Latest Windows operating system service packs were installed.

Dual Intel Pentium III (System 1): System 1 consists of an *ASUS* P2B-DS mainboard with *Intel* 440 BX chipset (*ASUSTeK* Computer Inc; Taiwan), equipped with dual Pentium III 550 MHz CPUs (*Intel*, Santa Clara, CA, USA), 512 MB PC100 SDRAM (*Crucial Technology*, Meridian, ID, USA), a 20 GB ATA33 hard disk drive, and a *NVIDIA* GeForce256 or GeForce2 AGP 2x graphics card with 32 MB DDR memory (*NVIDIA*; Santa Clara, CA, USA). The system was assembled in an IW-A500 mid-tower case with 300W power supply (*IN WIN Development Inc*., Taoyuan Hsien, Taiwan). The operating system is Windows NT 4 Workstation (*Microsoft*; Redmond, WA, USA).

AMD Athlon (System 2): System 2 consists of an ASUS A7V133 mainboard with *VIA* KT133A chipset and integrated RAID controller (*ASUSTeK* Computer Inc; Taiwan). It is equipped with a single *AMD* Athlon 1200 MHz CPU (*AMD*, Sunnyvale, CA, USA), 512 MB PC133 SDRAM (*Crucial Technology*, Meridian, ID, USA), 40 GB ATA66 hard disk drive, and a *NVIDIA* AGP 4x graphics card with 64 MB DDR RAM and GeForce 3 GTS GPU. The system was assembled in an EN-7520 mid-tower case with 340W power supply (*Enlight Corporation*, Taoyuan, Taiwan). The operating system is either Windows 2000 or Windows XP Professional (*Microsoft*; Redmond, WA, USA).

3.1.1.9.2 3D graphics acceleration

Great effort was made throughout development to take advantage of graphics cards capable of accelerating polygon based 3D rendering. Particularly hardware accelerated geometry transformations, lighting calculations and multi texture mapping capabilities are prerequisites for the implementation of some of the real-time visualization techniques discussed in section 2.1.9.

OpenGL (*SGI*, Mountain View, CA, USA), used in version 1.2, is an industry-standard, hardware and operating system independent application programming interface (API) to graphics hardware for the development of interactive 2D and 3D graphics applications (Woo *et al.* 1999). The library automatically enables hardware-accelerated functionality on graphics cards, provided that an OpenGL conform device driver is installed. OpenGL has been chosen over the Direct3D (*Microsoft*) graphics library, because it is specifically designed for scientific visualization instead of games, and because high quality, hardware accelerated implementations are available on all major computer hardware platforms and operating systems including Windows NT. Excellent documentation is available for OpenGL and it is easily extendable by graphics card driver developers to expose additional hardware functionality that is not part of the standard OpenGL library.

Graphics cards containing the GeForce line of GPUs (Graphics Processing Unit) from *NVIDIA* were chosen throughout the development because of unmatched 3D acceleration speed vs. price ratio of the hardware, as well as the availability of fast and stable OpenGL graphics drivers for the *Microsoft* Windows NT/2K/XP operating systems. Alternatives from *ATI* and *3D Labs* were tested and discarded because of price, performance or reliability issues.

3.1.1.9.3 Peripheral component interconnect (PCI) cards

Three PCI 2.1 bus-master compatible cards are used for image acquisition and control of light shutter, digital delay line phase shifter, frequency synthesizers, and CCD camera. The cards and associated software libraries used are available for a variety of computer platforms and operating systems. The peripheral component interconnect bus is an interconnection system between a microprocessor and attached devices in which expansion slots are spaced closely for high-speed operation. The standard PCI bus is 32-bit wide and is clocked at 33 MHz, thus it can offer a maximum bandwidth of 133 MB/s. For comparison, the transfer of 659 x 494 x 16 bit images at 26 fps as produced by the *Hamamatsu* C4880-81 CCD camera requires only about 16 MB/s bandwidth. Direct Memory Access (DMA) allows data to be sent directly from a card to the memory on the host computer's motherboard. The CPU is freed from involvement with the data transfer, thus speeding up overall computer operation. This operation mode is essential for video frame grabbers.

3.1.1.9.3.1 Frame grabber card

An EDT PCI-DV (*Engineering Design Team EDT*; Beaverton, OR, USA) digital video camera interface card (frame grabber) is used to transfer images from the camera to the host computer memory, to trigger image acquisition and to control camera functions (e.g. frame integration time).

The card basically implements a high-speed DMA channel between an external digital video camera and the computer memory and does not include frame buffer memory of its own. The device interface side of the board consists of 32 RS-422 compatible driver/receivers connected to a *Xilinx* RAM-based programmable gate array. The programmability of the *Xilinx* device ensures that it can interface with a variety of camera models such as the *Hamamatsu* C4880-81.

The PCI-DV uses a proprietary high-density 80-pin I/O connector and cable to interface with the camera. Besides the RS-422 lines the interface includes a RS-232 port to control basic camera functions and a TTL trigger line to trigger the acquisition of a new image by the camera.

EDT-PDV drivers are available for PC based Windows (NT, 2000 and XP) and Linux systems, as well as *Sun* workstation systems. Neither the VFW (Video for Windows) nor the WDM (Windows Driver Model) standard Windows video capture interfaces are supported. Instead, a customary SDK (Software Development Kit) with libraries for the C programming

language is provided along with sample source code and excellent documentation and support.

3.1.1.9.3.2 Multifunctional data acquisition (DAQ) card

A NI PCI-6025E (*National Instruments*; Austin, TX, USA) multi purpose digital/analog I/O card, connected to a BNC-2090 (also *National Instruments*) shielded BNC adapter rack, is used to control the light shutter and the digital delay line phase shifter. The card features 16 single-ended analog inputs with 12-bit resolution at a rate of 200000 Samples/s, two 12-bit analog outputs, 32 digital I/0 lines (5 V/TTL), and two 24-bit counter/timers.

A single digital I/O line is used to trigger the *Uniblitz* LS2Z2 shutter. Nine digital I/O lines are grouped into one parallel port to control the 9 bit digital delay line phase shifter (section 3.1.1.6).

NI-DAQ drivers are available for PC based Windows (98, ME, NT, 2000 and XP) and Linux systems, as well as *Sun* systems and include libraries for LabVIEW and C.

3.1.1.9.3.3 General purpose interface bus (GPIB) card

A NI PCI-GPIB (*National Instruments*; Austin, TX, USA) IEEE 488.2 compatible card with on-board bus master DMA controller is used to set the frequency and amplitude at the signal generators. NI-488.2 drivers include libraries for LabVIEW and C and are available for PC based Windows and Linux as well as *Sun* and *Apple* Macintosh systems.

3.1.1.9.4 Application development software

3.1.1.9.4.1 LabVIEW

National Instruments LabVIEW (*National Instruments*; Austin, TX, USA), used in versions 5 and 6, is an object-oriented, graphical development environment for rapid application development. It allows programming of complex control structures and design of user interfaces in a modular, integrated, graphical way that is reminiscent of designing electronic circuits respectively instrument front panels. Therefore LabVIEW is intuitive to use and easy to learn for scientists. Modules are called “Virtual Instruments” or VIs. LabVIEW includes a powerful library for measurement analysis and display and integrates with a wide variety of measurement devices. It produces compiled, multithreaded code for fast performance and is easily extendable via compiled C programs, dynamic link libraries (DLL) and ActiveX controls. LabVIEW is available for a variety of computer platforms and operating systems (*Microsoft* Windows, Linux, *Apple* MacOS, and *Sun* Solaris).

3.1.1.9.4.2 C/C++

C is a structured, procedural programming language that abstracts computer hardware at a relatively low level. Permitting direct access to memory via pointers makes it the preferred choice for programming low level tasks such as image acquisition and processing. C++ is an object-oriented programming language that supercedes the C language. It is widely used for programming application software throughout all major operating systems.

Microsoft Visual C++ Professional (*Microsoft*; Redmond, WA, USA), used in version 6, is the standard application programming environment for *Microsoft* Windows operating systems. It integrates a powerful development environment, a fast and robust C/C++ compiler, and support for the Microsoft Foundation Classes (MFC). MFC, used in version 6, are a collection of C++ classes that make accessible much of the Windows application programming interface (Win32 API) in an object-oriented way, and provides an overall framework for the development of standards-conform Windows application programs.

3.1.2 Software for fluorescence lifetime imaging

We have developed two complementary programs (FLImage and FlimFast) for personal computer systems in order to control the instrumentation (section 3.1.1), to acquire and calculate fluorescence lifetime images (section 2.1.8) and to visualize images and image statistics (section 2.1.9).

3.1.2.1 FLImage: Modular software for fluorescence lifetime imaging

FLImage focuses on fast fluorescence image acquisition in a single, linear phase-sweep and immediate subsequent lifetime analysis and display. The most relevant acquisition control parameters and results are accessible to the operator in a single panel for easy acquisition control and fast feedback on the results (see screenshot in Fig. 15). FLImage is a module that can be extended or controlled by other modules e.g. for repeated runs or advanced analysis.

The main program module was developed in LabVIEW (section 3.1.1.9.4.1). However in order to improve speed, the data analysis routines (section 2.1.8) were written in C, compiled and linked to the main module. The user is given control of the number of images per phase to be acquired, the frame integration time of the camera, the phase and modulation determined for the calibration standard, an arbitrary phase offset (“zero phase”) and a pre-exposure time (the time the light shutter stays open before the actual image acquisition begins). During image acquisition the program displays the currently acquired fluorescence intensity image, its one-dimensional image histogram and a plot of the mean image intensity vs. the phase.

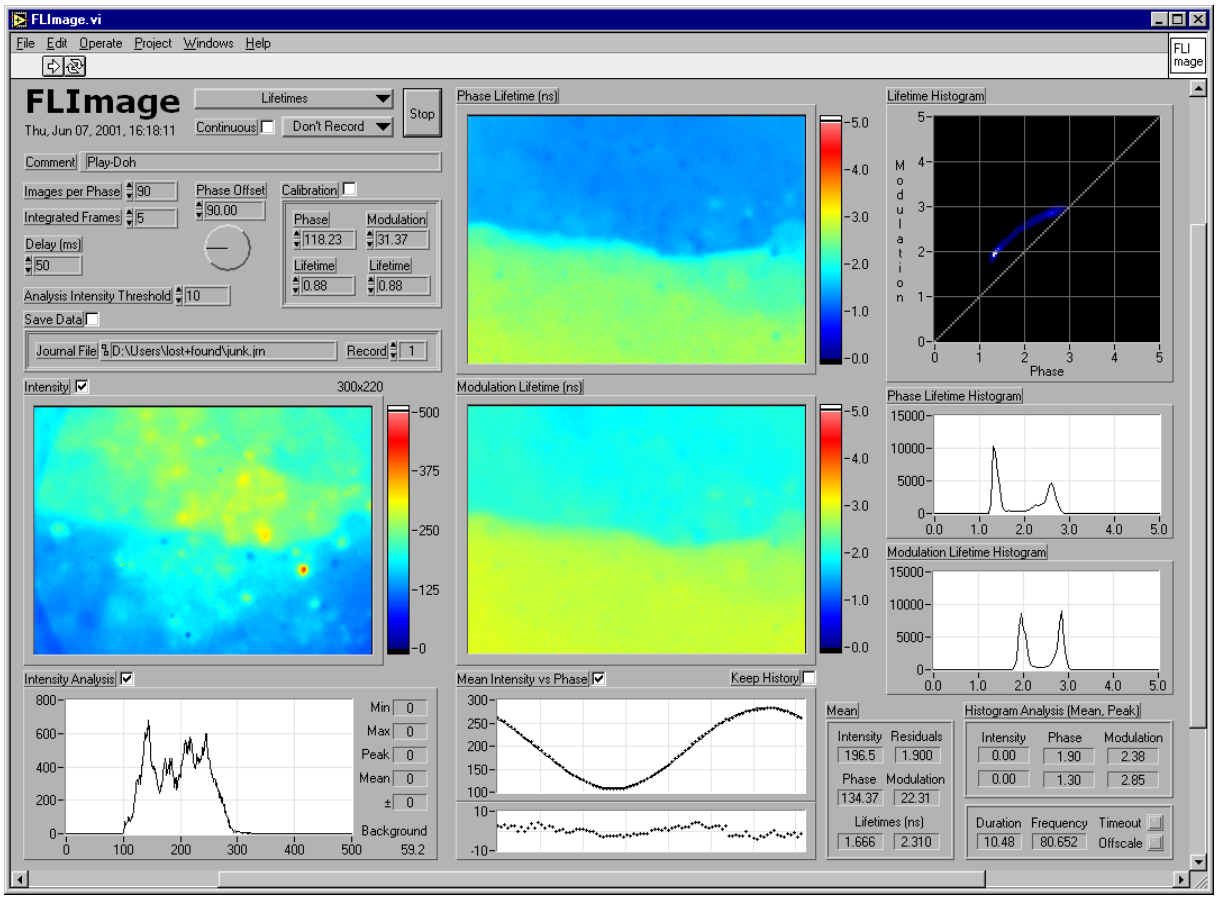

Fig. 15: Screenshot of FLImage
Screenshot of FLImage showing a measurement of two adjacent Play-Dohs. The upper left area contains controls to be adjusted by the user while the rest of the panel displays images, status and analysis results. The labeling of controls and indicators should make the various functions self explanatory. Lifetimes are given in ns.

Lifetime analysis (section 2.1.8) is performed after the image acquisition is complete. Color-coded bitmaps (section 2.1.9.1) of the three images resulting from fluorescence lifetime analysis are displayed side-by-side to their corresponding one-dimensional image histograms and two-dimensional lifetime histogram (section 2.1.9.3).

Several extensions have been developed for the FLImage module: (1) A module that remote controls and repeatedly executes FLImage and displays mean image statistics over time. This has been used to follow kinetic processes (in the range of seconds), to check for phase-stability of the instrumentation and to increase the precision of the instrument calibration (section 3.2.1.2) by averaging multiple measurements. (2) A sub module that buffers the acquired fluorescence intensity images for storage and later reuse. The image buffer can be written to or loaded from a file. The main module can read images from the image buffer instead of acquiring them from the camera. (3) A sub module allowing the user to interactively define an image mask based on an image region of interest as well as minimum and maximum threshold values of the fluorescence intensity and the lifetimes from phase shift

and demodulation. This image mask is used by the main module to mask image analysis, i.e. to limit analysis to certain objects of interest in the image.

FLImage has a number of limitations (some due to its design, others related to the LabVIEW development environment) that makes it inappropriate for applications, which require user interaction during run-time or continuous visual updates of fluorescence lifetime images at or near video-rate. While FLImage is able to acquire phase shifted fluorescence intensity images as fast as the instrumentation allows (up to 26 fps), the time required for the subsequent analysis and display of lifetime images and histograms does not allow repeated runs with video rate updates. Only 2-3 of a maximum of 8 fps are achieved on computer system 2. There is a performance overhead associated with using the object-oriented LabVIEW user interface for display and the graphical programming. Analysis and display have not been designed with video-rate measurements in mind but being done subsequently (not parallel) to rapid data acquisition. LabVIEW programs follow a 'batch oriented' paradigm, whereby they start, do something then stop, instead of being 'event driven' where they would start, wait for events, do something in response to those events, and only stop when told to do so - by an event. This makes LabVIEW unsuitable for programming user-interactive applications. LabVIEW recently obtained support for event handling, however fundamentally it remains batch oriented. The LabVIEW display library, although very powerful, does not provide built-in support for visualizing multi-parameter images beyond the side-by-side display of simple color-coded bitmaps; neither do any of the commercially available add-on libraries.

3.1.2.2 FlimFast: Fluorescence lifetime imaging at video-rate

FlimFast has been designed and programmed from scratch in order to complement the FLImage software, to overcome its limitations, and to unlock the full potential of the FLI instrumentation and modern personal computer hardware. Specifically, FlimFast enables continuous mode fluorescence lifetime imaging at video-rate with concurrent image analysis, user interaction, and advanced visualization of multi-parameter image information. Rates up to 26 fluorescence lifetime images per second are achieved for 320 x 240 pixel images. Image acquisition and lifetime analysis are optimized for speed and flexible operation modes such as continuous integration and non-sequential phase sweeps. If available, dual CPUs and a 3D graphics processor are made use of for parallelizing and distributing processing tasks and to increase responsiveness of user interactions. Real-time visualization of multi-parameter image information in form of multi-textured shaded surface renderings and combined 3D scatter plot / 2D histograms have been implemented to allow the operator to focus on the generally most

relevant aspects of the vast amount of image information that is generated at video rate. Operating the instrument has been automated to the possible extent and the user interface was streamlined to further hide much of the complexity of fluorescence lifetime imaging. A new file format, FLIF, was defined for archival and post-measurement analysis, containing all relevant parameters and acquired image information in a single file. While FlimFast has been developed with experimental applications in mind (e.g. fast sample screening), many of the concepts that are implemented are necessary in order to successfully introduce lifetime imaging to a medical environment (e.g. medical diagnostics using an endoscope). FlimFast has been developed in C++ using the Microsoft Foundation Classes (MFC 6) and OpenGL 1.2 (SGI). Interface libraries for PCI cards are loaded dynamically at runtime, so that FlimFast is capable of running on computers without installed device interface drivers.

3.1.2.2.1 Continuous, user-interactive fluorescence lifetime imaging at video-rate

As discussed in section 2.1.8, the determination of a single fluorescence lifetime image requires Fourier analysis of at least three fluorescence intensity images [$K \geq 3$; Equations (2.30)-(2.32)], acquired at phases, which are equidistantly distributed over one period. FlimFast is able to acquire fluorescence images in a single phase sweep with subsequent lifetime image analysis and visualization within 125 ms ($K = 3$; 1 frame exposure time; computer system 2).

The primary mode of operation is however the user interactive, continuous mode fluorescence lifetime imaging at video-rate with concurrent data visualization. FlimFast is capable to operate the instrumentation at its limit and acquire, analyze and visualize lifetime images of 320 x 240 pixels at a sustained rate of 26 fps ($K = 3$; 1 frame exposure time; no image enhancements; single multi-textured shaded surface display; computer system 2). This is achieved by continuously shifting the phase in equidistant $2\pi/K$ steps and analyzing the last K acquired intensity images such that one lifetime image is calculated and displayed for each newly acquired intensity image (Fig. 16). Hence, after an initial latency of K acquired intensity images, lifetime images are calculated and displayed at video-rate.

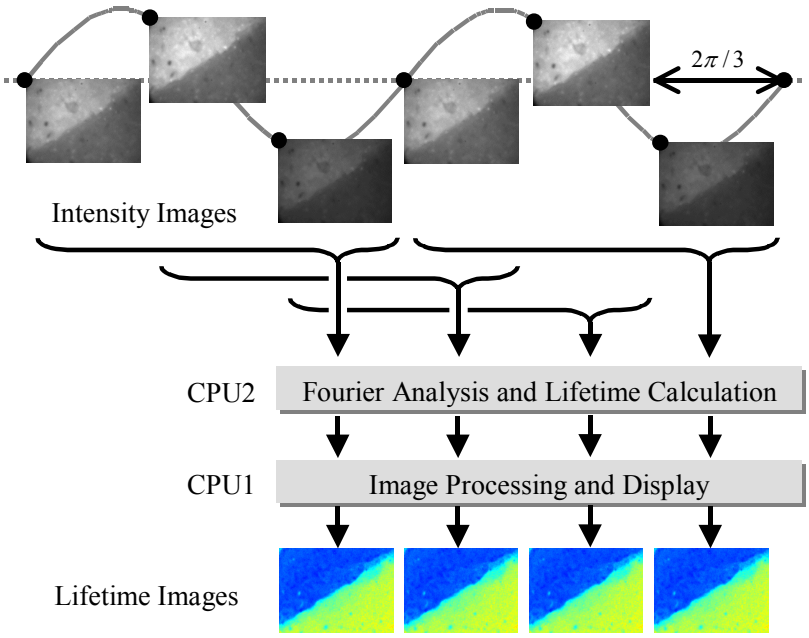

Fig. 16: Continuous-mode fluorescence lifetime imaging
Fluorescence intensity images are acquired continuously at equally distant phases. At least three images are required to determine a lifetime image. After a latency of three images, one lifetime image is calculated for each incoming intensity image. A new image is acquired by camera and frame grabber while the last three images are analyzed. A second processor analyzes newly incoming images while the main processor processes and displays current lifetime images.

It is not necessary to sweep through the equidistant phases of one period successively in a linear sequence. Optimized, nonlinear phase sequences can be used to minimize bleaching artifacts during continuous measurements (Gohlke *et al.* 2002). An image buffer, which stores the latest acquired K fluorescence intensity images, can be used to integrate newly acquired images with images previously acquired at the same phase. This allows for user controlled online integration during continuous measurements. Alternatively, bleaching artifacts can be almost completely circumvented by linearly sweeping through two periods in reverse order and averaging intensity images, which correspond to the same phase.

User interactivity, i.e. the ability of the user to control various software functions during run-time with a minimum latency feedback, has been an important design goal. While operating in continuous mode, the user can adjust at any time (via menu, toolbar or keyboard shortcuts) the measurement parameters (frame integration time, number of phases K), change the operation mode (online integration or phase sweep sequences), switch the lifetime analysis mode (phase and modulation images or fluorescence lifetime images calculated from phase and modulation), enable or disable image enhancements (software binning, smoothing, threshold masking, contrast enhancement, auto scaling), and alter display options (e.g. color palette). The operator can switch between the displays of either the mean intensity image or individual intensity images. The changes are put into effect after the currently integrated

image has been analyzed and the results visualized. If required, e.g. when changing the integration time or the number of phases K, acquisition is restarted automatically, which causes a minimum latency of display updates until K images are acquired again.

Operating in continuous mode at video-rate (26 fps) with concurrent analysis and visualization, the software has a time window of about 28 ms for the analysis and visualization of lifetime images until a new frame arrives in computer memory. Given the complexity of lifetime analysis (section 2.1.8) and the visualization of multi-parameter image information (section 2.1.9) this is not a trivial task, even given the excrescent computing power of today's CPUs. FlimFast makes heavy use of parallel processing and throughput optimized data processing routines in order to ensure soft real time processing and display. Image acquisition and lifetime analysis tasks are separated from visualization and user interaction tasks by executing them in a dedicated UI thread (multi-threading). The two threads can be executed in parallel on separate central processing units (CPUs) if available (Fig. 17). This almost doubles processing speed. Moreover, separating user interaction from acquisition tasks improves overall responsiveness to user inputs since image acquisition and control usually run at higher priority. The two software threads synchronize each other via the operating system messaging system. The camera continuously acquires images concurrently to the execution of the software threads. The actual image readout is triggered by software in order to synchronize with phase changes. Image processing and visualization tasks are optimized for speed instead of flexible analysis or visualization modes.

Parts of the Fourier analysis performed on previous intensity images are reused. An optimized image processing routine, which integrates the selection of an image region of interest (ROI), software binning, integration with previously acquired images, and on the fly Fourier term analysis, provides significantly improved throughput compared to the subsequent execution of the single, nonintegrated functions. Data structures, which are used by display routines, are calculated only on demand and are cached for potential reuse. Another major speed improvement is achieved by automatically setting the arbitrary zero phase of the instrument such that $\Delta\phi^{E\text{-}G} = 0$. Doing this significantly simplifies the determination of the fluorescence lifetime from the phase shift, eliminating two computationally very expensive trigonometric functions [see equation (2.37)].

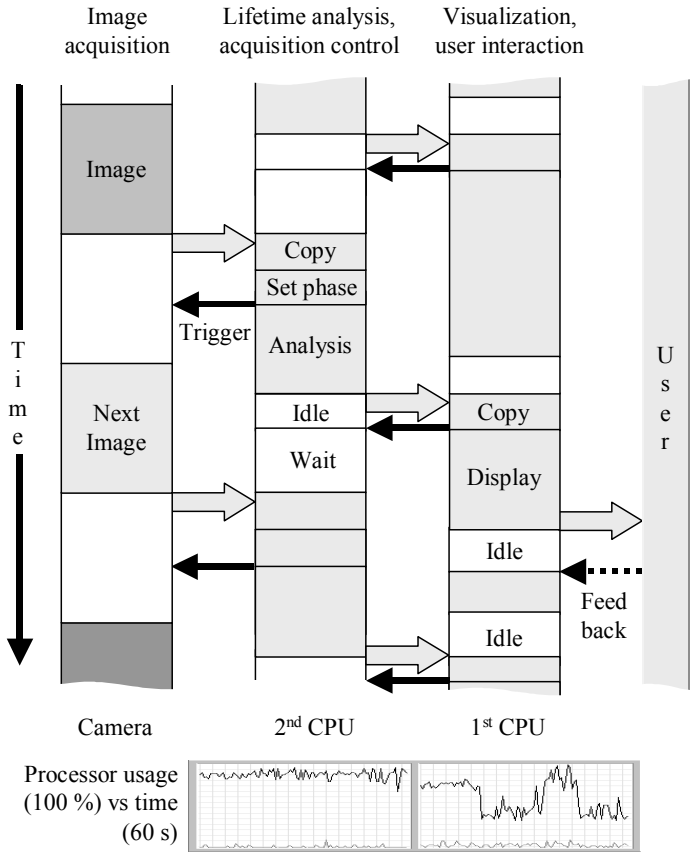

Fig. 17: Parallel processing
Distributing analysis and visualization tasks on separate processors (Multi-threading) while the camera acquires the next intensity image significantly improves processing speed. Separating user interaction from acquisition tasks improves overall responsiveness to user feedback since image acquisition and control usually run at higher priority. The two software threads synchronize each other via the operating system messaging system. The camera continuously acquires images, but the actual image readout is triggered by the software in order to synchronize with the phase changes.

3.1.2.2.2 Visualization of multi-parameter image information

Lifetime analysis provides at least three scalar images respectively three real number (floating point) parameters per pixel: the mean fluorescence intensity $\tilde{F}_0$ [equation (2.30)] and the apparent single fluorescence lifetimes calculated from phase shift τ_{phase} [equation (2.35)] and demodulation τ_{mod} [equation (2.36)]. FlimFast provides three different but consistent kinds of views of the analyzed and enhanced multi-parameter image data. The views are updated in real-time during a continuous measurement and are displayed in separate child windows that can be arranged for side-by-side display (compare the screenshot in figure 18).

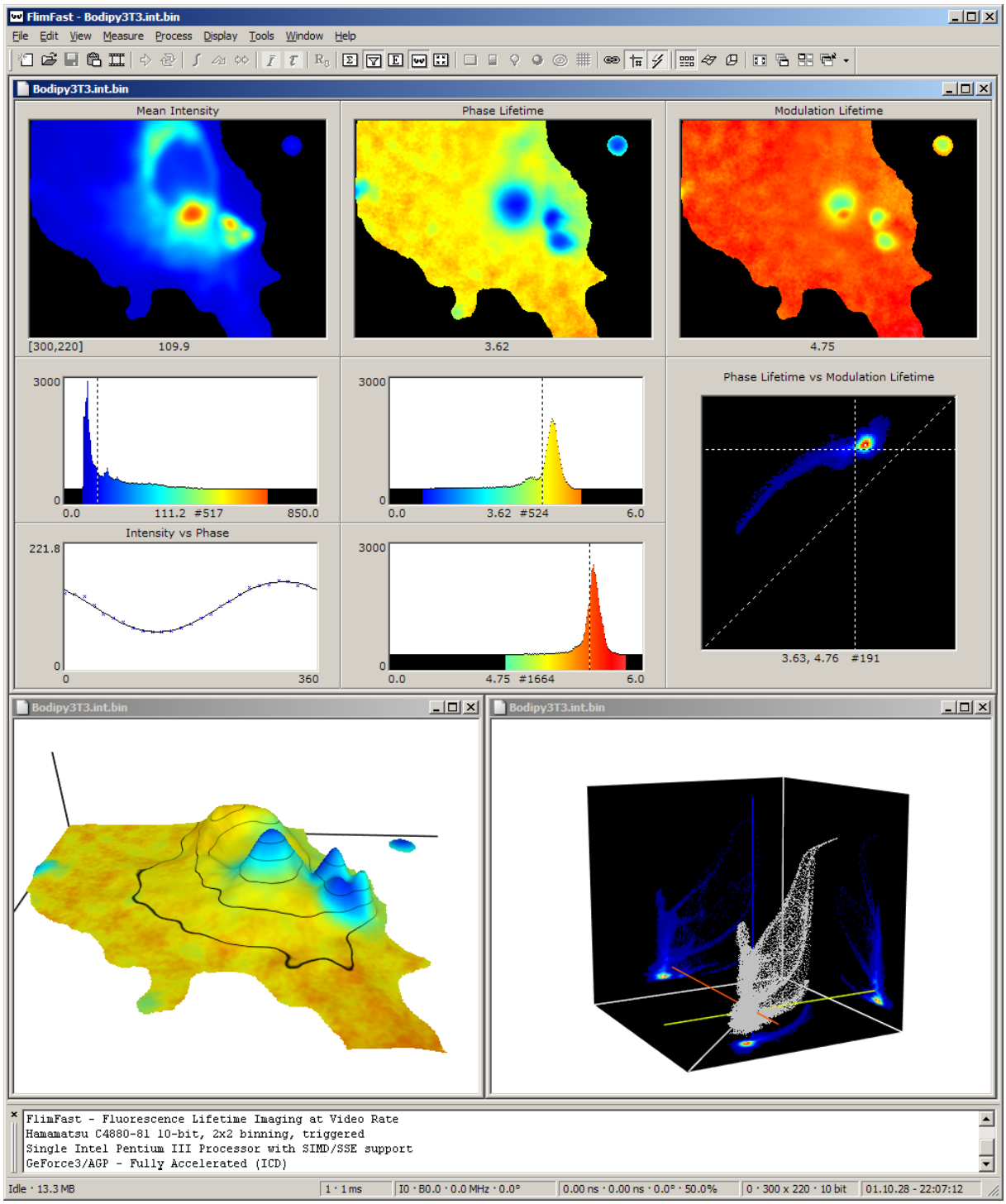

Fig. 18: Screenshot of FlimFast

Screenshot of FlimFast showing multiple, consistent views of fluorescence lifetime image data of a 3T3 cell stained with BODIPY FL C5-ceramide specifically for Golgi apparatus. *Upper panel*: two-dimensional side-by-side display of color-coded images (florescence intensity, lifetime from phase shift, and lifetime from demodulation), 1D image histograms, 2D lifetime histogram (demodulation vs. phase shift), and mean fluorescence intensity vs. phase plot*; Lower left panel*: multi-textured shaded surface rendering of a fluorescence intensity surface, color-coded lifetime image, and intensity iso-contours; *Lower right panel*: a 3D scatter plot of fluorescence intensity vs. lifetime from phase shift vs. lifetime from demodulation pixel data and 2D histograms mapped onto the cube faces. An intensity threshold mask is applied to all views. The lines in the histogram views indicate image mean values. The views are updated in real-time during a continuous measurement.

Multiple views of the same kind can be opened simultaneously. The color-coding, i.e. the minimum and maximum values for scaling and the color lookup table (Palette), is the same among all views of one document. Pixel data that do not fall within a global image mask do not show up in any view. The global color-coding and image mask facilitate the comparison of side-by-side displays of different views and allow caching and reuse of intermediate display data to increase overall processing speed. The views are drawn first into an invisible off-screen buffer, which reside either in the computer main memory or on the graphics card memory, and are then displayed by copying the off-screen buffer to the display buffer (bit-blitting) or by switching the off-screen and display buffers (double buffering). This ensures a flicker free, animated display. The graphics output of any window can temporarily be disabled and re-enabled if needed (e.g. to increase overall processing speed), copied into the clipboard, saved into a bitmap file, or streamed into an AVI video file for offline documentation or presentation. A wide variety of predefined color palettes of different file formats can be applied simply by drag-and-drop from the Windows file manager.

The main view provides a compact display of all the most relevant image data using conventional visualization techniques in one panel. Color-coded bitmaps (section 2.1.9.1) of the three images resulting from fluorescence lifetime analysis are displayed side-by-side to their corresponding one-dimensional image histograms, a two-dimensional histogram of the phase and modulation images (section 2.1.9.3), and a plot of the mean fluorescence intensity vs. phase. Individual values of pixels respectively bins of the images and histograms can be read out interactively, simply by pointing at them with the mouse cursor. The one-dimensional image histograms are displayed as bar charts using the same color code as the corresponding image. This greatly facilitates the comparison of different histograms and of histograms with their corresponding image. The drawing of the view does not depend on the presence of any hardware-accelerated feature on the graphics card and hence can be displayed on any Windows based computer system. The panel layout is automatically adjusted to different image sizes and display options.

Multi-textured shaded surface renderings provide a highly integrated view of the multi-parameter image data. Several advanced visualization techniques are integrated seamlessly such as interpolative surface plots or bar charts, shading (including Gouraud shading, per pixel lighting, bump- and environment-mapping), one- or multi-parameter color-coding (interpolative and anti-aliased), iso-contouring, image masking (surface clipping), and the display of image-metrics (such as a grid or ruler). Surface height, surface normal vectors (used for shading), color-code and iso-contours can each be independently derived from a

different image parameter. Color-code, iso-contours, transparency mask, and image metrics are texture-mapped onto the shaded surface (Fig. 19). A manifold of combinations are possible, although only some prove particularly useful for visualizing fluorescence lifetime data (chapter 2.1.9).

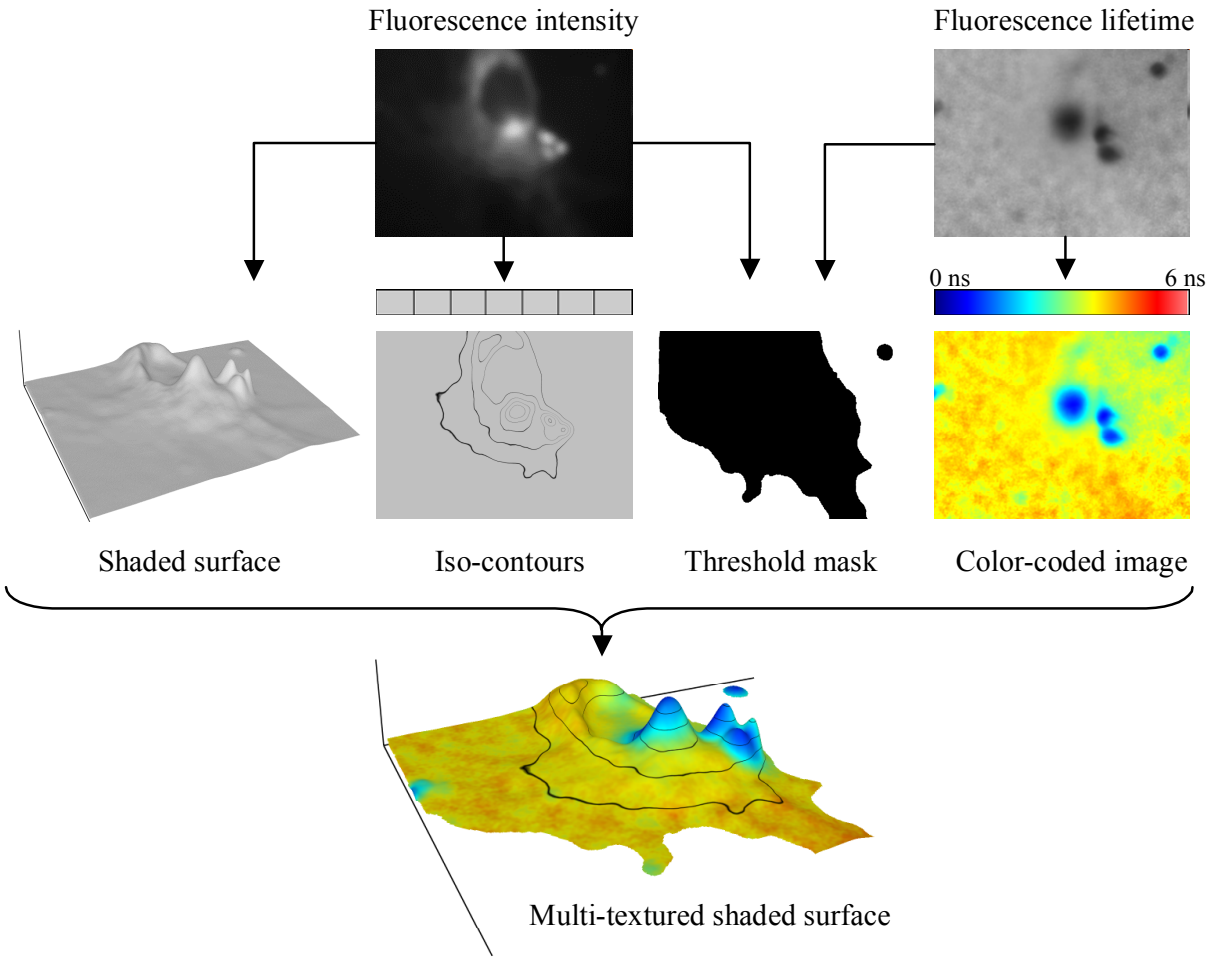

Fig. 19: Multi-textured shaded surface rendering
Polygon based surface rendering in combination with multi-texture mapping provides a single framework for the visualization of multi-parameter images. In this example the scalar fluorescence intensity and lifetime images are each normalized and clamped to a region of interest and are then used to index one-dimensional textures for iso-contouring and color-coding. The textures are overlaid on top of one another onto a shaded surface plot, which has a height proportional to the fluorescence intensity. The surface is clipped by a multi-parameter threshold and ROI mask. The surface is linearly interpolated and the texture lookup occurs filtered such that the final rendering appears smooth and anti-aliased. The rendering can be rotated and scaled interactively in real-time. The example shows fluorescence lifetime image data of a 3T3 cell stained with BODIPY FL C5-ceramide specifically for Golgi apparatus.

The implementation of this technique will be described in detail in (Gohlke *et al.* 2002). It relies heavily on the presence of hardware accelerated 3D rendering and multi-texture mapping capabilities on the graphics card. Besides integrating several visualization techniques and being accelerated by inexpensive graphics hardware, the technique seamlessly enables correct linear interpolative image scaling and anti-aliased color-coding. This is achieved by loading a color palette as a one-dimensional texture and using normalized and

clamped image data as texture coordinates. When linear texture magnification filtering is enabled, color interpolation occurs within the one-dimensional space of the color palette, whereas in case of the mapping of a color-coded bitmap as a two-dimensional texture, the interpolation would occur in between the colors of the bitmap. Another advantage of using one- instead of two-dimensional texture-mapping for color-coding is the avoidance of generating an intermediate color bitmap. Anti-aliasing is accomplished by enabling linear texture minification filtering and/or MIP-mapping. Multi-parameter color-coding is a straightforward extension: a multi-dimensional color palette is loaded as multi-dimensional texture and multiple image parameters are used as independent texture coordinates. One-dimensional texture-mapping also enables fast generation of iso-contours by using a transparent one-dimensional texture with nontransparent color entries at certain levels. Similarly, image metrics (such as a grid or ruler) can be overlaid onto an image/surface via a two-dimensional texture that is transparent except for the display of the metrics. Specific image regions can be rendered invisible by means of loading an image mask as a two-dimensional alpha channel (transparency) texture. Multiple layers of textures of different dimensionality, parameters and mapping functions can be subsequently mapped onto the same geometry using a variety of different ways to combine (blend) them into one final appearance (multi texture mapping). The rendering can be rotated and scaled interactively and intuitively via a virtual trackball. The minimum intensity threshold value of the image mask can be adjusted in real time.

An integrated view of the image statistics is provided by a **three-dimensional scatter plot and two-dimensional image histograms**. For each pixel the mean fluorescence intensity is plotted vs. the lifetime calculated from phase shift and the lifetime from demodulation. Color-coded images of the three possible two-dimensional image histograms are projected onto the corresponding faces of the coordinate system. Measurement artifacts and anomalies, such as off-scale intensities, bit-noise or bleaching, can easily be detected. The two-dimensional lifetime histogram (lifetime from demodulation vs. lifetime from phase shift) allows fast recognition of the presence of multiple lifetime components (see section 2.1.9.3 for a discussion).

3.1.2.2.3 Image analysis and enhancements

A number of commonly used image analysis and enhancement functions can be applied and adjusted on the fly during the measurement.

Software binning, i.e. the combination of 2x2 neighboring pixels to one pixel, is implemented on the level of the intermediate Fourier images (equations (2.30)-(2.32)), before the lifetime analysis is performed. It increases the signal to noise ratio and reduces the spatial image resolution by a factor of 4. Subsequent lifetime analysis and display tasks are speeded up proportionally.

Images are scaled and clamped (normalized) to minimum and maximum values prior to display and histogram analysis. These values can either be specified manually for each image parameter to specifically select region of interests or can be automatically determined to yield a maximum dynamic range (auto scaling). “Smart auto scaling” has been implemented to automatically select reasonable regions of interest that still provide a good dynamic range while also allowing for comparison of subsequent images during a measurement.

Contrast enhancement is implemented by histogram equalization, where each pixel of the image is scaled by the so-called cumulative distribution function, such that each bin of the outcoming image histogram has about equal counts. Image smoothing is implemented via a 3x3 Gaussian convolution filter. Contrast enhancement and smoothing are applied to the final fluorescence intensity respectively lifetime images, before display and histogram analysis.

Image analysis and display can be masked by minimum and maximum thresholds of the three image parameters and by an image region of interest.

It has to be noted that these functions are computationally very expensive and -with the exception of software binning- drastically slow down the overall speed of measurement.

3.1.2.2.4 Miscellaneous features

FlimFast uses a proprietary file format (FLIF) as default for data import and export. A FLIF file contains all relevant parameters and acquired image information, including user comments and precise timing. Streaming of unprocessed fluorescence intensity images into a FLIF file during data acquisition is (although supported by the file format) not implemented. For display purposes only a number of file formats can be imported, including 8 and 32 bit Windows bitmap files (BMP), FLImage binary files (BIN), and 16 bit integer and 32 bit floating-point image files used in the Laboratory for Fluorescence Dynamics (INT, PHS, MOD and DAT). Images and three-dimensional histogram volume data can be exported as ASCII worksheets or 32 bit floating-point binary files for analysis and visualization in external programs.

FlimFast automates the control of the instrumentation as far as possible. At program startup it attempts to load and link the EDT-PDV, NI-DAQ, and PCI-GPIB device driver libraries and if successful tries to initialize the frequency synthesizers, CCD camera, phase shifter and light shutter to default values. If any of these steps fail to complete, the program automatically falls back to emulating all functions of the instrumentation in software. This offline mode can be used to calculate the influence of special measurement conditions (e.g. the effects of bit noise) or to verify the correct functioning of the program (e.g. of analysis routines), and it enables FlimFast to run on computers without installed interface drivers or cards.

FlimFast was developed using standard Microsoft Windows user interface elements and concepts. Hence it provides the users with a familiar application environment. It uses a multiple document interface (MDI) where multiple documents and multiple views per document can be opened simultaneously inside one mainframe window. Program functions are exposed to the user by means of a main menu, popup menus, a toolbar, dialog boxes and keyboard shortcuts. The status of the instrumentation and progress of the measurement are displayed in a status bar. Non-critical error and other messages are directed to a text output window instead of annoying dialog boxes. FlimFast can be run in a full screen or topmost window mode.

3.2 Application Project: Fluorescence Lifetime Imaging Microscopy (FLIM) of non-photochemical quenching mutant cells of the green alga *Chlamydomonas reinhardtii*: Inter- and intracellular lifetime heterogeneities of single alga cells and the fluorescence lifetime transient

3.2.1 Materials and methods

3.2.1.1 Fluorescence transient and lifetime measurements

For lifetime measurements of fluorescence, the data acquisition must take place during defined time periods of irradiation where the fluorescence signal is constant. If the fluorescence intensity changes during the time of the measurement, artifacts will arise. The artifacts are due to distortions of the sine curve (fluorescence *versus* phase delay) in the frequency domain[32]. If the decay characteristics of the fluorescence change during the measurement time, then any measurement of the lifetime must take place in a period of time short compared to these kinetics, or the measurement (no matter whether it takes place in the frequency or time domain) will be affected.

Dark-adapted photosynthetic systems change their chlorophyll fluorescence intensity (fluorescence transient; see the photosynthesis introduction given in 2.2) when irradiated. The fluorescence level of photosynthetic systems increases upon sufficient irradiation to a maximum (F_{max}), 5-10 times the original level F_0, and this usually takes place in time scales ranging from 100 ms up to 1 s. The intensity can increase by a factor of four within 0.2 ms. Under certain conditions the changes in fluorescence intensity of photosynthetic systems directly reflect changes in the lifetime of the fluorescence as discussed in a review by Govindjee (1995).

In the frequency domain (that we use for data acquisition), the fluorescence transient (the Kautsky curve) will be convoluted with the sinusoidal fluorescence emission signal (Fig. 20), and unless the measurement is very short compared to the time of the induction curve, or is made in a region of constant fluorescence, the analysis would also be distorted through this convolution. Rapid lifetime measurements therefore have been performed in the transient region of relatively constant and maximum (P-level) intensity following initial illumination and during the P-to-S (or T) decay (P stands for peak; S for quasi-steady state and T for terminal steady state), during which the intensity changes of the transient are negligible in the short measurement time interval.

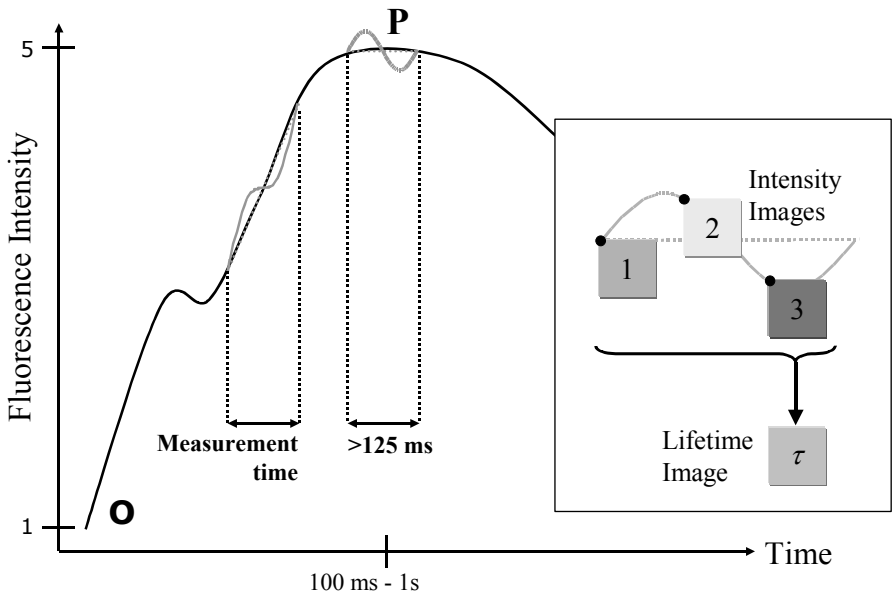

Fig. 20: The fluorescence transient and lifetime measurements
Three or more phase-delayed images (images of the fluorescence intensity with a different incremented phase difference $\Delta\phi^{E\text{-}G}$) are necessary to obtain a fluorescence lifetime image (see *insert*). The lifetime measurements were done at the P-level, where one usually obtains several seconds of constant fluorescence intensity. This allows analysis of the modulated fluorescence emission signal without corrections for additional changes in the intensity, as they occur for example at the rapid intensity increase in the beginning of the fluorescence transient. The minimal necessary measurement time for a lifetime image (3 phase-delayed images of 328×247 superpixel; 2×2 binning) is down to 125 ms in the described setup. Such fast measurement times allow the imaging at the P-level.

3.2.1.2 Instrument calibration with a lifetime standard

The lifetime measurement must be calibrated either against the phase and modulation depth of the excitation light, or from the dynamic signal from a known fluorescence sample. We have found it convenient, robust and accurate to use a fluorescent plastic standard (purple CD SlimLine jewel case; InterAct, Florida, USA) that was selected for its spectral emission at 690±40 nm, and reproducible phase and modulation lifetimes (τ_{phase} = 1.02 ns and τ_{mod} = 1.26 ns). The lifetimes of the plastic standard have been accurately determined relative to two well known standards: fluorescein in NaOH, which has a single-exponential lifetime of 4.1 ns (Sjöback *et al.* 1995), and rhodamine 101 (Lambda Physik GmbH, Göttingen, Germany) that has a temperature independent single-exponential lifetime of 4.34 ns in ethanol (Drexhage 1973; Karstens and Kobs 1980; Vogel *et al.* 1988). The solutions have been filled in micro-capillaries (see 3.2.1.5). In addition the plastic standard has been verified by measuring the short lifetimes of dandelion leaves under high light conditions.

The importance of lifetime calibration and the problems related with this procedure have been addressed by Hanley *et al.* (2001). They present a beautiful method for the lifetime calibration, which does not require the knowledge of the lifetime of the reference fluorophore in solution. They use different solutions of the same fluorophore, which show different

degrees of dynamic quenching. This procedure allows lifetime calibration, if the fluorophore exhibits a single exponential decay in all solutions. But to ensure this point is not unproblematic (without multifrequency or time domain measurement). The procedure could not be used in our case due to the small and unfavorable spectral emission window at 690±40 nm. The fluorescence emission of many of the common fluorophores, used as lifetime standards, is rather low at this wavelength, which makes concentrated solutions necessary to obtain a sufficient signal. The lifetime of the solutions was changing depending on the concentration, probably due to aggregate formation. It is well known that in general the preparation of accurate standard solutions is not unproblematic, due to their sensitivity to concentration, temperature, solvent (and solvent and compound purity), excitation and emission wavelength. The sensitivity to these parameters is different for each fluorophore, depending on its chemical constitution. For the selection of a lifetime standard it is of importance that the calibration can be performed under identical instrumental conditions especially with respect to the used objective, neutral density and emission filters and sample position. Otherwise the difference in the path-length Δl of the light will give rise to a phase difference $\Delta\phi = \Delta l\ \omega/c$, if the path-length change occurs in a medium with a refractive index of unity, or to a phase difference of $\Delta\phi = -\ n\ \Delta l\ \omega/c$, if an optical element of refractive index n is introduced or removed. Especially changes after the dichroic mirror give rise to double path-length changes, because the light is passing this region two times.

Calibration with reflected or scattered excitation light has certain disadvantages. First, changes in the optical path are necessary. The fluorescence emission filter has to be removed and different neutral density filter have to be inserted in order to decrease the high light intensities. But different filters with identical thickness and refractive index can be inserted (see also instrument description in 3.1.1.4.2) in order not to introduce unwanted phase differences.

Second, it has to be ensured that the reflected or scattered light originates from the object plane of the microscope. A microscope slide has been painted with barium sulfate suspension (white reflectance coating 6080, Eastman Kodak Co., Rochester, NY, USA), a very efficient non-fluorescent scatter coating. If the image intensifier gain had been adjusted for the detection of the scattered light, the signal was still composed to a considerable part of reflected light from the optical surfaces in the microscope (e.g. dicroic mirror, objective, lenses) as could be measured by replacing the scattering slide with a sooted microscope slide (positioned in an angle on the microscope stage, far removed from the objective, in order to prevent back reflection). In such a case phase and modulation of the scattered light can only

be determined if one corrects for the microscope-internal reflections. A FlimFast module has been developed, which does correct for this case. The average intensity value for all pixels is recorded first for a measurement with the scatter coating. After that the measurement is performed with the sooted microscope slide. For each phase setting the measured average intensity of the sooted slide (the reflections) are subtracted from the scatter signal and a single Fourier analysis is performed on the corrected signal.

Instead of the scatter coating a mirror can be placed under the objective. We found that in this case at lowest intensifier amplification (and according laser light attenuation with neutral density filters) the light intensity originating from the object plane is so high in comparison to the microscope-internal reflections that the above-mentioned correction is not necessary any more. Phase and modulation measured from corrected scattering and from reflection at a mirror gave identical results.

But for a calibration with reflected excitation light, strong interferences due to the light reflections on the optical surfaces of the microscope are the case. If these interference patterns in the image are averaged, reflections of excitation light can also be used as a stable calibration. But it should be noted that such average signal, although stable and reproducible, was found not to correspond absolutely to the zero phase and modulation (lifetime of 0 ns). Constant phase offset and modulation factor have to be taken into account, if reflection is used for the instrument calibration.

We find it most convenient to use a fluorescent plastic standard for the instrument calibration. First it allows fast calibration (and calibration control) without changes in the optical setup of the instrument. Second it ensures reproducibility and correct measurement comparisons, if the identical standard is used for all measurements. A solution in comparison might change over time (to a higher degree than a fluorophore in plastic) or might differ slightly every time prepared.

It has to be emphasized that a lifetime standard does not need to be a fluorophore with single exponential fluorescence decay, although this is the case for the fluorophores commonly used as lifetime standards. If reproducibility is ensured, a standard can be used even without the knowledge of the different exponential components. For the selected plastic standard, we could determine the lifetimes calculated from phase and modulation at the selected light modulation frequency by comparisons with known (single component) lifetime standards as mentioned above. This procedure has to be performed only once correctly. After that all measurements are only compared against the selected standard with $\tau_{phase} < \tau_{mod}$.

Before each measurement the instrument has been calibrated using a FLImage module for repeated measurements (see section 3.1.2.1). For a lifetime measurement the module uses the average intensity from all pixels at every phase setting and performs a single Fourier analysis on this data. The module repeatedly executes FLImage and displays mean image statistics over time. It therefore repeatedly measures and plots the fluorescence signal from the plastic lifetime standard (the image average) as a function of time and determines the average of multiple measurements. This offers a higher precision (with automatic phase-stability check) than the alternatively build-in function, which employs a single measurement for calibration. After each measurement the procedure is repeated to assure phase stability during the measurement. This calibration check is especially important for the acquired time series of lifetime measurements, during which the phase might have changed.

3.2.1.3 Experimental conditions for the fluorescence lifetime measurements

The 488 nm line of the argon-ion laser, modulated at a frequency of 80.652 MHz, was used for illumination. For the presented measurements the FLIM instrument equipped with the Zeiss fluorescence microscope (as described in 3.1.1.4.2) was used. The wavelength of the measured fluorescence was 690±40 nm (bandpass filter for fluorescence emission, Omega XF70/690DF40; Omega Optical, Brattleboro, VT, USA). The intensity of the excitation light was adjusted by neutral density filters (see 3.1.1.4.2) and ranged between 50 and 8600 μmol photons m^{-2} s^{-1}. However, for most experiments it was typically between 300 or 2500 μmol photons m^{-2} s^{-1}. The cells were dark adapted for at least five minutes before each measurement. The cells were then pre-exposed to the light for 1 s before 8, 16 or 32 incrementally phase delayed images were acquired. Each image was averaged for 100 ms, so that the total illumination time of the measurement was about 1, 2.1 or 3.9 s. The time range was chosen to keep the measurement within the constant plateau region of the transient (at the "P" level). The lifetime measurement must be carried out rapidly, so that during the time of measurement no transient intensity changes occur (see above and Holub *et al.* 2000). For all ensemble measurements (samples on nitrocellulose filter paper, micro-capillaries and lifetime transients) an objective magnification of x10 has been used. The single cell measurements were made with a 100x objective.

Fluorescence lifetime transient measurements were begun at the P-level fluorescence. Eight incrementally phase delayed measurements were taken at 100 ms intervals, and the measurement time for each transient time point was 0.9 s. Such time for each single measurement has been found to be sufficiently fast for the P-to-S fluorescence decline, but the

instrument allows faster measurements (see above). In addition higher camera binning modi can increase the measurement speed. The special measurement of fluorescence lifetime transients still makes use of the imaging setup, but globally analyzes the signal of all pixels[33]. In addition each pixel still averages the fluorescence signal from many cells immobilized on nitrocellulose filter paper at low magnification (x10 objective).

3.2.1.4 Determination of the excitation light intensity

The radiant flux was measured with a radiant power meter (model 70260 with 70286 Si diode detector; Oriel Instruments, Stratford, USA) directly in the focal plane of the objective. The illumination intensity profile is Gaussian, due to the use of a single mode fiber. Therefore the irradiation intensity is higher in the middle than at the side of the image. With a thin and homogeneous layer of a fluorescent sample and a micro scale the Gaussian illumination profile can be measured under the microscope. The area under the normalized Gauss curve from a fit of the illumination profile corresponds to the diameter of a (hypothetical) circular area of constant irradiation. If this area has been determined once for the objective, the photon flux density in the center of the image can always be directly calculated from the radiant power measurement.

We measured diameters of 79/650 μm for 100x/10x objectives. The irradiation variations in the image are dependent on the zoom optics used in the microscope. Lifetime measurements at different defined excitation intensities are therefore possible in a single image.

3.2.1.5 Algal growth conditions and measurement preparation

Cells of *Chlamydomonas reinhardtii* were grown photoheterotrophically during constant illumination with 100 μmol photons m^{-2} s^{-1} in tris-acetate phosphate (TAP) medium (17.4 mM acetate; pH 7) (Harris 1989) at 25° C. The cells were grown in Erlenmeyer glasses, which were constantly shaken. Cells were harvested at late logarithmic growth phase. Cells in the TAP medium were always kept under motion (as the culture flasks were kept over either shaking table or magnetic stirrer) until the measurement was performed. The cells under these conditions showed high motility and have high photosynthetic activity.

The following protocol was followed at room temperature. When used, the protonophore nigericin (Sigma; St. Louis, MO, USA) was added to the cell suspension (10 μM final concentration; 10 minutes incubation) after cells have been centrifuged down and buffer changed to minimum High Salt (HS) medium (Harris 1989). When used, methyl viologen (Gramoxone, Sigma) was added to the cell suspension (100 μM final concentration), followed

by a 10 minute incubation. Prior to the fluorescence lifetime measurements, the cell suspension was dark adapted for 5 minutes. When needed, the electron transfer inhibitor 3-(3,4-dichlorophenyl)-1,1-dimethylurea (DCMU, Diuron; Sigma) was added in darkness to the cell suspension (10 μM final concentration), followed by a 5 minute incubation in the dark.

The fluorescence transients as presented by Govindjee and Seufferheld (2002; also Fig. 12) have been acquired from an ensemble of alga cells swimming in buffer. To compare with these studies, we have used three different experimental procedures to measure the fluorescence signals from an ensemble of cells at low magnification (the same procedures were also used for single cell observations in combination with high magnification optics and reduced cell numbers):

1) by depositing a sufficiently large number of cells from suspension on a nitrocellulose filter paper using a mild vacuum so that they form a continuous layer of immobilized cells.
2) by filling the cells in rectangular micro-capillaries and
3) by deposition of cells on a thin film of agar between two microscope cover slips.

The first and the second method allow a direct comparison of the xanthophyll cycle mutants and WT in a single image, allowing an accurate differential measurement. This is accomplished by cutting the pieces of filter paper and arranging them side by side under the microscope or by putting the three micro-slides next to each other in the same field of view. Procedures two and three also allow transmission light images to be recorded, whereas method one can only observe the Chl fluorescence. In procedure two the cells are not immobilized. Single cell lifetime measurements can be carried out on cells that have stopped their movement (as discussed later for the case of geotaxis). Ensemble measurements of swimming cells are still possible, if the cell number is high and the resolution low enough so that the average signal is not affected any more by the movements of the single cells during the measurement time.

The three methods involved the following detailed procedures:

1) Using a mild vacuum, cells were deposited on a nitrocellulose filter (pore size 1.2 microns, Millipore; Bedford, MA, USA) that had been soaked previously in minimum HS medium; this was done to avoid out-of-focus movement of the cells under the microscope due to the water uptake of the filter. The filter was then covered with minimum HS medium (pH 7) and a cover slip. For comparative measurements the pieces of filterpaper with deposited WT, npq1 and npq2 could be cut and arranged under a single cover slip.

2) Before the cells were filled in micro-capillaries (precision rectangle glass capillary tubes, called microslides or Vitrotubes; inner diameter 0.03 x 0.3 mm; VitroCom Inc., Mountain Lakes, NJ, USA), the cell suspension was centrifuged, supernatant nearly completely removed and the cells were then resuspended in the drop of medium left in the tube. This produced a highly concentrated cell suspension in the capillaries.

3) Thin agar films were created by applying a drop of warm agar (agar bacteriological; Sigma) prepared with HS medium between two large microscope cover slips. After cooling down, one cover slip could be lifted, the cell suspension was applied and then it was covered by the cover slip.

At the beginning of the series of measurements the cells were illuminated in the microscope with lower light intensity (300 μmol photons m^{-2} s^{-1}) for focusing purposes. Then the cells were illuminated briefly with the chosen excitation light intensity (in most cases about 2500 μmol photons m^{-2} s^{-1}) to adjust the image intensifier gain for an optimal dynamic range of the camera. This was followed by dark adaptation of the cells for 5 min. For the acquisition of a measurement series the gain adjustment had to be performed only once.

3.2.2 Results and discussion

3.2.2.1 The lower fluorescence intensity of the npq2 mutant in comparison to WT and npq1 mutant is correlated with a shorter fluorescence lifetime

When photosynthetic organisms are irradiated constantly after being dark-adapted, the fluorescence intensity undergoes large changes with time. This is usually referred to as the "fluorescence induction" or the "fluorescence transient", and is also known as the Kautsky effect (see the photosynthesis introduction given in section 2.2).

The transients in the fluorescence intensity of the xanthophyll cycle mutants npq1, npq2 and the WT (without cell walls) have been measured and have been discussed in a previous publication (Govindjee and Seufferheld 2002). The fluorescence intensity of npq2 is significantly reduced (about 25-35% at the P-level for the unnormalized data) in comparison to WT and npq1 (both of which showed similar levels) even in the presence of DCMU and nigericin. In our experiments, the goal was to determine whether the reduced fluorescence is due to a reduction in the quantum yield of fluorescence or whether it might originate from differences in the absorption cross section of the fluorescent pigment bed (i.e. static quenching) e.g. by state changes (Delosme *et al.* 1996).

Fig. 21 shows the Chl *a* fluorescence of WT, npq1 and npq2 (cell ensembles deposited on nitrocellulose filter paper) taken simultaneously in a single measurement. In this experiment,

all the samples were adjusted to have the same concentration of cells, as measured by scattering at 750 nm. The fluorescence intensity and lifetime images were taken over 3.9 s during the P-level of the Chl fluorescence transient. npq2 shows 30% lower fluorescence intensity than npq1.

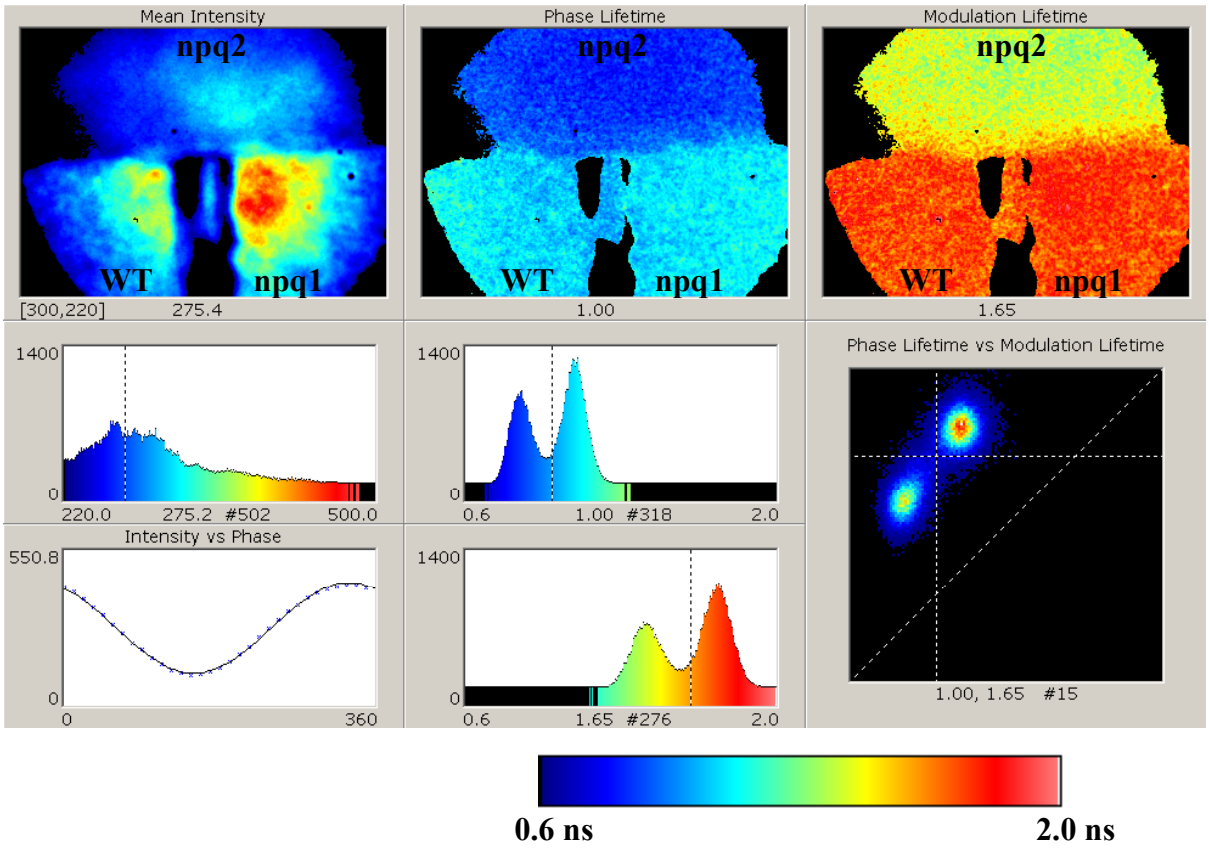

Fig. 21: Comparison of the Chl *a* fluorescence from WT, npq1 and npq2 mutants of *Chlamydomonas reinhardtii* in a single image
Cells immobilized on nitrocellulose filter paper. Shown are the images of the fluorescence intensity, apparent single lifetime form phase τ_{phase} and from demodulation τ_{mod}. The mutant npq2 displays shorter intensity and lifetimes than WT/npq1. Irradiance, 2500 µmol (photons) m^{-2} s^{-1}; total irradiation time 3.9 s.

WT and npq1 in the image show similar intensities (WT fluorescence is 10% less than npq1). The decreased fluorescence intensity in npq2 is correlated with a shorter apparent single lifetime calculated from both the phase (τ_{phase}) and from demodulation (τ_{mod}) analysis. At the high light intensity used (2500 µmol photons m^{-2} s^{-1}), WT in the image shows τ_{phase} = 1.11 ns and τ_{mod} = 1.78 ns ($\tau_{phase} < \tau_{mod}$ if there is more than one lifetime; see Appendix 5.5). Multiple pixels have been analyzed globally for these average values (that is, the intensities of all the pixels in the selected region are added for each incrementally phase delayed image, and a single Fourier analysis is performed on this data). Therefore the measurement error of the given lifetimes is less than 10 ps. The measurement error for the single pixel analysis (Fourier analysis for every pixel) can be determined directly from the histograms and is in this case

about 50 ps for τ_{phase} and 70 ps for τ_{mod}.

The fluorescence lifetime of npq1 is very similar to the WT with τ_{phase} = 1.12 ns and τ_{mod} = 1.79 ns, while npq2 displays significantly shorter τ_{phase} = 0.85 ns and τ_{mod} =1.44 ns.

A discussion of how these values relate to the lifetime compositions can be found in the Appendix 5.5.

In addition the measurements with the ensembles of cells display a heterogeneity in the intensities and lifetimes, which are significantly larger than the measurement error (data not shown). While the variation usually is less than 10%, changes of 25% could be observed in certain cases. Possible reasons for this heterogeneity will be addressed in the next sections, especially the way these differences manifest themselves on the single cell level. For example we could observe that cells that form clusters have longer lifetimes, whereas non-swimming cells (in the state of negative geotaxis) display shortened lifetimes even on the ensemble level.

For all average measurements the lifetimes of the zeaxanthin accumulating mutant npq2 are 20-30 % shorter. Zeaxanthin therefore quenches dynamically the Chl *a* fluorescence of PSII in *Chlamydomonas reinhardtii* by decreasing its quantum yield.

That is, these changes are due to an increased rate of de-excitation from the excited state, and the decreased fluorescence intensity is not simply due to a decrease in the absorption cross section in PSII (see e.g., Gilmore *et al.* 1995; Gilmore *et al.* 1998). Our results are consistent with a dynamic quenching by zeaxanthin of the Chl *a* fluorescence of PSII in *Chlamydomonas reinhardtii*.

And this result applies to cells even when electron transfer is inhibited by DCMU, and even when the proton gradient is decreased by nigericin and after treatment with the PSI-electron-acceptor methyl viologen (images not shown, but see lifetime transients below). These results imply that the quenching process includes contributions from non-qE related processes.

3.2.2.2 The fluorescence lifetime transient: Measuring how the fluorescence lifetime changes during the transient

Many researchers have used measurements of the fluorescence transient as a powerful tool for probing excitation energy transfer among PSII units and electron flow in PSII (Govindjee 1995; Stirbet *et al.* 1998; Steffen *et al.* 2001). We have extended such studies by measuring the transients in the fluorescence lifetimes, which shall be further referred to as the fluorescence lifetime transient: We have simultaneously measured the fluorescence intensity, τ_{phase} and τ_{mod} for each time point of the fluorescence transient.

Figs. 22 and 23 show fluorescence lifetime transients, starting from the "P" level during P-to-S decay, for WT, npq1 and npq2 cells exposed to two different excitation intensities for untreated cells and cells treated with the electron transfer inhibitor DCMU, the protonophore nigericin and the PSI-electron-acceptor methyl viologen (Chl concentrations have been adjusted to be the same for all samples as in Fig. 21).

It should be noted that the presented lifetime transients are single measurements from a cell ensemble. As mentioned for the lifetime images in the previous section, the cells display remarkable heterogeneities between measurements. Therefore the presented transients might not represent the average of many measurements. The averages of multiple measurements for the fluorescence intensity alone have been already presented previously (see Fig. 12). The goal for the presented lifetime transients has been to establish the method, to compare intensity and lifetime changes and to obtain qualitative and quantitative order of magnitude information about the relation between mutants and WT under the different treatments.

At the lower excitation light intensity (300 μmol photons m^{-2} s^{-1}), photoinhibition is avoided; not so at high light exposure (2750 μmol photons m^{-2} s^{-1}), as discussed in detail in section 3.2.2.4.2.

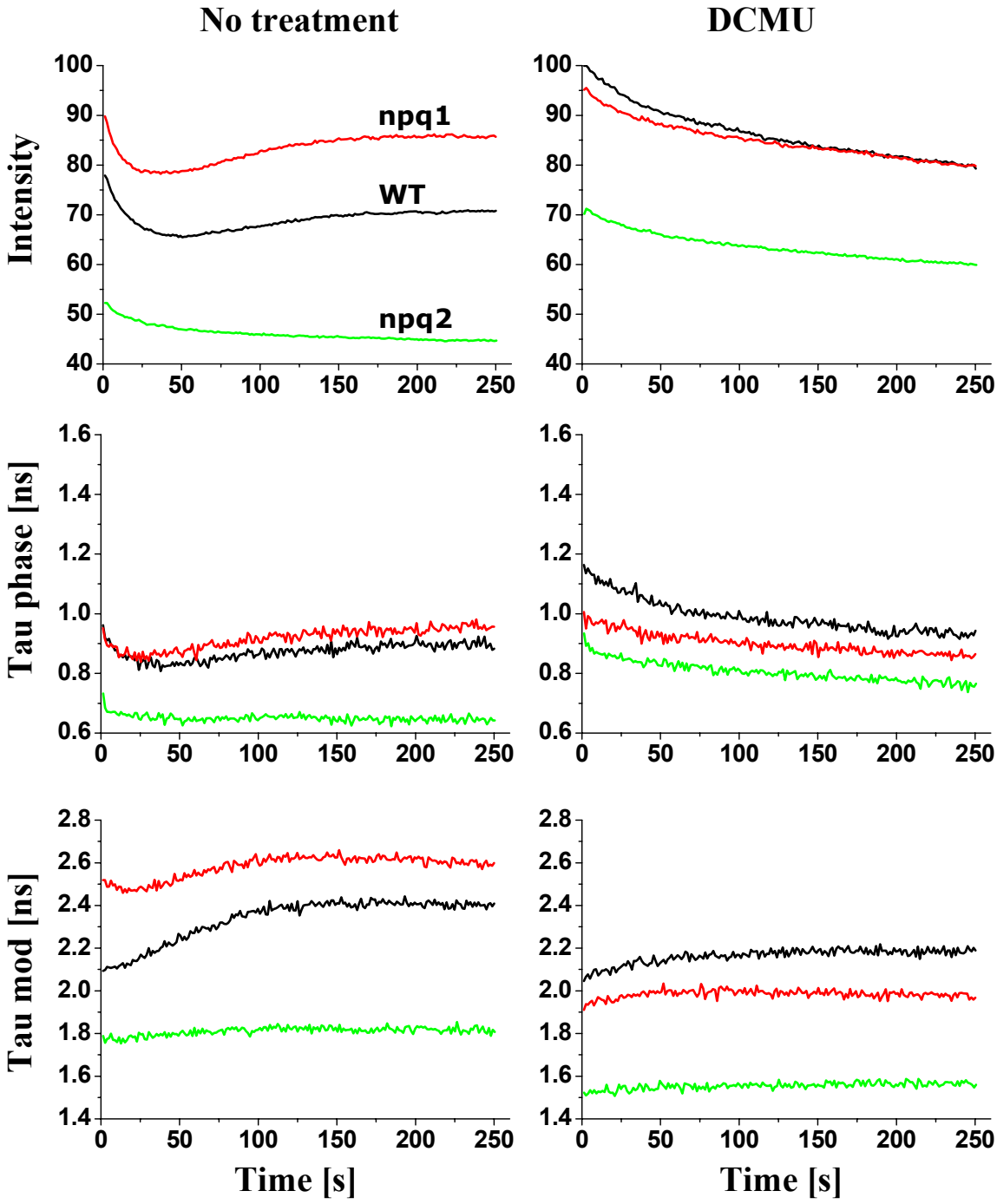
No treatment
DCMU
Intensity
Tau phase [ns]
Tau mod [ns]
Time [s]
Time [s]
npq1
WT
npq2

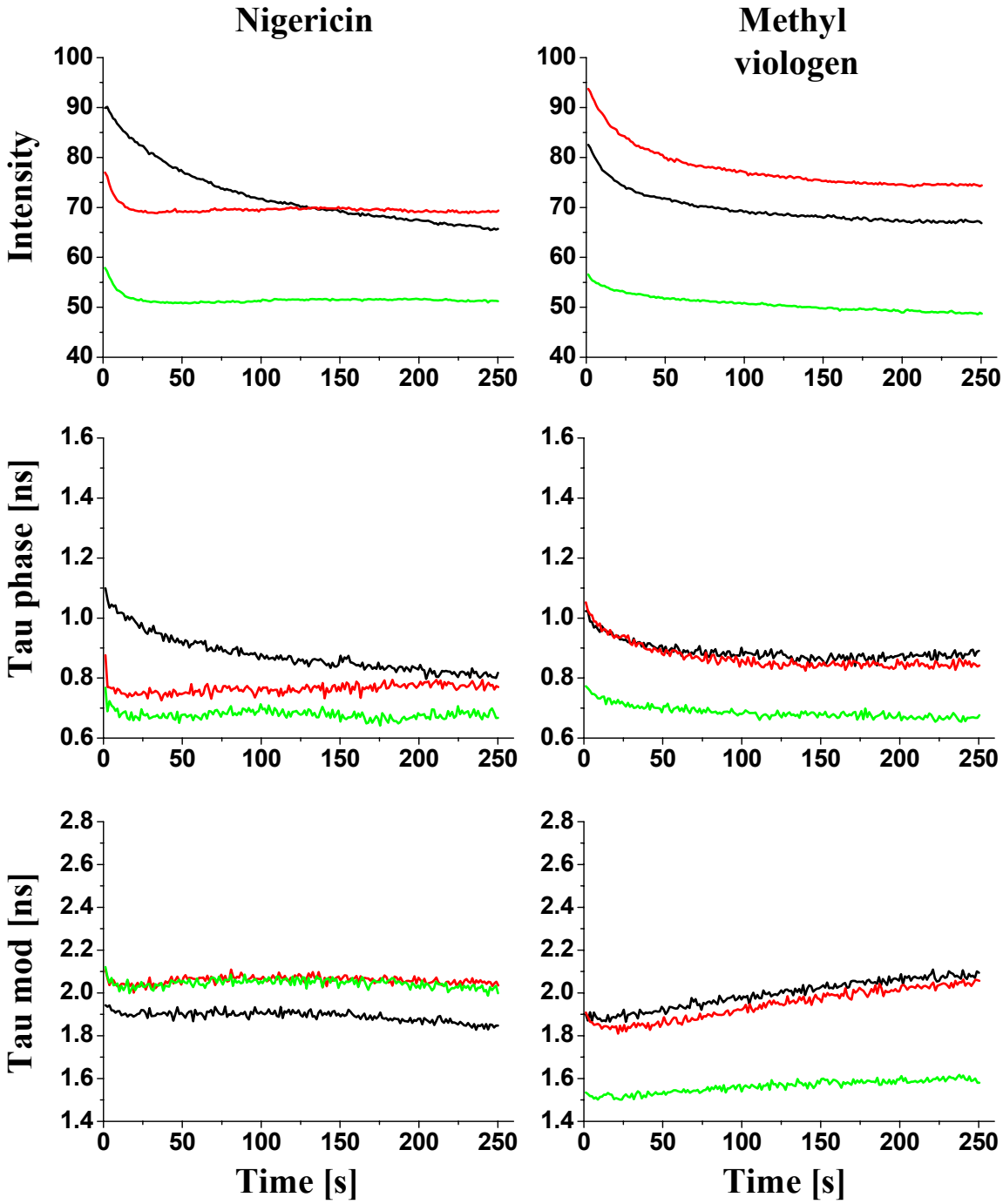

Fig. 22: Fluorescence lifetime transients at 2750 µmol (photons) m^{-2} s^{-1}, starting at the "P"level
Chl *a* fluorescence intensity (relative units) and apparent single lifetimes from phase and modulation for WT (black), npq1 (red) and npq2 (green) mutants of *Chlamydomonas reinhardtii*, with and without 10 µM DCMU, 10 µM nigericin or 100 µM methyl viologen.

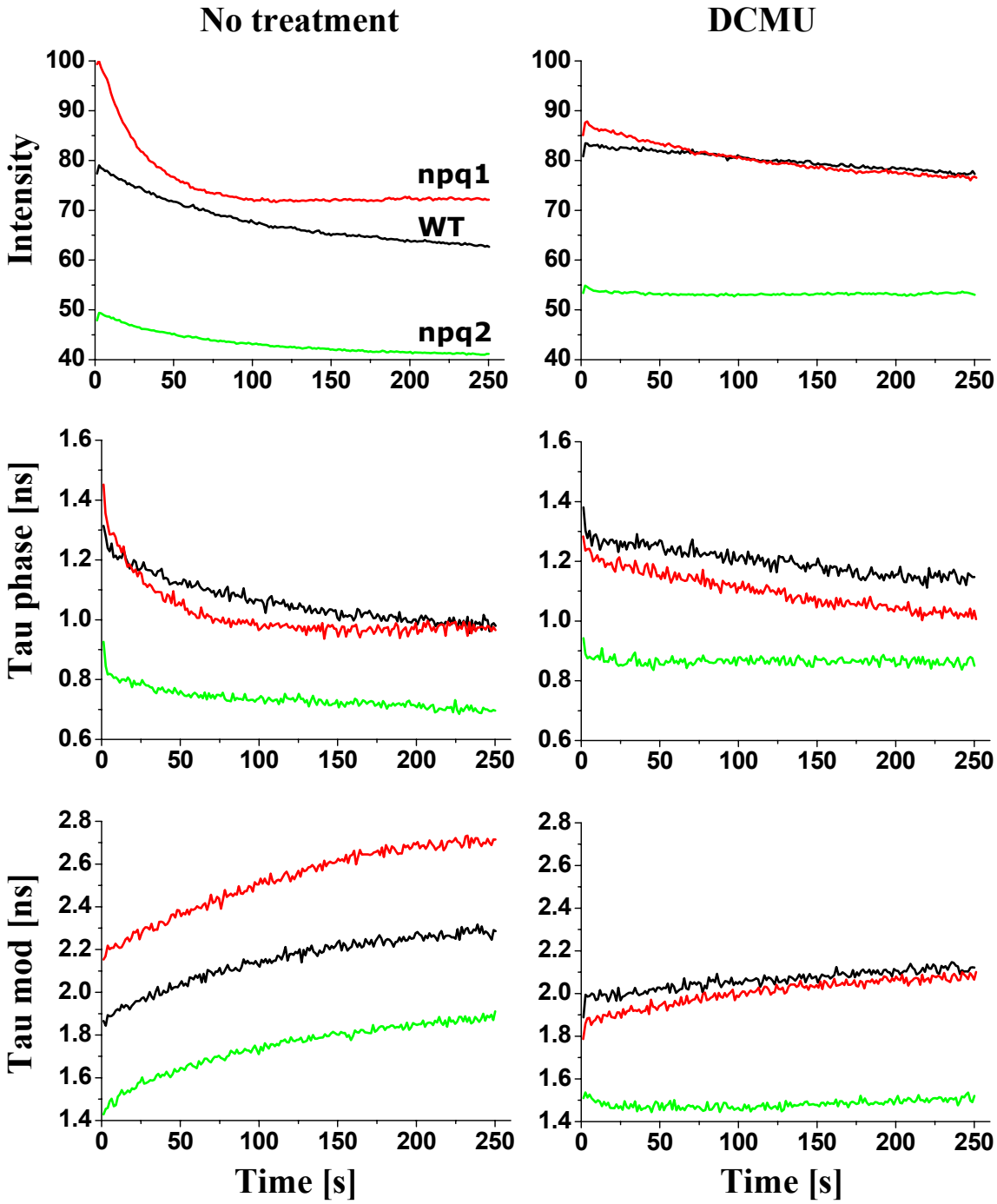
No treatment
DCMU
Intensity
Tau phase [ns]
Tau mod [ns]
Time [s]
Time [s]
npq1
WT
npq2

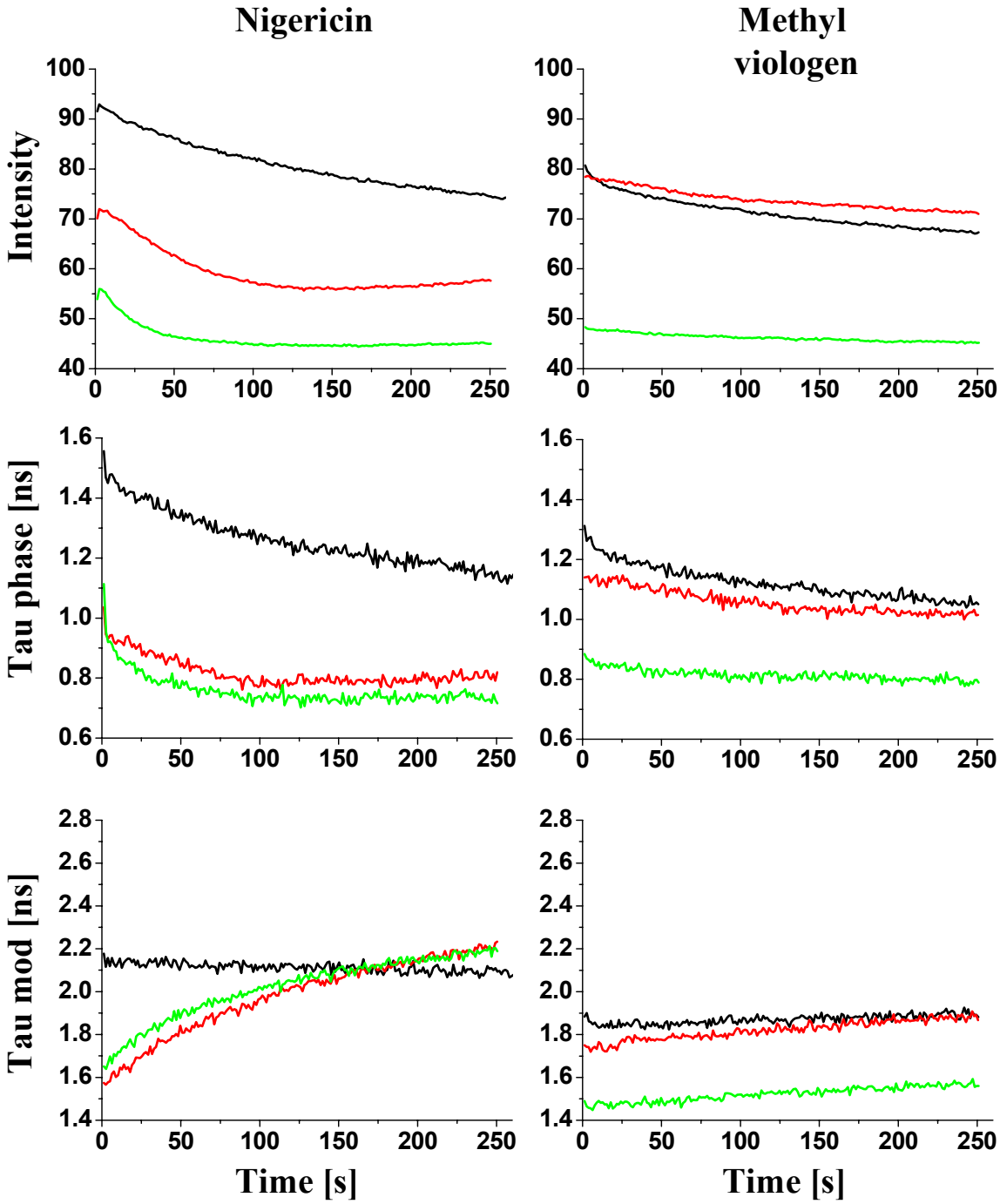

Fig. 23: Fluorescence lifetime transients at 300 µmol (photons) m^{-2} s^{-1}, starting at the "P"level
Transient Chl *a* fluorescence intensity (relative units) and apparent single lifetimes from phase and modulation for WT (black), npq1 (red) and npq2 (green) mutants of *Chlamydomonas reinhardtii*, with and without 10 µM DCMU, 10 µM nigericin or 100 µM methyl viologen.

The electron transfer inhibitor DCMU, the protonophore nigericin and the PSI-electron-acceptor methyl viologen have well known effects on the progress of the fluorescence transient (see Fig. 24 for an overview of their chemical interactions).

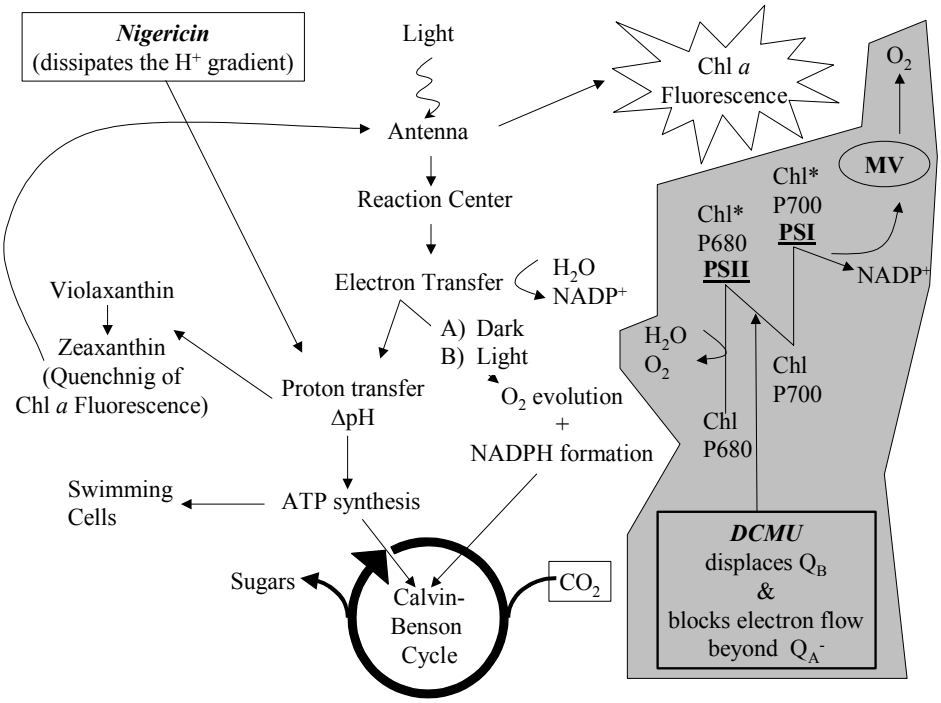

Fig. 24: Overview of the chemical interferences of DCMU, nigericin and methyl viologen in photosynthetic samples
The electron transfer inhibitor DCMU is known to replace the plastoquinone Q_B of PSII and thereby to close the PSII reaction center and block the electron transport from PS2 to PS1. The protonophore nigericin dissipates the proton gradient of the thylakoid membrane. Methyl viologen (MV) is one of the most efficient electron acceptors of PSI. Its removal of electrons prevents the usual "blockage" of the electron flow during photosynthesis and thereby the accumulation of reduced Q_A.

While the differences induced by the drug treatments are not quite as pronounced as reported earlier from swimming cells (Govindjee and Seufferheld 2002), similar trends can be observed in the lifetime transients of the immobilized cells.

DCMU: DCMU is known to replace the plastoquinone Q_B of PSII and thereby to close the PSII reaction center and block the electron transport from PSII to PSI (Velthuys 1981; Wraight 1981). A major effect of DCMU is in the faster rise from F_0 to the P level, but this could not be followed by the lifetime measurements here (as discussed in 3.2.1.1). However, we measured the so-called P-to-S (or T) decay that is a result of both, internal acidification (Briantais *et al.* 1979) and state changes (Allen and Forsberg 2001). Without any treatment by inhibitors, the fluorescence intensity is reduced considerably when passing from the P- to the S-level, and this is observed in all 3 samples. It is known that DCMU abolishes the P to S intensity decay. The resulting general increase in fluorescence intensity (due to the closure of the reaction centers) and the decrease in the difference between P- and S-level are clearly

visible in Figs. 22 and 23. The intensity increase is accompanied by an increase in τ_{phase}; however, there is a decrease in τ_{mod} (see Appendix 5.6 for analysis).

It is of significance that the lifetime of fluorescence of the npq2 mutant is much shorter than that of the WT/npq1 mutant even in the presence of DCMU. It establishes that the quantum yield of fluorescence is greatly reduced in npq2 even when the electron transfer is blocked. That is, a quenching process persists, even at blocked electron transfer. Since the lifetime decreases parallel the intensity decreases, the latter are not due to "state changes". Further, when the linear flow of electrons is blocked by DCMU, one does not expect to have an accumulation of protons inside. Thus, a change in the "xanthophyll cycle" (and the related qE quenching mechanism, which involves the thylakoid ΔpH; see Fig. 11) is only possible if we suggest that a cyclic reaction around PS1 accumulates protons. An alternative is to suggest that zeaxanthin may also be quenching by a process that is independent of the normal xanthophyll cycle.

Nigericin: The importance of the proton gradient for fluorescence quenching is well known (see Fig. 11 and the photosynthesis introduction given in section 2.2). Addition of nigericin, that dissipates the proton gradient, therefore is known to decrease (or eliminate) the P-to-S fluorescence decline (see e.g., Briantais *et al.* 1979, 1980; Govindjee and Spilotro 2002). This effect is very distinct for npq1 at high and low excitation light intensities (Fig. 22 and 23), but not obvious for WT and npq2. In this context one has to remember that the effect can be hidden by the heterogeneities displayed by the cell ensembles.

Methyl viologen: Methyl viologen is one of the most efficient electron acceptors of PSI (Munday and Govindjee 1969a, b). As a result it is known to lower the P-level (reduced Q_A cannot accumulate as there is no "blockage" of the electron flow) and thereby to diminish the P-to-S fluorescence decline. This effect can be observed clearly at lower excitation light intensities (Fig. 23). It is correlated with the observed shortening of τ_{mod}. At high light intensities the effect is not obvious.

Distinct general effects can be observed, if one compares all measurements. All the fluorescence lifetime transients, starting at the "P" level, of the measured immobilized ensembles show lower fluorescence amplitudes and shorter lifetimes for npq2 in comparison to WT/npq1 for all treatments and excitation light conditions.

Qualitatively for every species the fluorescence intensities seem to follow τ_{phase} (but not τ_{mod}). This raises the question whether the transient intensity curve can also be understood

quantitatively as a simple consequence of the measured lifetime changes. A discussion of this point can be found in the Appendix 5.6.

Summarizing, the results of measurements on the WT and two mutants, in conjunction with our experiments using molecular inhibitors that interfere with specific steps in the photosynthetic process, support our contention that the lower fluorescence intensity in the presence of zeaxanthin is accompanied by a shortening of the fluorescence lifetime, presumably involving a dynamic energy transfer.

Comparing the progress of the fluorescence transient in WT, npq1 and npq2 cells:

A comparison of the datasets for WT, npq1 and npq2 cells with each other reveals the following additional experimental observations, which in this case are listed only for intensity-lifetime comparisons and not for a discussion of any treatment effects (it should always kept in mind that the reported lifetime transients are single transient measurements of cell ensembles and not averages of multiple lifetime transients):

1) (Fig. 22; no treatment) shows that the lifetimes correlate with the intensity. npq1 has higher fluorescence intensity and also shows longer lifetimes τ_{phase} and τ_{mod}.

2) However in (Fig. 22; DCMU), WT and npq1 display identical intensities at the end of the measured transient, although the WT has longer τ_{phase} and τ_{mod}.

3) In (Fig. 23; DCMU), npq1 shows a higher intensity at the P-level than the WT, although the WT displays the longer lifetimes.

4) Quite substantial intensity differences between npq1 and npq2 can be obtained even when the lifetimes are similar (Fig. 23; nigericin).

5) In (Fig. 22; methyl viologen) the lifetimes of WT and npq1 are similar, the lifetime of npq1 being slightly shorter. Nevertheless npq1 displays 10% higher fluorescence intensity.

In interpreting these results we have to remember that there are more than one lifetime decay, as seen from the difference in lifetimes determined by the demodulation and phase. This is in addition a well-established fact for photosynthetic samples and is considered by all kinetic models, which describe their fluorescence characteristics (for review see Holzwarth 1991). In addition there is no guarantee that all the fluorophores (emitting species) will be in identical molecular environments in all the measurements for the different conditions and for the different types of cells. The lifetime of a fluorophore depends not only on the rates of decay along different pathways from the excited state, but also on the intrinsic radiative lifetime [compare equation (2.4)]. Both, the radiative lifetime and all other deactivation rates can be affected by strong interactions of the fluorophore with its environment. Therefore the

observed intensity differences very well can be simply the result of changes in the lifetime components and their amplitudes (as demonstrated for fluorescence lifetime transients with the global analysis given in the Appendix 5.6).
But for fluorescence transient measurements the same warnings apply in an even more severe form, as always has been emphasized (Govindjee 1995). The measured intensity is not only a function of the complex quantum yield with all its lifetime components but also of the direct absorption properties of the sample. These properties strongly change during the so called "state changes" (Allen and Forsberg 2001), during which LHC's move from the strongly fluorescent PSII region of the photosynthetic apparatus to the weakly fluorescent PSI regions. While the measured fluorescence lifetime transients still will show these absorption changes in the transient intensity, they cannot show up in the measured transient lifetimes. When comparisons between fluorescence transients are used to answer specific questions about the photosynthetic system, assumptions about comparable molecular environments always are implied. Therefore in all cases, in which the study of fluorescence transients is useful, the measurement of fluorescence lifetime transients will be advantageous.

If the assumption of similar molecular environments should allow a comparison between the different mutants under identical treatment conditions (and again, this very well might not be the case), then the differences between intensities and lifetimes as pointed out in 1)-5) above have to be understood as differences in the antenna constitution between the samples and their dynamic changes and rearrangements. If state changes (in a certain fraction of the multitude of single cells) change the absorption cross section of the cells (to a certain amount), differences in fraction and amount will necessarily heterogenise the average fluorescence intensity signals.

If one wants to compare the fluorescence lifetime transients at the two different irradiation intensities, it should be noted that the scale for the fluorescence intensity in Fig. 22 is about a factor 9 higher than in Fig. 23 (following approximately the difference in excitation intensity). At the lower intensity (Fig. 23) τ_{phase} in general is longer and τ_{mod} slightly shorter than at the higher intensity (Fig. 22). Some lifetime transients have also been measured at the very high irradiation intensity of 8600 μmol (photons) m^{-2} s^{-1} (data not shown). Both observed lifetimes were shorter than for 2750 μmol (photons) m^{-2} s^{-1}. These short lifetime values are due to photoinhibition at the very high intensities used (see 3.2.2.4.2 for a discussion of the relation of fluorescence intensity and lifetime at different excitation intensities).

3.2.2.3 Comparison of swimming and resting cells: Fluorescence changes during the state of negative geotaxis

The cells kept under motion (see Materials and methods 3.2.1.5) showed high motility. But it is known that cells left for 1-2 hr in a capillary tube in the dark reduce motility and tend to accumulate at the top of the tube, which is called negative geotaxis (Bean 1977; Fornshell 1978; Bean 1984; Harris 1989, pg. 216). Resting Chlamydomonas cells have decreased photosynthetic activity, and they loose their variable fluorescence (Govindjee and Reto Strasser, personal communication).

Provided that the sample was kept under light, cells filled in micro-capillaries (see section 3.2.1.5) did not stop their movement, even for the duration of one day. However, in darkness, after a few hours, all cells stopped swimming. They began a "shaking" movement, whereby each cell moved only slightly about its center. Some cells performed a rotation involving the movement of only one of their two flagella. About 70% of the cells showed what has been called negative geotaxis and 30% showed positive geotaxis. Eventually, after a sufficiently long time (2-5 h) in the dark, the shaking and rotating motions stopped.

Fig. 25 shows signals acquired from ensembles of WT, npq1 and npq2 in micro-capillaries. The same sample is displayed two times. First, directly after filling the cells into the capillary (swimming cells) and second after 2 h in the dark (resting cells in the state of negative geotaxis). The lifetimes of the npq2 swimming cells are 20 % shorter than the lifetimes of the WT/npq1 samples. This is in agreement with the results presented above. However, in this case an additional effect can be seen; at high concentrations of cells, which were accomplished by centrifugation, some cells form clusters. These clusters, which can be seen especially for npq1 in Fig. 25 (swimming sample), show fluorescence lifetimes that are 30 % longer than for the non-clustered swimming cells. The resting cells have reduced intensities and reduced lifetimes. In Fig. 25, the fluorescence intensity for the WT and npq1 samples are reduced, as compared to the swimming cells, by over 40%; τ_{phase} is reduced by 70% and τ_{mod} is reduced by 30 %. On the other hand, npq2 shows only a 10 % reduction in both the intensity and τ_{phase}. Interestingly, in this case npq2 has even longer lifetimes than WT/npq1.

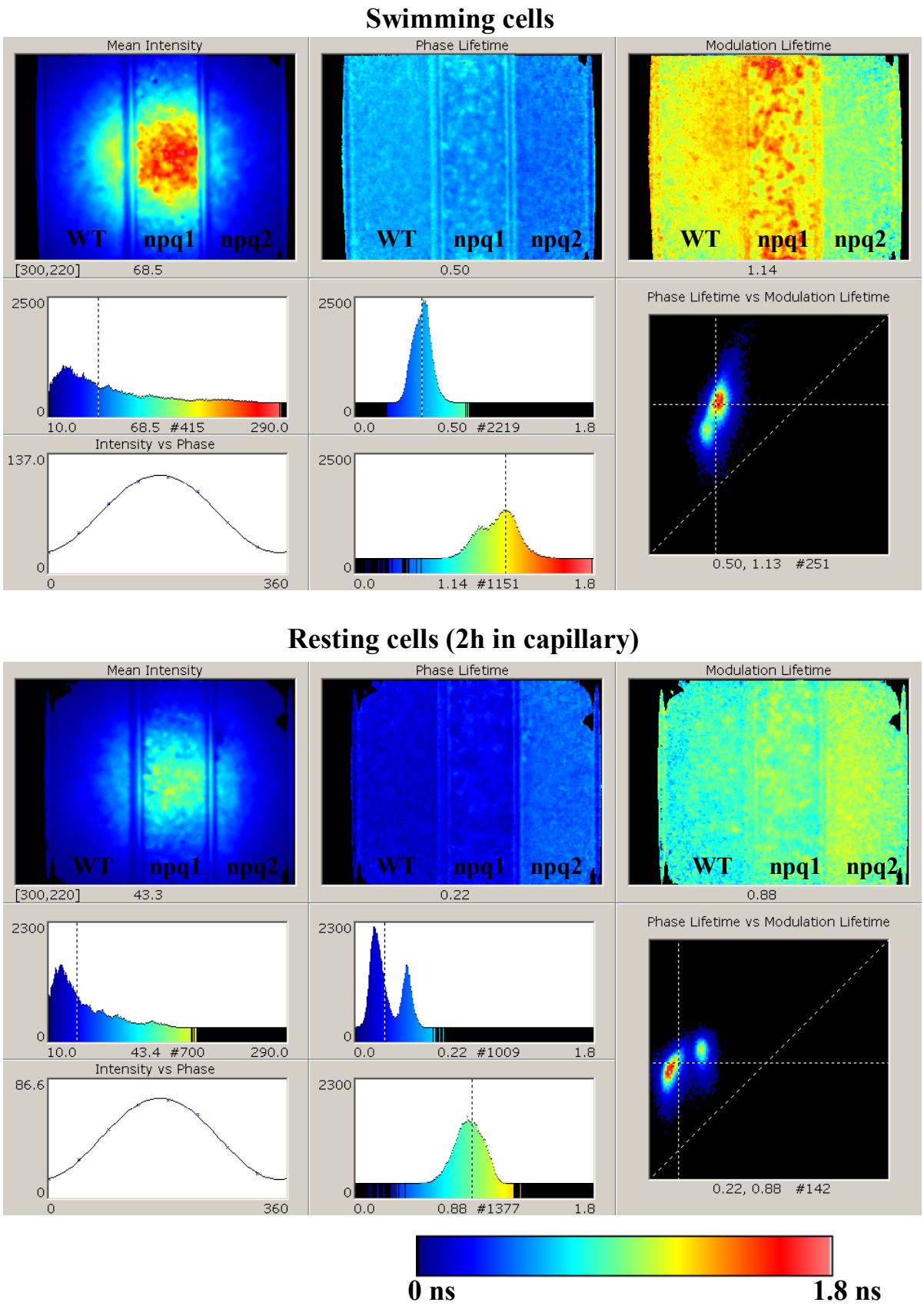

Fig. 25: Chlorophyll *a* fluorescence changes due to the state of negative geotaxis. Comparison of swimming and resting cells

Ensemble signals of cells of WT, npq1 and npq2 mutants of *Chlamydomonas reinhardtii* in micro-capillaries. First, swimming cells directly after filling the capillaries and second, the same sample after 2 h in the dark (resting cells in the state of negative geotaxis). In the resting state (geotaxis), the cells display reduced intensities and lifetimes. Irradiance, 1400 µmol (photons) m^{-2} s^{-1}.

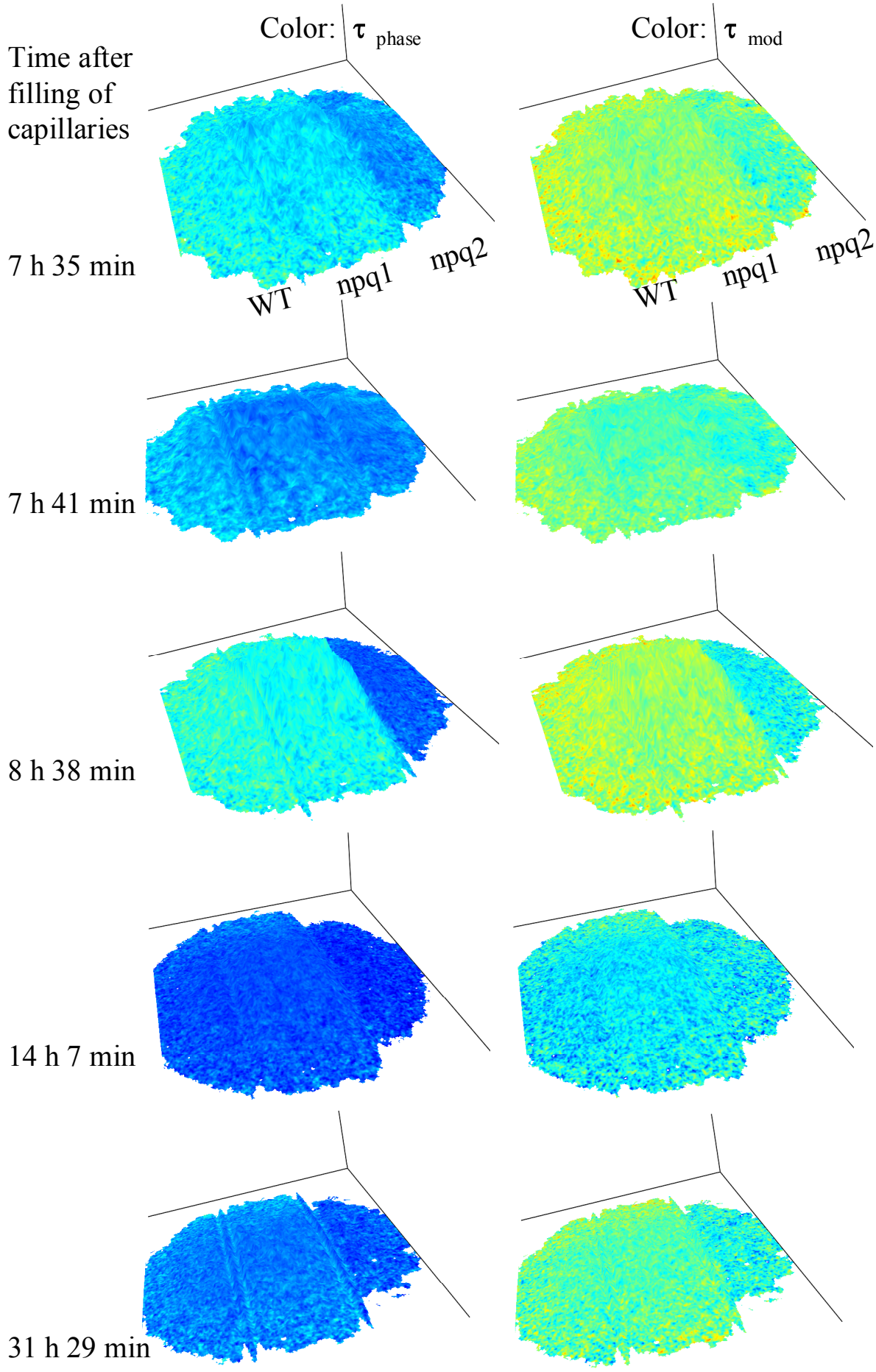
Color: τ phase
Color: τ mod
Time after filling of capillaries
7 h 35 min
7 h 41 min
8 h 38 min
14 h 7 min
31 h 29 min
WT
npq1
npq2
WT
npq1
npq2

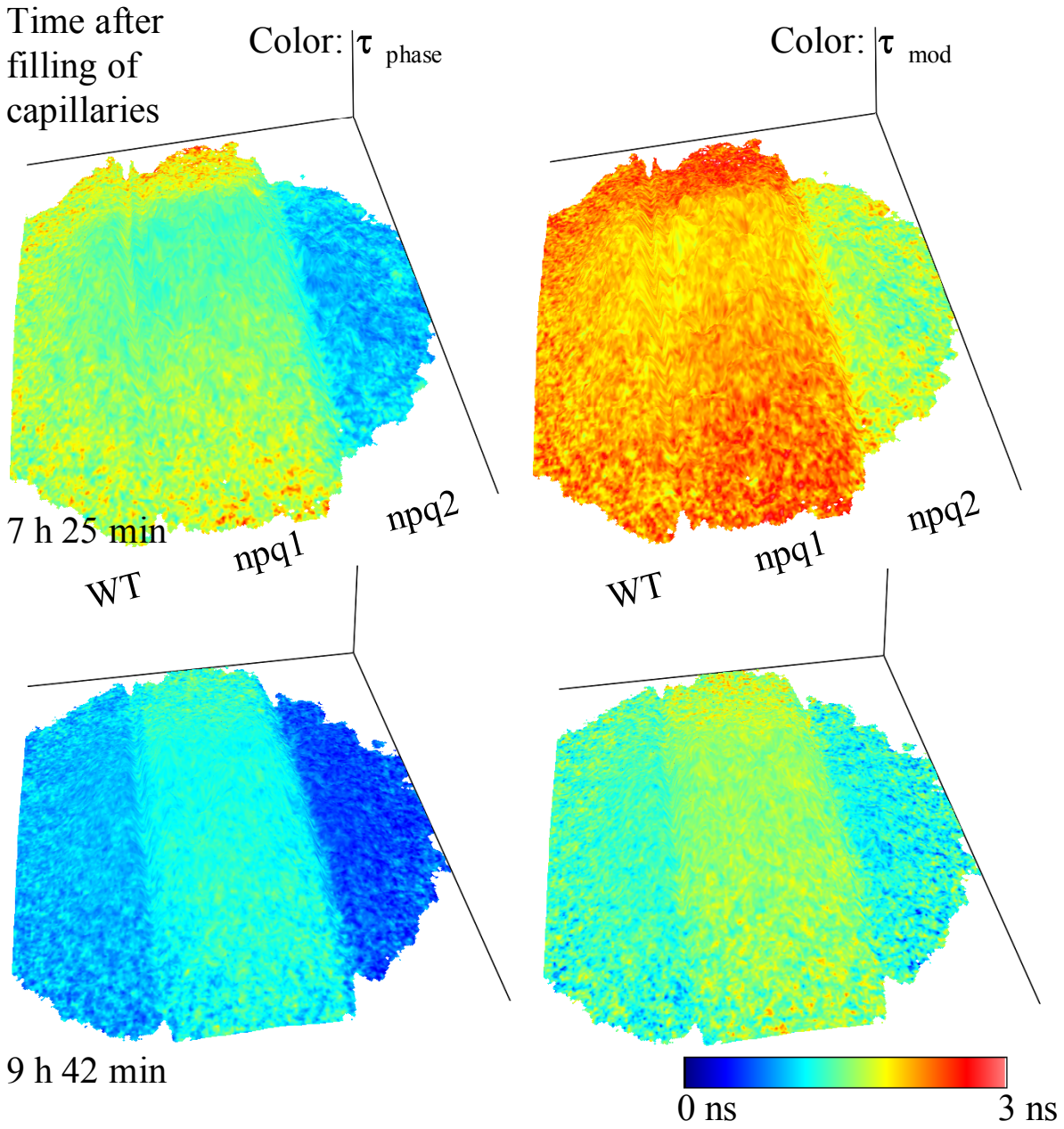

Fig. 26: Chlorophyll *a* fluorescence changes during the state of negative geotaxis
Changes of ensemble Chl *a* fluorescence signals of resting *Chlamydomonas reinhardtii* cells during the state of negative geotaxis (due to storage in the dark) are shown in two cases. In each of these cases the same sample of cells (WT, npq1 and npq2) in micro-capillaries in the dark was measured after certain time intervals (given is time after filling of cells in capillaries).
Irradiance, 2000 µmol (photons) m^{-2} s^{-1}; total irradiation time 1.2 (2.4) s; Height: relative fluorescence intensity; Color: apparent single lifetime calculated from phase or modulation.

In addition, if one observes one sample that is already in the state of geotaxis for several hours, Fig. 26 shows that large changes (up to 50 %) in intensity and lifetimes still take place. These ensemble changes are time-dependent and are different for WT and the two mutants, so that npq2 sometimes does not have the shortest lifetimes. Although, on the average, the pronounced differences between WT/npq1 and npq2 are preserved. The reasons behind these long-term changes are not yet understood.

It can be concluded that both, Chl *a* fluorescence intensity and lifetimes of *Chlamydomonas reinhardtii* also strongly depend on the physiological state of the cells, which can be observed in this case on the ensemble level.

The precise physiological state of swimming or (darkness induced) resting cells is unknown as several factors are involved (Harris 1989): (1) negative geotaxis, as noted above; (2) cell cycle[34] as regulated by biological timers (Donnan and John 1983); (3) changes in cell division; and (4) most importantly, differences in the bioenergetics, e.g., swimming cells use ATP for motion, whereas in resting state, many biochemical reactions are turned off.

3.2.2.4 Fluorescence lifetime images of single cells: Lifetime heterogeneity between and on single chloroplasts

3.2.2.4.1 The fluorescence lifetimes are usually homogeneous within each cell, but the lifetimes of individual cells can change over time.

Measurements of single cells immobilized on a thin film of agar are shown in Figs. 27 - 29.

In Fig. 27 lifetime changes of individual cells over time are compared to the multi-cellular averages. Images of Chl *a* fluorescence intensity, τ_{phase} and τ_{mod} for multiple untreated WT cells are shown for four consecutive measurements (with at least 5 minutes dark adaptation before each measurement). Three transmission images of the cells are also displayed, each image focused at different depths. These transmission images allow to identify the single chloroplast structures (each *Chlamydomonas* cell has one chloroplast) as the origin of the Chl *a* fluorescence. The lifetimes are homogenous over the single chloroplasts and identical between most chloroplasts and they do not change significantly in the four measurements. However, changes over time can be observed for some cells, for instance the two cells marked as one and two in the figure. Homogeneous over their chloroplast the lifetimes change (see figure legend for details), which pronounces these cells in the image in comparison to the multi-cellular average. The observation that the Chl *a* fluorescence of individual cells changes its lifetime homogeneously over the whole chloroplast in comparison to other chloroplasts, which do not follow such changes (as shown in Fig. 27), clearly speaks for cell internal physiological processes, which affect all PSII units of the chloroplast simultaneously.

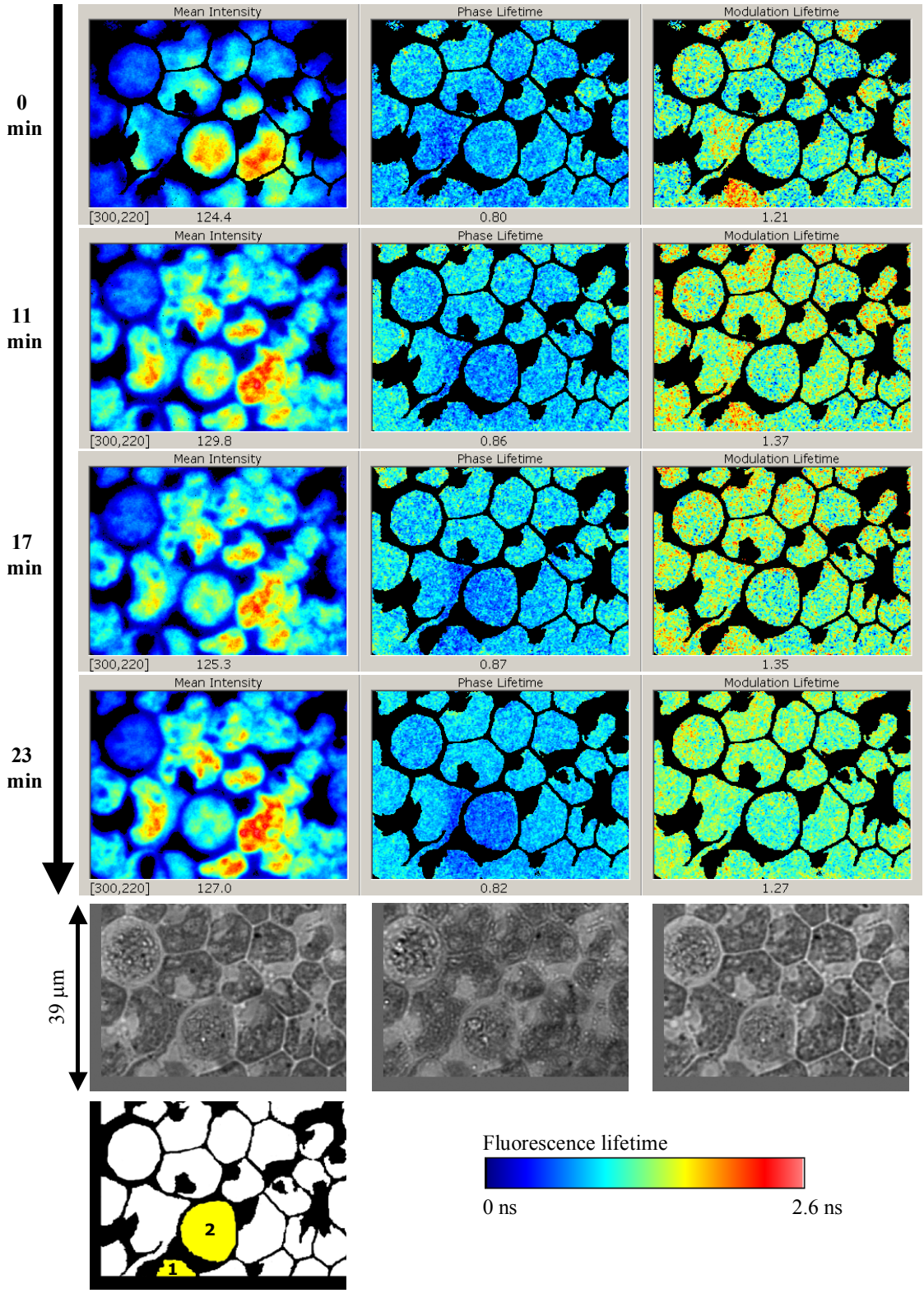

Fig. 27: Intercellular Chl *a* fluorescence lifetime heterogeneities in their kinetic development
Images of the Chl *a* fluorescence intensity, apparent single lifetimes calculated from phase τ_{phase} and modulation τ_{mod} and transmission images of multiple single cells of WT immobilized on an agar film. Two cells are marked as one and two (bottom left mask). In the first measurement the lifetimes of cell two are identical with the lifetimes of the other cells in the image. But from the first to the last measurement τ_{phase} drops from 0.75 to 0.61 ns. This lifetime difference (in comparison to the other cells) pronounces cell 2 in the image. The same effect can be observed for the τ_{phase} of cell one. But cell one shows a longer τ_{mod} of 1.77 ns in the first measurement, which changes to 1.19 ns in the last measurement and thereby becomes identical with most other cells in the image. Irradiance, 2800 µmol (photons) m^{-2} s^{-1}; total irradiation time 1.04 (last row 2.1) s.

3.2.2.4.2 Fluorescence lifetime measurements are often not correlated with the fluorescence intensity

A change in fluorescence intensity in an image can be due either to a change in the number of fluorophores or to a change in the quantum yield of each fluorophore. Even if the number of molecules remains constant in the sample, the number of fluorophores with a certain quantum yield can decrease during "state changes" (Allen and Forsberg 2001), as mobile antenna move from fluorescent PSII to weakly fluorescence PSI. This affects the measured fluorescence intensity, without changing the quantum yield of the remaining fluorophores. On the contrary, the measured intensity can also change due to a change in the quantum yield of the individual fluorophores. The quantum yield decreases if the rate of non-radiative transitions from the excited state increases. This dynamic effect leads to a decrease in the fluorescence lifetime concomitant with a decrease in the fluorescence intensity. By measuring the lifetime we can determine whether such a dynamic effect contributes to observed intensity changes. In addition, the lifetime is also independent of the concentration of the fluorophore. Thus fluorescence lifetimes help us distinguish whether intensity variations are due to concentration or quantum yield changes (unless physical or chemical reactions are coupled to concentration variations). This is especially important in the fluorescence images of photosynthetic biological cells. Due to large variable concentrations of Chl in different cells, the lifetime differences are often not correlated with fluorescence intensities. Some cells with shorter lifetimes have greater intensities than cells with lower intensities (compare cell two with the other cells in Fig. 27). Because we cannot control the Chl concentrations in the cells, the intensity differences between cells are impossible to interpret unless the lifetimes are measured.

Of course, the illumination profile of the excitation light (see Materials and methods 3.2.1.4) effects the intensity distribution of the fluorescence in the image, too. The irradiation variations in the image are dependent on the zoom optics used in the microscope. In Fig. 27 the excitation intensity is 2800 μmol photons m^{-2} s^{-1} in the middle of the image, but at the left and right side the intensity is 60 % of this value. Nevertheless the lifetimes are not effected by this inhomogeneous illumination in the case shown. This is also true for the average of cells shown in Fig. 21. In general lifetime measurements are not dependent on the excitation intensity, because different excitation intensities do not change the deactivation rate constants for most fluorophores. However for photosynthetic samples the excitation intensity is convoluted with the rates of photosynthetic reactions and other physiological processes. Because these physiological changes depend on the level of the irradiation, it is essential that

the illumination intensity be carefully monitored so that different samples can be compared. If the inhomogeneous illumination includes the resulting fluorescence intensity region from F_o to F_{max} level, it will clearly have an effect on the measured lifetimes: For example longer lifetimes have been reported for higher excitation intensities by Briantais *et al.* (1972). They attributed this to a higher fraction of closed reaction centers, which reduces the rate constant of photochemistry. Of course, the fluorescence lifetimes and intensities are not necessarily correlated in a simple way; increased excitation light can increase the fluorescence intensity simply because more fluorophores become excited per unit time. This would not necessarily change the lifetimes (indeed, this is one of the major reasons for making lifetime determinations).

At very high light intensities approaching sunlight (2000 µmol photons m^{-2} s^{-1}), however, photoinhibition sets in, and thus, the quantum yield of fluorescence is expected to decrease. Indeed, we observe a shortening of the lifetimes with increasing irradiation intensities as can be seen in some of the irradiation profiles of Fig. 26 and as it has been mentioned for the fluorescence lifetime transients above. This trend (shortening of lifetimes upon increasing the excitation intensity to that in sunlight) has also been seen in measurements with single cells (see Fig. 28) comparing different excitation intensities. The shortened lifetime values are due to photoinhibition at the very high intensities used. A shortening of the lifetimes with increasing irradiation intensities might be understood as an increase in the rate constant of the quenching at closed reaction centers.

Also the independence of the lifetimes from the fluorescence intensities seen in Figs. 21 and 27 presumably results because the reaction centers are already closed, indicating that the measurements are done in a regime that is already dominated by quenching. Here, increased excitation light will cause increased fluorescence intensity, but not increased lifetimes.

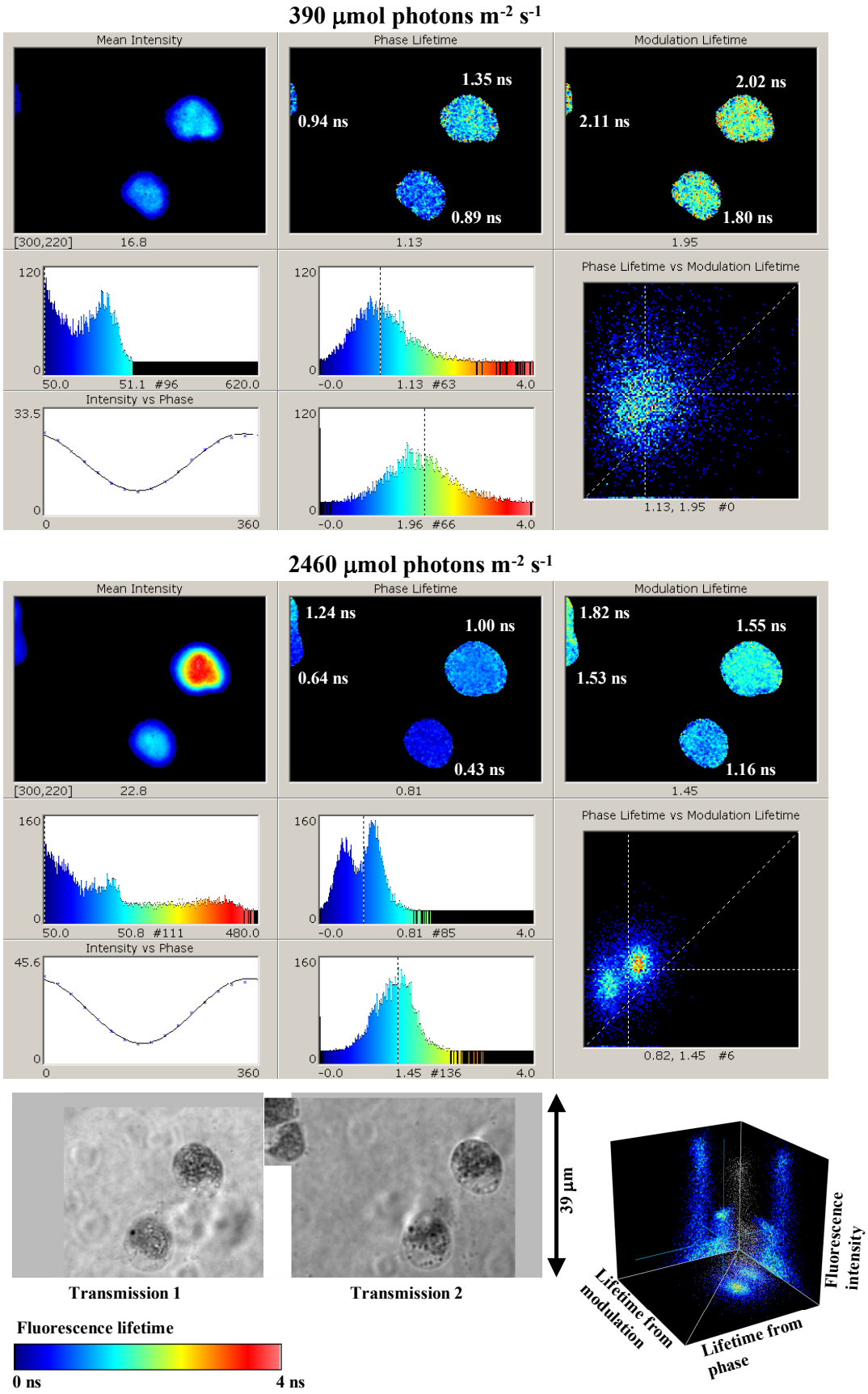

Fig. 28: Intercellular lifetime heterogeneities measured at two different intensities of excitation
Lifetime of Chl *a* fluorescence in single cells of *Chlamydomonas reinhardtii* measured at two different intensities of excitation (390 and 2460 µmol (photons) m^{-2} s^{-1}) displaying shorter lifetimes at the higher excitation intensity. WT cells on agar film; total irradiation time 1.96 s (at the P-level).

3.2.2.4.3 Heterogeneities of fluorescence lifetimes between and within individual cells

Multiple lifetimes are indicated in all our measurements because the demodulation lifetimes are longer than the phase lifetimes. If the fluorescence is averaged over an entire cell, the signal contains contributions from several fluorescence lifetime components if they are present. Averaging pixel readings in an image is similar to making ensemble measurements on cell suspensions in a cuvette. Similarly, if the spatial distributions of heterogeneous lifetimes are below the spatial resolution of the image, the fluorescence signal from the separate pixels would also consist of multiple lifetime components.

An example of multiple lifetime distributions within single cells is shown in Fig. 29, where four untreated cells of npq1 are shown that have been immobilized on agar film. One of the cells is dividing and therefore has two chloroplasts. One of these two chloroplasts shows lifetimes similar to the other three cells (τ_{phase} = 0.96 ns; τ_{mod} = 1.45 ns). But for the second chloroplast the lifetimes of phase and modulation are 26 % shorter (at the right side of the cell τ_{phase} is even 55 % shorter). These differences are well outside of the measurement error.
Differences can sometimes be observed even within single chloroplasts. The τ_{mod} image of the first chloroplast of the dividing cell shows localized spots (diameter 0.5 - 1 μm) of long lifetime about 2.2 ns. Similar locations are also visible on the other three cells, but too close in these cases to the resolution limit given by the chloroplast lifetime distribution to be considered as resolved. We have not been able to relate all of these lifetime inhomogeneities to perceptible chloroplast structures. Although intracellular lifetime heterogeneities were evident in some measurements, a homogenous lifetime distribution over the chloroplast was observed in most cases.

The reasons for these observed heterogeneous lifetimes are not yet known. The lifetime is dependent on processes in the antenna and on the trapping at reaction centers. Therefore multiphasic kinetics are expected for chloroplasts. Only for individual light-harvesting complexes LH-2 (isolated antenna systems without the reaction centers) from anoxygenic photosynthetic purple bacteria the fluorescence lifetimes have been reported to be initially homogeneous and monoexponential. The lifetime spectrum changes only after some time of illumination (Bopp *et al.* 1997). For LHCII biphasic decay kinetics are observed while for aggregated LHCII a three-exponential decay has been reported (Vasil'ev *et al.* 1997). The situation becomes even more complicated with chloroplasts or with systems with many complexes and quenching centers.

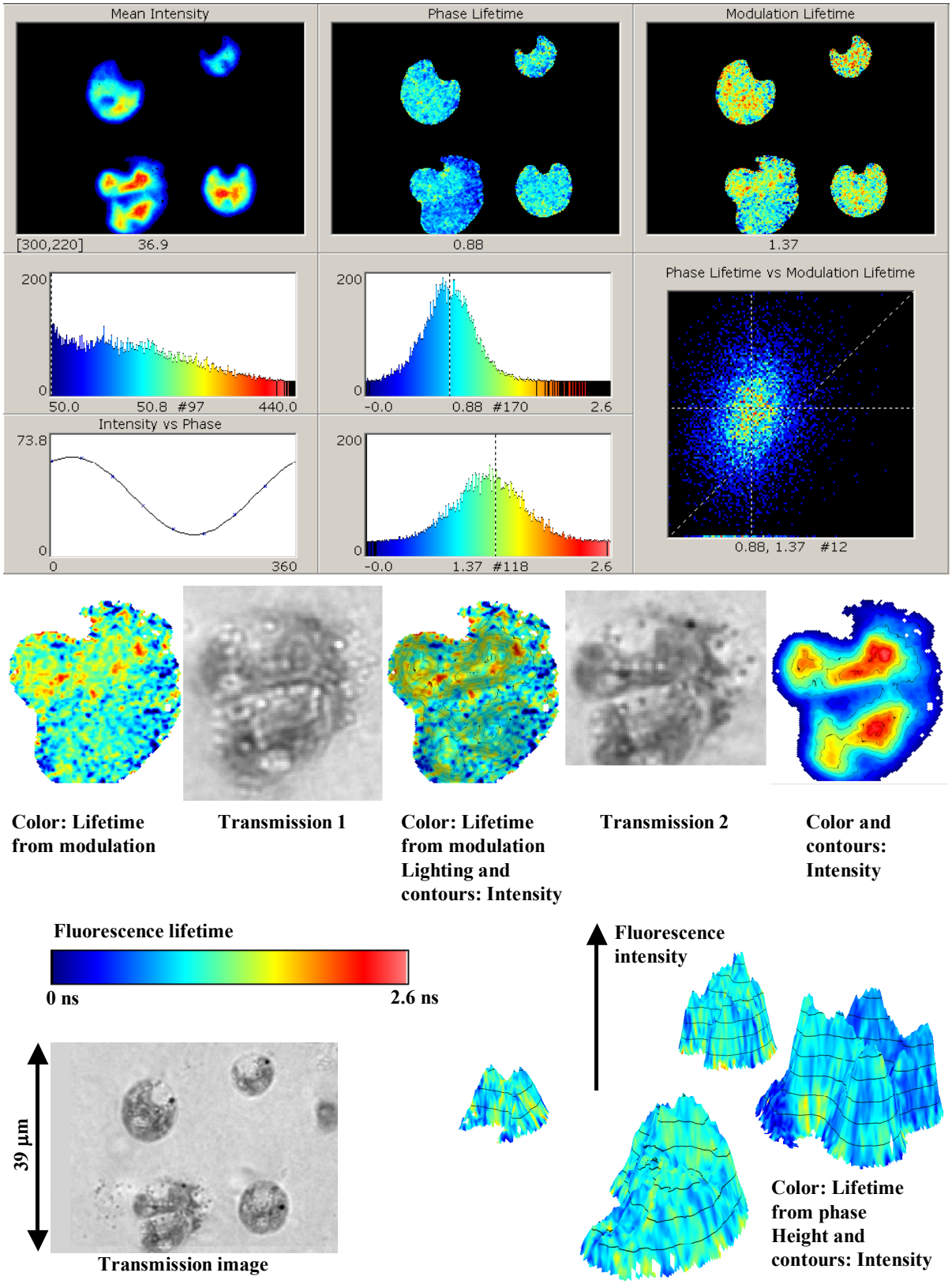

Fig. 29: Inter- and intracellular lifetime heterogeneities of single alga cells
Chlorophyll *a* fluorescence of four cells of the npq1 mutant of *Chlamydomonas reinhardtii* immobilized on agar film. Shown are intensity-, τ_{phase}- and τ_{mod}-images with histograms for each image; transmission image; plot of average intensity of every incrementally phase delayed image against phase; two-dimensional histogram of τ_{mod} against τ_{phase} for all pixels in the image and different displays.
Irradiance, 2200 µmol (photons) m^{-2} s^{-1}; total irradiation time 1.04 s (at P-level).

Different pigment-protein complexes can lead to lifetime heterogeneities. Roelofs *et al.* (1992) attributed multi-exponential fluorescence decay of PSII membranes to the presence of different (α and β) reaction centers. The lifetimes could also depend on the area over which the excitation energy migrates during the lifetime of the excitation (producing a diffusing excitation domain – i.e. an exiton) as well as a distribution of different concentrations of the quenchers in this area. Such structural heterogeneities can give rise to lifetime heterogeneities provided that one has the necessary spatial resolution to observe these differences. Barzda *et al.* (2001) resolved lifetime heterogeneities within single aggregates of LHCII using FLIM. They applied a lattice model to explain the inhomogeneities. According to this model, the measured lifetimes are a result of kinetic competition between migration and trapping times. Therefore the measured lifetimes depend very strongly on the number of chromophores constituting the lattice and the number of traps in the domain. Both these populations vary in the concentration of the aggregates. They concluded that all macroscopic measurements average out such lifetime differences. Our data supports this notion, but on different levels. The extent to which this can be observed depends on the spatial extent of the inhomogeneities compared to the imaging resolution. A PSII particle is about 190 Å wide (Zouni *et al.* 2001) and the packing of photosystems in the thylakoid membranes is in the order of several thousand/μm^2 (Olive *et al.* 1981; Harris 1989). The signal of each pixel in Fig. 29 corresponds approximately to 0.032 μm^2. Therefore, this area would correspond to an average of over 100 particles (not considering the fact that the measurement is not confocal). This makes it understandable why in most imaging experiments, homogenous lifetimes are observed throughout the chloroplast. The grid of inhomogeneities leading to different lifetimes is usually too fine to be observed with optical resolution.

The clear lifetime differences between single chloroplasts and their changes seem to have a strong physiological connection. Macroscopic lifetime measurements of living cells therefore average over (1) a general lifetime influenced (a) directly by the external conditions as light, temperature, growth media…and (b) by the overall physiological state of the cells, which at least partially is the result of the external conditions (2) cells in special states or formations (like the observed differences in the lifetime of cell clusters or dividing cells) (3) lifetime differences between single chloroplasts, which might be the result of a certain distribution of the physiological state for each single cell (4) lifetime differences on single chloroplasts and probably (not measured in this work) (5) lifetime differences between single PSII units and perhaps even (indicated by the results cited before) (6) lifetime differences on single PSII units.

3.2.3 Concluding remarks

The model for energy-dependent Chl *a* fluorescence quenching (qE; an important form of non-photochemical quenching), which allows to monitor photoprotection during photosynthesis, can be summarized as follows (see introduction given in section 2.2; especially the model given in Fig. 11):

Under intense irradiation that exceeds a plant's capacity for CO_2 fixation, lumen acidification leads to the enzymatic conversion of violaxanthin to zeaxanthin *via* antheraxanthin (xanthophyll cycle). In addition, the buildup of the thylakoid ΔpH leads to protonation of and conformational changes in the LHCIIs, which might favor the binding of zeaxanthin. The combination of these two events leads to a quenched state of PSII with lowered Chl fluorescence intensity and lifetime, during which potentially harmful energy is dissipated as heat.

Another form of non-photochemical quenching is state-transition quenching (qT), during which LHC's move from the strongly fluorescent PSII region of the photosynthetic apparatus to the weakly fluorescent PSI regions. These and other changes in the absorption cross-section of the PSII antenna cannot be distinguished from true differences in the lifetime of fluorescence when only fluorescence intensities are compared.

Therefore the lifetime differences in the Chl *a* fluorescence between WT and xanthophyll-cycle mutants npq1 and npq2 of *Chlamydomonas reinhardtii* have been investigated in this work using the constructed instrument for rapid fluorescence lifetime-resolved imaging.

The violaxanthin-accumulating mutant npq1 shows similar fluorescence intensities and lifetimes as the WT, whereas the zeaxanthin accumulating mutant npq2 displays a reduced fluorescence intensity and shorter phase and modulation lifetimes. This lifetime difference between the mutants was also observed for cells treated with the electron transfer inhibitor DCMU, the protonophore nigericin and the PSI-electron-acceptor methyl viologen. These results show that the reduced fluorescence intensities in the npq2 mutant are not exclusively a result of simple static quenching of the zeaxanthin that is accumulated in this mutant. It can be concluded that dynamic quenching, possibly brought about by Förster energy transfer, is important. Additional two-component analysis of possible lifetime compositions shows that the reduction of the fluorescence intensity can be interpreted as increase in the fraction of a short lifetime component (see Appendix 5.5 and 5.6). The strong fluorescence quenching of npq2 agrees with the known involvement of zeaxanthin in non-photochemical quenching as stated above.

It is of significance that the lifetime of fluorescence of the npq2 mutant is much shorter than that of theWT/npq1 mutant even in the presence of DCMU. That means, a quenching process persists, even at blocked electron transfer. In this case one does not expect proton accumulation in the lumen, which activates the xanthophyll cycle conversion. Possible explanations are, that a cyclic reaction around PS1 accumulates protons or that zeaxanthin may also be quenching by a process that is independent of the normal xanthophyll cycle.

The shorter fluorescence lifetime of the npq2 mutant even when the proton gradient is decreased by nigericin, especially supports the second implication that the quenching includes contributions from non-qE related processes that involve zeaxanthin.

The similar lifetimes of the violaxanthin-accumulating mutant npq1 and the WT support the assumption that other carotenoids might compensate for the missing zeaxanthin in npq1 to reach a level of quenching, which is comparable to the WT.

In this work, we have introduced the measurement of Fluorescence Lifetime Transients, which provide additional information for the interpretation of transients, due to their independence on changing absorption properties of the sample. The Fluorescence Lifetime Transients shows that the P-to-S decay in the fluorescence transient of *Chlamydomonas reinhardtii* is not solely due to state changes (change in absorption cross section of PSII) but also due to true changes in the quantum yield of fluorescence (see also Briantais *et al.* 1972).

In addition to evidence for dynamic quenching of the Chl *a* fluorescence by zeaxanthin, we have also observed lifetime heterogeneities in the algae on the ensemble and single cell level by using our fast fluorescence lifetime imaging capabilities. Lifetime changes over periods of time have also been observed. Cells, which stopped swimming and are in the state of negative geotaxis induced by darkness for some hours, show drastically shortened lifetimes. Individual chloroplasts mostly show homogeneous lifetimes, but in some cases also heterogeneities within single chloroplasts have been observed. Although many chloroplasts display similar lifetimes, differences in the lifetimes between single chloroplasts are always detectable. These heterogeneities in lifetimes are not correlated with the fluorescence intensity. The total intensity is related to the total Chl contents in the cells.

It is striking that the Chl fluorescence characteristics are influenced strongly by physiological processes on the single-cell level, which affect all PSII units of the chloroplast simultaneously. The physiological effects have been found to manifest itself also on the ensemble level, where an average signal from many cells is observed. This can lead to complexities in interpreting ensemble experiments.

4 Summary

Fluorescence lifetimes provide valuable information that is not available from steady state fluorescence. However, due to the complexity of the required acquisition hardware, analysis and visualization, fluorescence lifetime imaging has not yet attained the rapid and continuous operation required by many biological applications.

The achievements of this work are twofold:

1) An instrument was designed and constructed for fast Fluorescence Lifetime-resolved Imaging (FLI) – it can provide fluorescence lifetime images at video-rate.

2) The rapid image acquisition capabilities afforded by the new instrument were used to answer important questions concerning the photoprotection mechanisms of photosynthetic samples.

The first of its kind, the FLI instrument described in this work enables continuous image acquisition with concurrent data analysis and visualization of fluorescence lifetime images at video-rate. Sustained rates of up to 26 fluorescence lifetime images per second can be obtained for images of 320 x 220 pixels. This was achieved by a combination of new and conceptually different hardware and software design, which integrates modern opto-electronic components and custom built software for personal computers.

The instrument is based on the principle of the phase and modulation method in homodyne operation mode: In a fluorescent sample, high frequency modulated light excites an emission signal that is modulated at the same frequency, but that exhibits a lifetime dependent phase shift and demodulation. Using a modulatable image intensifier, it is possible to detect both measurement parameters with a fast charge-coupled device (CCD)-camera. Excitation and detection optics can be variable adapted to the samples under investigation. For the most part, an inverted microscope or an upright microscopic stage-scanning setup with long working-distance objectives were used.

In this frequency domain instrument, LASER light provides full field sample illumination, which is high frequency modulated by an acousto-optical modulator. The high frequency modulation at the detecting image intensifier is under rapid phase control due to the fast phase shift abilities of implemented digitally controlled delay-line phase shifters. Intensity images are acquired at different phase settings and analyzed for their fluorescence lifetime properties at each pixel.

The inexpensive computational power of PC-based systems with their powerful graphics handling and display capabilities was harnessed by custom designed C++ and LabVIEW-based control programs. This combination allows to accelerate the instrument to its hardware dictated limitations.

The software has been designed and implemented for instrumentation control, image acquisition and analysis, and data visualization. Pixel by pixel lifetime determination via fundamental Fourier component analysis, a method previously reserved for high precision measurements, could be facilitated for the rapid measurements. This method of analysis was accomplished at video rate concurrent with data acquisition by reusing and reanalyzing the previously acquired two (or more) intensity images at different phase settings with every new incoming image.

Among other features, the software for continuous fluorescence lifetime imaging includes user interactivity: the user can control various software functions during run-time with a minimum latency feedback and data visualization, (for example, with multi-textured shaded surface renderings that provide a highly integrated view of the multi-parameter image data).

Under intense irradiation, plants and photosynthetic algae activate photoprotection mechanisms to thermally dissipate potentially harmful energy that exceeds their photosynthetic capacity. Photoprotection of this kind can be monitored by non-photochemical quenching (npq) of the chlorophyll (Chl) *a* fluorescence produced in photosystem II. The so-called xanthophyll-cycle is known to be involved in photoprotection by conversion of violaxanthin to zeaxanthin under intense irradiation.

The new capabilities for rapid fluorescence lifetime-resolved imaging microscopy were used to investigate differences between the Chl *a* fluorescence of wild type (WT) and xanthophyll-cycle npq mutants, npq1 and npq2 of the photosynthetic alga *Chlamydomonas reinhardtii*.

When photosynthetic samples are brought from darkness to constant irradiation, fluorescence intensity undergoes large changes with time. Rapid measurements are necessary to determine the fluorescence lifetimes during this so-called Chl *a* fluorescence transient (induction). Lifetime measurements have been carried out at maximum (P level) fluorescence and during the following transient decay into a steady state (S, quasi-steady state or T, terminal steady state).

WT and the mutant npq1, (which accumulates violaxanthin), show similar fluorescence intensities and lifetimes while the npq2 mutant, (which accumulates zeaxanthin), displays

reduced fluorescence intensity, (about 25-35% at P-level), compared to WT/npq1 cells. This reduction in fluorescence intensity is correlated with 20-30% shorter apparent single lifetimes from phase and modulation. Additional two-component analysis of possible lifetime compositions shows that the reduction of the fluorescence intensity can be interpreted as increase in the fraction of a short lifetime component.

These results support the important function of zeaxanthin in the photoprotection mechanism of photosynthetic samples.

Similar reductions at P-level and P-to-S decay in fluorescence intensities and lifetimes for the npq2 mutant compared to WT/npq1 are also found for cells that were treated with the electron inhibitor DCMU (3-(3,4-dichlorophenyl)-1,1-dimethylurea), the protonophore nigericin and the efficient PSI electron acceptor methyl viologen. These results might imply that the quenching process includes contributions from additional processes not dependent on the npq mechanisms.

We present the first fluorescence lifetime transients: the simultaneous measurements of transient changes of fluorescence intensity and lifetime during the fluorescence induction for the WT as well as for the mutants. The fluorescence lifetime transients provide additional information for interpreting the transient phase. They clearly show that the P-to-S decay in the fluorescence transient of *Chlamydomonas reinhardtii* is not solely due to state changes, (change in absorption cross section of PSII), but also due to true changes in the quantum yield of fluorescence. A special nonlinear least squares curve-fitting procedure allows the comparison of possible lifetime compositions during the transient under certain assumptions.

Lifetime heterogeneities were observed in ensemble experiments (averaged over multiple cells) as well as at the single cell level. Cells in the state of negative geotaxis, (induced by several hours of darkness), show shortened lifetimes.

Zusammenfassung:

Bildgebende Messung von Fluoreszenzlebensdauern im Phasenbereich mit Video-Rate – eine neue Technik in der Photosynthese Forschung.

Fluoreszenzlebensdauern, also die Lebensdauern von molekularen Anregungszuständen, die unter Aussendung von Fluoreszenz in ihren Grundzustand zurückkehren, können wertvolle Informationen über die Umgebung der Fluorophore, die Freiheitsgrade ihrer Bewegungen und über Geometrie und Dynamik der angeregten Zustände liefern. Fluorezenzlebensdauermessungen ermöglichen somit den Zugang zu quantitativen Informationen, die nicht mittels Steady-state Techniken zugänglich sind und die besonders im Falle bildgebender Messungen häufig erst Quantifizierungen ermöglichen.

Allerdings haben bildgebende Messungen von Fluoreszenzlebensdauern aufgrund der Komplexität der erforderlichen Instrumentierung für die Datenaufnahme, Analyse und Visualizierung noch nicht den erforderlichen schnellen und kontinuierlichen Betrieb erreicht, der für eine Vielzahl von biologischen Anwendungen erforderlich ist.

Die Ziele, die im Rahmen dieser Arbeit verfolgt und erreicht wurden, sind:

1) Entwicklung und Aufbau einer Apparatur zur bildgebenden Messung von Fluoreszenzlebensdauern (FLI: Fluorescence Lifetime Imaging), die Bilder von Fluoreszenzlebendauern mit Video-Rate liefert.

2) Anwendung der schnellen Meßmöglichkeiten des neuen Gerätes auf die Untersuchung von Photosynthese betreibenden Proben, um Antworten auf wichtige Fragen bezüglich der Photoschutzmechanismen während der Photosynthese zu erhalten.

Die im Rahmen dieser Arbeit entwickelte Apparatur stellt die erste betriebene Anlage zur Aufnahme, Berechnung und Visualisierung von Fluoreszenzlebensdauerbildern mit Video-Rate dar. Bildwiederholraten von 26 Lebensdauerbildern pro Sekunde für Bilder mit 320 x 220 Pixeln wurden erreicht. Dies konnte durch eine konzeptionell neue Kombination von instrumentellen Systemkomponenten, die neuste optoelektronische Elemente enthalten, und speziell entwickelten Programmen für Personal Computer erreicht werden.

Die Apparatur beruht auf dem Prinzip der Phasen-und-Modulationsmethode im Homodyn-Modus: Hochfrequent moduliertes Anregungslicht löst in einer fluoreszierenden Probe ein mit der gleichen Frequenz moduliertes Emissionssignal aus, das gegenüber der Anregung eine lebensdauerbedingte Phasenverschiebung und Demodulation aufweist. Mit Hilfe eines modulierbaren Bildverstärkers werden diese beiden Meßgrößen der Detektion durch eine

schnelle CCD-Kamera zugänglich gemacht. Die Anregungs- und Detektionsoptik kann je nach Aufgabenstellung variabel an die zu untersuchende Probe angepaßt werden. In den meisten Fällen wurde ein invertiertes Mikroskop oder eine aufrechte mikroskopische Vergrößerungsoptik mit xy-Tisch und Objektiven mit großem Arbeitsabstand benutzt.

Das gesamte Beobachtungfeld der fluoreszierenden Probe wird von einem Laser ausgeleuchtet, dessen Licht von einem akusto-optischen Modulator mit hoher Frequenz moduliert wird. Die hochfrequente Modulation am detektierenden Bildverstärker ist unter schneller Phasenkontrolle durch eingebaute digital gesteuerte Phasenschieber. Fluoreszenzintensitätsbilder werden bei unterschiedlichen Phasenverschiebungen aufgenommen und auf ihre Fluorezenzlebensdauern in jedem Pixel untersucht. Die preisgünstige Rechenleistung moderner Personal Computer Systeme mit ihren beschleunigten dreidimensionalen Grafikfunktionen und Unterstützung für zwei Prozessoren wurde mittels speziell für die Aufgabenstellung entwickelter Computerprogramme ausgenutzt. Diese Kombination erlaubt den Betrieb der Apparatur an dem Geschwindigkeitslimit, das durch die elektronischen Komponenten vorgegeben wird.

Die Programme wurden für Instrumentkontrolle, Bildaufnahme und Analyse und Datenvisualisierung entwickelt. Pixel für Pixel Lebensdauerbestimmung mittels der Bestimmung der fundamentalen Fourier-Komponenten – eine Methode die zuvor nur für zeitaufwendige Präzisionsmessungen verwendet wurde – konnte für die Analyse von schnellen Messungen zugänglich gemacht werden. Diese Analyse konnte mit Video-Rate betrieben und gleichzeitig während der Datenaufnahme durchgeführt werden, indem die zuvor aufgenommen und für die vorhergehende Analyse verwendeten zwei (oder mehr) Intensitätsbilder an unterschiedlichen Phaseneinstellungen in der Analyse für jedes neu aufgenommene Intensitätsbild wiederverwendet wurden.

Das Computerprogramm fuer kontinuierliche bildgebende Messungen von Fluoreszenzlebensdauern unterstützt neben einer Vielzahl von Funktionen interaktive Nutzerhandhabung: Der Benutzer kann mit minimaler Verzögerung Programmfunktionen kontrollieren während kontinuierlicher Datenaufnahme und Visualisierung (z. B. mit multi-texturierten beleuchteten Reliefdarstellungen, die eine sehr kompakte Darstellung von mehreren unterschiedlichen Bildparametern ermöglicht).

Pflanzen und Photosynthese betreibende Algen aktivieren Photoschutz-Mechanismen, wenn sie intensiver Bestrahlung ausgesetzt werden, um die potentiell schädliche absorbierte Überschußenergie, die nicht mehr für die Phototosynthese verwendet werden kann, als Wärme zu dissipieren. Photoschutz dieser Art kann mittels Nicht-photochemischer Löschung (npq: non-photochemical quenching) der Chlorophyll (Chl) *a* Fluoreszenz von Photosystem (PS) II verfolgt werden. Es ist bekannt, dass der sogenannte Xanthophyll-Zyklus durch Umwandlung von Violaxanthin in Zeaxanthin unter Starklicht eine Rolle in dem Photoschutz-Mechanismus spielt.

Die neuen Möglichkeiten für schnelle bildgebende Messungen von Fluoreszenzlebensdauern wurden genutzt, um Unterschiede zwischen der Chl *a* Fluoreszenz von dem Wildtyp (WT) und den Xanthophyll-Zyklus-Mutanten, npq1 und npq2 der photosynthetischen Alge *Chlamydomonas reinhardtii* zu untersuchen.

Wenn Photosynthese betreibende Proben nach Dunkelheit einer konstanten Bestrahlung ausgesetzt werden, dann ändert sich ihre Fluoreszenzintensität stark mit der Zeit. Schnelle Messungen sind notwendig, um die Fluoreszenzlebensdauer während dieses sogenannten Chl *a* Fluoreszenz-Transienten (Induktion) zu bestimmen. Fluoreszenzmessungen wurden bei maximaler Fluoreszenz (P-Level) und während des nachfolgenden Abfalls in einen Steady-State-Zustand (S, Quasi-Steady State oder T, Terminaler Steady-State) durchgeführt.

Der WT und die Mutante npq1, die Violaxanthin akkumuliert, weisen ähnliche Fluoreszenzintensitäten und Lebensdauern auf, während die npq2 Mutante, die Zeaxanthin akkumuliert, im Vergleich zu WT/npq1 eine deutlich reduzierte Fluoreszenzintensität aufweist (etwa 25-35% am P-Level). Diese Reduktion in der Fluoreszenzintensität ist mit 20-30% kürzeren Fluoreszenzlebensdauern von Phase und Modulation (den „scheinbaren“ Fluoreszenzlebensdauern, berechnet für eine einzelne Lebensdauerkomponente) verbunden. Eine zusätzliche Analyse von möglichen Lebensdauerkompositionen für ein System mit zwei Lebensdauerkomponenten zeigt, daß die geringere Fluoreszenzintensität durch Zunahme in der Fraktion einer kurzen Lebensdauerkomponente verstanden werden kann.

Diese Ergebnisse sind im Einklang mit einer Vielzahl von Messungen, die zeigen, daß Zeaxanthin im Photoschutzmechanismus während der Photosynthese eine wichtige Rolle zukommt.

Auch Zellen die mit dem Elektroneninhibitor DCMU (3-(3,4-dichlorophenyl)-1,1-dimethylurea), dem Protonophor Nigericin und dem effizienten PSI Elektronenakzeptor Metyl Viologen behandelt wurden, wiesen ähnlich reduzierte Fluoreszenzintensität und Lebensdauern fuer die npq2 Mutante (im Vergleich zu WT/npq1) auf. Diese Ergebnisse könnten darauf hindeuten, dass zusätzliche, von dem gewöhnlichen npq Mechanismus unabhängige, Prozesse an dem Fluoreszenzlöschvorgang beteiligt sind.

Die ersten Fluorezenzlebensdauer-Transienten konnten gemessen werden: während in einer gewöhnlichen Fluoreszenz Transienten Messung nur die Fluoreszenzintensität aufgenommen wird, konnten Intensität und Lebensdauern während des Verlaufs der Fluoreszenzinduktion für den WT und die Mutanten gemessen werden. Fluorezenzlebensdauer-Transienten liefern zusätzliche Informationen für die Interpretation und den Vergleich von Transientenverläufen. Sie zeigen deutlich, daß der Abklingungsverlauf der Transienten von P zu S von *Chlamydomonas reinhardtii* nicht allein auf sogenannte „State-Changes“ – Veränderungen in dem Absorptionsquerschnitt von PSII – zurückzuführen ist, sondern daß er auch mit wirklichen Veränderungen der Fluoreszenzquantenausbeute verbunden ist. Eine speziell entwickelte Marquardt-Fitprozedur für einen globalen Transientenfit erlaubt (unter bestimmten Annahmen) den Vergleich möglicher Lebensdauerkompositionen in ihrer Veränderung über den Transienten.

Lebensdauer-Heterogenitäten konnten sowohl in Ensemble-Messungen (gemittelt über eine Vielzahl von Zellen) als auch auf der Ebene von einzelnen Zellen festgestellt werden. Zellen im Zustand negativer Geotaxis (ausgelöst von einigen Stunden Dunkelheit), weisen deutlich verkürzte Fluoreszenzlebensdauern auf.

5 Appendix

5.1 References

Abraham, H. and Lemoine, J.: Disparition instantanée du phénomène de Kerr. C. R. Acad. Sci. Paris **129**, 206-208 (1899).

Alcala, J.R., Gratton, E. and Prendergast, F.G.: Interpretation of fluorescence decays in proteins using continuous lifetime distributions. Biophysical Journal **51** (6), 925-936 (1987a).

Alcala, J.R., Gratton, E. and Prendergast, F.G.: Fluorescence lifetime distributions in proteins. Biophysical Journal **51** (4), 597-604 (1987b).

Alcala, J.R., Gratton, E. and Prendergast, F.G.: Resolvability of fluorescence lifetime distributions using phase fluorometry. Biophysical Journal **51** (4), 587-596 (1987c).

Allen, J.F. and Forsberg, J.: Molecular recognition in thylakoid structure and function. Trends in Plant Science **6** (7), 317-326 (2001).

Andersson, J., Walters, R.G., Horton, P. and Jansson, S.: Antisense inhibition of the photosynthetic antenna proteins CP29 and CP26: Implications for the mechanism of protective energy dissipation. Plant Cell **13** (5), 1193-1204 (2001).

Badea, M.G. and Brand, L.: Time-resolved fluorescence measurements. Methods Enzymol. **61**, 378-425 (1979).

Barzda, V., de Grauw, C.J., Vroom, J., Kleima, F.J., van Grondelle, R., van Amerongen, H. and Gerritsen, H.C.: Fluorescence lifetime heterogeneity in aggregates of LHCII revealed by time-resolved microscopy. Biophysical Journal **81** (1), 538-546 (2001).

Bassi, R., Sandona, D. and Croce, R.: Novel aspects of chlorophyll a/b-binding proteins. Physiologia Plantarum **100** (4), 769-779 (1997).

Bassi, R., Pineau, B., Dainese, P. and Marquardt, J.: Carotenoid-binding proteins of photosystem II. European Journal of Biochemistry. **212** (2), 297-303 (1993).

Bastiaens, P.I.H. and Squire, A.: Fluorescence lifetime imaging microscopy: spatial resolution of biochemical processes in the cell. Trends in Cell Biology **9** (2), 48-52 (1999).

Bean, B.: Geotactiv behavior of Chlamydomonas. Journal of Protozoology. **24** (3), 394-401 (1977).

Bean, B.: Microbial geotaxis. In "Membranes and sensory transduction", G. Colombetti and F. Lenci [eds.] (Plenum Press: New York), pp. 163-198 (1984).

Bergmann, A., Eichler, H.J., Eckert, H.J. and Renger, G.: Picosecond laser-fluorometer with simultaneous time and wavelength resolution for monitoring decay spectra of photoinhibited Photosystem II particles at 277 K and 10 K. Photosynthesis Research **58** (3), 303-310 (1998).

Bilger, W. and Björkman, O.: Relationships among violaxanthin deepoxidation, thylakoid membrane conformation, and non-photochemical chlorophyll fluorescence quenching in leaves of cotton (*Gossypium hirsutum L.*). Planta **193** (2), 238-246 (1994).

Bilger, W. and Schreiber, U.: Energy-dependent quenching of dark-level chlorophyll fluorescence in intact leaves. Photosynthesis Research **10** (3), 303-308 (1986).

Bopp, M.A., Jia, Y.W., Li, L.Q., Cogdell, R.J. and Hochstrasser, R.M.: Fluorescence and photobleaching dynamics of single light-harvesting complexes. Proceedings of the National Academy of Sciences of the United States of America **94** (20), 10630-10635 (1997).

Briantais, J.-M., Merkelo, H. and Govindjee: Lifetime of the excited state (τ) *in vivo*. III. Chlorophyll during fluorescence induction in *Chlorella pyrenoidosa*. Photosynthetica **6**, 133-141 (1972).

Briantais, J.-M., Vernotte, C., Picaud, M. and Krause, G.H.: A quantitative study of the slow decline of chlorophyll *a* fluorescence in isolated chloroplasts. Biochimica et Biophysica Acta **548**, 128-138 (1979).

Briantais, J.-M., Vernotte, C., Picaud, M. and Krause, G.H.: Chlorophyll fluorescence as a probe for the determination of the photo-induced proton gradient in isolated chloroplasts. Biochimica et Biophysica Acta **591**, 198-202 (1980).

Buehler, C., Dong, C.Y., So, P.T.C., French, T. and Gratton, E.: Time-resolved polarization imaging by pump-probe (stimulated emission) fluorescence microscopy. Biophysical Journal **79** (1), 536-549 (2000).

Buist, A.H., Müller, M., Gijsbers, E.J., Brakenhoff, G.J., Sosnowski, T.S., Norris, T.B. and Squier, J.: Double-pulse fluorescence lifetime measurements. J. Microsc. **186**, 212-220 (1997).

Buurman, E.P., Sanders, R., Draaijer, A., Gerritsen, H.C., van Deen, J.J.F., Houpt, P.M. and Levine, Y.K.: Fluorescence lifetime imaging using a confocal laser scanning microscope. Scanning **14**, 155-159 (1992).

Chow, W.S., Funk, C., Hope, A.B. and Govindjee: Greening of intermittent-light-grown bean plants in continuous light: Thylakoid components in relation to photosynthetic performance and capacity for photoprotection. Indian Journal of Biochemistry & Biophysics **37** (6), 395-404 (2000).

Clegg, R.M.: Fluorescence resonance energy transfer. In "Fluorescence imaging spectroscopy and microscopy", X.F. Wang and B. Herman [eds.], Chemical analysis series Series Vol. 137, J.D. Winefordner [ed.] (John Wiley & Sons, Inc.: New York), pp. 179-252 (483) (1996).

Clegg, R.M. and Schneider, P.C.: Fluorescence Lifetime-resolved Imaging Microscopy: A general description of the lifetime-resolved imaging measurements. In "Fluorescence Microscopy and Fluorescent Probes", J. Slavik [ed.] (Plenum Press: New York), pp. 15-33 (1996).

Clegg, R.M., Schneider, P.C. and Jovin, T.M.: Fluorescence lifetime-resolved imaging microscopy (FLIM). In "Biomedical optical instrumentation and laser-assisted biotechnology", A.M. Verga Scheggi, S. Martellucci, A.N. Chester and R. Pratesi [eds.], NATO ASI Series E: Applied Sciences Series Vol. 325 (Kluwer Academic Publishers: Dordrecht, Boston, London), pp. 143-156 (1996).

Clegg, R.M., Feddersen, B., Gratton, E. and Jovin, T.M.: Time resolved imaging fluorescence microscopy. Proc. SPIE **1604** (Time-resolved Laser Spectroscopy in Biochemistry III), 448-460 (1992).

Condon, E.U.: A theory of intensity distribution in band systems. Phys. Rev. **28**, 1182-1201 (1926).

Condon, E.U.: The Franck-Condon principle and related topics. Am. J. Phys. **15**, 365-374 (1947).

Conn, P.M.: Green Fluorescent Protein. Methods in Enzymology Vol. 302 (Academic Press: San Diego), pp. 490 (1999).

Crimi, M., Dorra, D., Bösinger, C.S., Giuffra, E., Holzwarth, A.R. and Bassi, R.: Time-resolved fluorescence analysis of the recombinant photosystem II antenna complex CP29 - Effects of zeaxanthin, pH and phosphorylation. European Journal of Biochemistry **268** (2), 260-267 (2001).

Crofts, A.R. and Yerkes, C.T.: A molecular mechanism for qE-quenching. FEBS Letters **352** (3), 265-270 (1994).

Cubeddu, R., Canti, G., Taroni, P. and Valentini, G.: Time-gated fluorescence spectroscopy and imaging of porphyrins and phthalocyanines. Proc. SPIE **1525**, 17-25 (1991).

Cubeddu, R., Canti, G., Pifferi, A., Taroni, P. and Valentini, G.: A real time system for fluorescence lifetime imaging. Proceedings of SPIE **2976**, 98-104 (1997).

Cubeddu, R., Pifferi, A., Taroni, P., Torricelli, A., Valentini, G., Rinaldi, F. and Sorbellini, E.: Fluorescence lifetime imaging: An application to the detection of skin tumors. IEEE **5** (4), 923-929 (1999).

Cundall, R.B. and Dale, R.B.: Time-resolved fluorescence spectroscopy in biochemistry and biology. NATO Advanced Science Institutes Series A: Life Sciences Vol. 69 (Plenum Press: New York), pp. 785 (1983).

Delosme, R., Olive, J. and Wollman, F.A.: Changes in light energy distribution upon state transitions - an in vivo photoacoustic study of the wild type and photosynthesis mutants from *Chlamydomonas reinhardtii*. Biochimica et Biophysica Acta - Bioenergetics **1273** (2), 150-158 (1996).

Demmig, B., Winter, K., Krüger, A. and Czygan, F.-C.: Zeaxanthin and the heat dissipation of excess light energy in *Nerium oleander* exposed to a combination of high light and water stress. Plant Physiology **87**, 17-24 (1988).

Demmig-Adams, B.: Carotenoids and photoprotection in plants: a role for the xanthophyll zeaxanthin. Biochimica et Biophysica Acta **1020** (1), 1-24 (1990).

Demmig-Adams, B. and Adams III, W.W.: Photosynthesis - Harvesting sunlight safely. Nature **403** (6768), 371-374 (2000).

Demmig-Adams, B., Gilmore, A.M. and Adams III, W.W.: Carotenoids 3: in vivo function of carotenoids in higher plants. FASEB Journal **10** (4), 403-412 (1996).

Dexter, D.L.: A theory of sensitized luminescence in solids. J. Chem. Phys. **21**, 836-850 (1953).

Dong, C.Y., So, P.T.C., French, T. and Gratton, E.: Fluorescence lifetime imaging by asynchronous pump-probe microscopy. Biophysical Journal **69** (6), 2234-2242 (1995).

Dong, C.Y., So, P.T.C., Buehler, C. and Gratton, E.: Spatial resolution in scanning pump-probe fluorescence microscopy. Optik **106** (1), 7-14 (1997).

Donnan, L. and John, P.C.: Cell cycle control by timer and sizer in Chlamydomonas. Nature **304** (5927), 630-633 (1983).

Dowling, K., Dayel, M.J., Hyde, S.C.W., Dainty, C., French, P.M.W., Vourdas, P., Lever, M.J., Dymoke-Bradshaw, A.K.L., Hares, J.D. and Kellett, P.A.: Whole-field fluorescence lifetime imaging with picosecond resolution using ultrafast 10-kHz solid-state amplifier technology. IEEE **4** (2), 370-375 (1998).

Drexhage, K.H.: Structure and properties of laser dyes. In "Dye lasers", F.P. Schäfer [ed.], Topics in Applied Physics Series Vol. 1 (Springer: Berlin), pp. 144-193 (1973).

Duschinsky, F.: Der zeitliche Intensitätsverlauf von intermittierend angeregter Resonanzstrahlung. Z.Phys. **81**, 7-22 (1933a).

Duschinsky, F.: Eine allgemeine Theorie der zur Messung sehr kurzer Leuchtdauern dienenden Versuchsanordnungen (Fluorometer); A general theory of the instruments for the measurement of very short after-glows (Fluorometer). Z.Phys. **81**, 23-42 (1933b).

Eggeling, C., Berger, S., Brand, L., Fries, J.R., Schaffer, J., Volkmer, A. and Seidel, C.A.M.: Data registration and selective single-molecule analysis using multi-parameter fluorescence detection. Journal of Biotechnology **86** (3 Special Issue SI), 163-180 (2001).

Einstein, A.: Zur Quantentheorie der Strahlung. Physik. Z. **18**, 121-128 (1917).

Elrad, D., Niyogi, K.K. and Grossman, A.R.: A major light-harvesting polypeptide of photosystem II functions in thermal dissipation. Plant Cell **14**, 1801-1816 (2002).

Fornshell, J.A.: An experimental investigation of bio convection in 3 species of microorganisms. Journal of Protozoology **25** (1), 125-133 (1978).

Förster, T.: Energiewanderung und Fluoreszenz. Naturwissenschaften **6**, 166-175 (1946).

Förster, T.: Zwischenmolekulare Energiewanderung und Fluoreszenz. Ann. Phys. (Leipzig) **6** (2), 55-75 (1948).

Förster, T.: Fluoreszenz organischer Verbindungen pp. 315 (Vandenhoeck & Ruprecht: Göttingen), (1951).

Franck, J.: Elementary processes of photochemical reactions. Trans. Faraday Soc. **21**, 536-542 (1925).

Franck, J.: Über eine Rotverschiebung der Resonanzfluoreszenz durch vielfach wiederholte Streuung. Naturwissenschaften **15**, 236-238 (1927).

Frank, H.A., Bautista, J.A., Josue, J.S. and Young, A.J.: Mechanism of nonphotochemical quenching in green plants: Energies of the lowest excited singlet states of violaxanthin and zeaxanthin. Biochemistry **39** (11), 2831-2837 (2000).

Frank, H.A., Das, S.K., Bautista, J.A., Bruce, D., Vasil'ev, S., Crimi, M., Croce, R. and Bassi, R.: Photochemical behavior of xanthophylls in the recombinant photosystem II antenna complex, CP26. Biochemistry **40** (5), 1220-1225 (2001).

French, T.: The development of fluorescence lifetime imaging and an application in immunology. Ph.D.-Thesis, Department of Physics, Laboratory for Fluorescence Dynamics, University of Illinois at Urbana-Champaign, Urbana-Champaign (1996).

Gadella Jr., T.W.J.: Fluorescence Lifetime Imaging Microscopy (FLIM): Instrumentation and applications. In "Fluorescent and luminescent probes for biological activity", W.T. Mason [ed.], Biological techniques Series, D.B. Sattelle [ed.] (Academic Press: San Diego), pp. 467-479 (1999).

Gadella Jr., T.W.J., Jovin, T.M. and Clegg, R.M.: Fluorescence lifetime imaging microscopy (FLIM): Spatial resolution of microstructures on the nanosecond time scale. Biophys. Chem. **48**, 221-239 (1993).

Gadella Jr., T.W.J., Clegg, R.M. and Jovin, T.M.: Fluorescence lifetime imaging microscopy: pixel-by-pixel analysis of phase-modulation data. Bioimaging **2** (3), 139-159 (1994).

Gaviola, E.: Die Abklingungszeiten der Fluoreszenz von Farbstofflösungen. Z. Physik **35**, 748-756 (1926a).

Gaviola, E.: Die Abklingungszeiten der Fluoreszenz von Farbstofflösungen. Annalen der Physik **81**, 681-710 (1926b).

Gaviola, E.: Ein Fluorometer. Apparat zur Messung von Fluoreszenzabklingungszeiten. Z. Physik **42**, 853-861 (1927).

Gilmore, A.M. and Yamamoto, H.Y.: Linear models relating xanthophylls and lumen acidity to non-photochemical fluorescence quenching: evidence that antheraxanthin explains zeaxanthin-independent quenching. Photosynth. Res. **35**, 67-78 (1993).

Gilmore, A.M. and Govindjee: How higher plants respond to excess light: Energy dissipation in photosystem II. In "Concepts in Photobiology : Photosynthesis and Photomorphogenesis." G.S. Singhal, G. Renger, K.D. Irrgang, Govindjee and S. Sopory [eds.] (Narosa Publishers/Kluwer Academic Publishers), pp. 513-548 (1999).

Gilmore, A.M., Hazlett, T.L. and Govindjee: Xanthophyll cycle-dependent quenching of Photosystem II Chlorophyll *a* fluorescence - Formation of a quenching complex with a short fluorescence lifetime. Proceedings of the National Academy of Sciences of the USA. **92** (6), 2273-2277 (1995).

Gilmore, A.M., Itoh, S. and Govindjee: Global spectral-kinetic analysis of room temperature chlorophyll *a* fluorescence from light-harvesting antenna mutants of barley. Phil. Trans. Roy. Soc. London, Biology Series **355** (1402), 1371-1384 (2000).

Gilmore, A.M., Hazlett, T.L., Debrunner, P.G. and Govindjee: Photosystem II Chlorophyll *a* fluorescence lifetimes and intensity are independent of the antenna size differences between barley wild-type and chlorina mutants - Photochemical quenching and Xanthophyll cycle-dependent nonphotochemical quenching of fluorescence. Photosynthesis Research. **48** (1-2), 171-187 (1996).

Gilmore, A.M., Shinkarev, V.P., Hazlett, T.L. and Govindjee: Quantitative analysis of the effects of intrathylakoid pH and Xanathophyll cycle pigments on Chlorophyll *a* fluorescence lifetime distributions and intensity in thylakoids. Biochemistry. **37** (39), 13582-13593 (1998).

Gohlke, C., Holub, O. and Clegg, R.M.: unpublished data (2002).

Goss, R., Böhme, K. and Wilhelm, C.: The xanthophyll cycle of *Mantoniella squamata* converts violaxanthin into antheraxanthin but not to zeaxanthin - consequences for the mechanism of enhanced non-photochemical energy dissipation. Planta **205** (4), 613-621 (1998).

Gottling, P.F.: The determination of the time between excitation and emission for certain fluorescent solids. Phys. Rev. **22**, 566-573 (1923).

Govindjee: Sixty-three years since Kautsky - Chlorophyll *a* fluorescence. Australian Journal of Plant Physiology. **22** (2), 131-160 (1995).

Govindjee: A role for a light-harvesting antenna complex of photosystem II in photoprotection. Plant Cell **14**, 1663-1668 (2002).

Govindjee and Seufferheld, M.J.: Non-photochemical quenching of chlorophyll *a* fluorescence: Early history and characterization of two xanthophyll cycle mutants of *Chlamydomonas reinhardtii*. Journal of Functional Plant Biology **29** (10), 1141-1155 (2002).

Govindjee and Spilotro, P.: An *Arabidopsis thaliana* mutant, altered in the γ-subunit of ATP synthase, has a different pattern of intensity-dependent changes in non-photochemical quenching and kinetics of the P-to-S fluorescence decay. Functional Plant Biology **29** (4), 425-434 (2002).

Gratton, E. and Limkeman, M.: A continuously variable frequency cross-correlation phase fluorometer with picosecond resolution. Biophysical Journal **44** (3), 315-324 (1983).

Gratton, E., Feddersen, B. and vande Ven, M.: Parallel acquisition of fluorescence decay using array detectors. Proc. SPIE **1204** (Time-resolved Laser Spectroscopy in Biochemistry III), 21-25 (1990).

Haehnel, W., Holzwarth, A.R. and Wendler, J.: Picosecond fluorescence kinetics and energy transfer in the antenna chlorophylls of green algae. Photochemistry & Photobiology **37** (4), 435-443 (1983).

Hanley, Q.S., Subramaniam, V., Arndt-Jovin, D.J. and Jovin, T.M.: Fluorescence lifetime imaging: Multi-point calibration, minimum resolvable differences, and artifact suppression. Cytometry **43** (4), 248-260 (2001).

Harris, E.H.: The *Chlamydomonas* Sourcebook: A comprehensive guide to biology and laboratory use (Academic press: San Diego), (1989).

Haugland, R.P.: Handbook of fluorescent probes and research products. 8 ed. (Molecular Probes: Eugene, Oregon, USA), (2001).

Henry, B.R. and Siebrand, W.: Radiationless transitions. In "Organic molecular photophysics", J.B. Birks [ed.] Vol. 1 (John Wiley & sons: London), pp. 153 (1973).

Holub, O.: Orientierungsabhängigkeit bei Förster-Fluoreszenz-Resonanz-Energie-Transfer zwischen gleichartigen Farbstoffmolekülen in doppelsträngiger DNA. Diplom-Thesis, Fakultät für Physik & Max-Planck-Institut für biophysikalische Chemie, Abteilung Molekulare Biologie, Georg-August-Universität, Göttingen, pp. 103 (1996).

Holub, O. and Schneider, P.C.: unpublished data (1997).

Holub, O., Seufferheld, M.J., Gohlke, C., Govindjee and Clegg, R.M.: Fluorescence lifetime imaging (FLI) in real-time - a new technique in photosynthesis research. Photosynthetica **38** (4), 581-599 (2000).

Holzwarth, A.R.: Excited-state kinetics in chlorophyll systems and its relationship to the functional organization of the photosystems. In "Chlorophylls", H. Scheer [ed.] (CRC Press: Boca Raton), pp. 1125-1151 (1991).

Horton, P., Ruban, A.V. and Walters, R.G.: Regulation of light harvesting in green plants: indication by non-photochemical quenching of chlorophyll fluorescence. Plant Physiology **106**, 415-420 (1994).

Horton, P., Ruban, A.V. and Young, A.J.: Regulation of the structure and function of the light-harvesting complexes of photosystem II by the xanthophyll cycle. In "The

photochemistry of carotenoids", H.A. Frank, A.J. Young, G. Britton and R.J. Cogdell [eds.], Advances in photosynthesis Series Vol. 8, Govindjee [ed.] (Kluwer Academic Publishers: Dordrecht, The Netherlands), pp. 271-291 (1999).

Itoh, H., Evenzahav, A., Kinoshita, K., Inagaki, Y., Mizushima, H., Takahashi, A., Hayakawa, T. and Kinosita, K.J.: Use of a gain modulating framing camera for time-resolved imaging of cellular phenomena. Proceedings of SPIE **2979**, 733-740 (1997).

Jablonski, A.: Efficiency of anti-Stokes fluorescence in dyes. Nature **131**, 839-840 (1933).

Jablonski, A.: Über den Mechanismus der Photolumineszenz von Farbstoffphosphoren. Z. Physik **94**, 38-46 (1935).

Jablonski, A.: Decay of photoluminescence of solutions. Acta Phys. Pol. **16**, 471-479 (1957).

Jablonski, A.: On the notion of emission anisotropy. Bull. Acad. Polon. Sci., série des sci. math., astr. et phys. **8**, 259-264 (1960).

Jameson, D.M.: The seminal contributions of Gregorio Weber to modern fluorescence spectroscopy. In "Methods and applications of fluorescence spectroscopy" (Springer: Heidelberg) (2001).

Jameson, D.M. and Gratton, E.: Analysis of heterogeneous emissions by multifrequency phase and modulation fluorometry. In "New directions in molecular luminescence, ASTM STP 822", D. Eastwood [ed.] (American Society for Testing and Materials: Philadelphia), pp. 67-81 (1983).

Jameson, D.M., Gratton, E. and Hall, R.D.: The measurement and analysis of heterogeneous emissions by multifrequency phase and modulation fluorometry. Applied Spectroscopy Reviews **20** (1), 55-106 (1984).

Karstens, T. and Kobs, K.: Rhodamine B and Rhodamine 101 as reference substances for fluorescence quantum yield measurements. J. Phys. Chem. **84**, 1871-1872 (1980).

Kasha, M.: Characterization of electronic transitions in complex molecules. Disc. Faraday Soc. **9**, 14-19 (1950).

Kautsky, H. and Hirsch, A.: Neue Versuche zur Kohlensäureassimilation. Naturwissenschaften **19**, 964 (1931).

Kemnitz, K., Pfeifer, L. and Ainbund, M.R.: Detector for multichannel spectroscopy and fluorescence lifetime imaging on the picosecond timescale. Nuclear Instruments & Methods in Physics Research Section A **387** (1-2), 86-87 (1997).

Kohl, M., Neukammer, J., Sukowski, U., Rinneberg, H., Wörle, D., Sinn, H.J. and Friedrich, E.A.: Delayed observation of laser-induced fluorescence for imaging of tumors. Applied Physics B - Photophysics & Laser Chemistry **B56** (3), 131-138 (1993).

Krause, G.H.: The high-energy state of the thylakoid system as indicated by chlorophyll fluorescence and chloroplast shrinkage. Biochimica et Biophysica Acta. **292** (3), 715-728 (1973).

Lakowicz, J.R.: Principles of fluorescence spectroscopy. 2nd ed. (Kluwer Academic/Plenum Publishers: New York), (1999).

Lakowicz, J.R. and Berndt, K.W.: Lifetime-selective fluorescence imaging using an RF phase-sensitive camera. Review of Scientific Instruments **62** (7), 1727-1734 (1991).

Lakowicz, J.R., Szmacinski, H., Nowaczyk, K., Berndt, K.W. and Johnson, M.: Fluorescence lifetime imaging. Analytical Biochemistry **202** (2), 316-330 (1992).

Lazar, D.: Chlorophyll *a* fluorescence induction. Biochimica et Biophysica Acta - Bioenergetics. **1412** (1), 1-28 (1999).

Lewis, G.N. and Kasha, M.: Phosphorescence and the triplet state. J. Am. Chem. Soc. **66**, 2100-2116 (1944).

Li, X.P., Björkman, O., Shih, C., Grossman, A.R., Rosenquist, M., Jansson, S. and Niyogi, K.K.: A pigment-binding protein essential for regulation of photosynthetic light harvesting. Nature **403** (6768), 391-395 (2000).

Lord Rayleigh: On the measurement of certain very short intervals of time. Nature **69** (1798), 560-561 (1904).

Marriott, G., Clegg, R.M., Arndt-Jovin, D.J. and Jovin, T.M.: Time resolved imaging microscopy. Phosphorescence and delayed fluorescence imaging. Biophysical Journal **60** (6), 1374-1387 (1991).

McGown, L. and Bright, F.: Phase-resolved fluorescence spectroscopy. Anal. Chem. **56**, 1400A-1415A (1984).

Minami, T. and Hirayama, S.: High quality fluorescence decay curves and lifetime imaging using an elliptical scan streak camera. J. Photochem. Photobiol., A: Chemistry **53**, 11-21 (1990).

Mizeret, J., Stepinac, T., Hansroul, M., Studzinski, A., van den Bergh, H. and Wagnieres, G.: Instrumentation for real-time fluorescence lifetime imaging in endoscopy. Review of Scientific Instruments **70** (12), 4689-4701 (1999).

Morgan, C.G., Mitchell, A.C. and Murray, J.G.: Nanosecond time-resolved fluorescence microscopy: Principles and practice. Trans. R. Microsc. Soc. **1**, 463-466 (1990).

Morgan, C.G., Mitchell, A.C. and Murray, J.G.: Prospects for confocal imaging based on nanosecond fluorescence decay time. J. Microscopy **165**, 49-60 (1992).

Müller, P., Li, X.P. and Niyogi, K.K.: Non-photochemical quenching. A response to excess light energy. Plant Physiology **125** (4), 1558-1566 (2001).

Munday, J.C., Jr. and Govindjee: Light-induced changes in the fluorescence yield of chlorophyll *a* in vivo. 3. The dip and the peak in the fluorescence transient of *Chlorella pyrenoidosa*. Biophysical Journal **9** (1), 1-21 (1969a).

Munday, J.C., Jr. and Govindjee: Light-induced changes in the fluorescence yield of chlorophyll *a* in vivo. IV. The effect of preillumination on the fluorescence transient of *Chlorella pyrenoidosa*. Biophysical Journal **9** (1), 22-35 (1969b).

Ni, T. and Melton, L. Applied Spectroscopy **45**, 938-943 (1991).

Nickel, B.: Pioneers in photochemistry: From the Perrin diagram to the Jablonski diagram. EPA Newsletter **58**, 9-38 (1996).

Nickel, B.: Pioneers in photophysics: From the Perrin diagram to the Jablonski diagram. Part 2. EPA Newsletter **61**, 27-60 (1997).

Nickel, B.: Pioneers in photophysics: From Wiedemann's discovery to the Jablonski diagram. EPA Newsletter **64**, 19-72 (1998).

Niyogi, K.K.: Photoprotection revisited: Genetic and molecular approaches. Annual Review of Plant Physiology & Plant Molecular Biology **50**, 333-359 (1999).

Niyogi, K.K., Björkman, O. and Grossman, A.R.: *Chlamydomonas* Xanthophyll cycle mutants identified by video imaging of chlorophyll fluorescence quenching. Plant Cell. **9** (8), 1369-1380 (1997).

Niyogi, K.K., Shih, C., Chow, W.S., Pogson, B.J., DellaPenna, D. and Björkman, O.: Photoprotection in a zeaxanthin- and lutein-deficient double mutant of Arabidopsis. Photosynthesis Research **67** (1-2), 139-145 (2001).

Oida, T., Sako, Y. and Kusumi, A.: Fluorescence lifetime imaging microscopy (flimscopy). Methodology development and application to studies of endosome fusion in single cells. Biophysical Journal **64** (3), 676-685 (1993).

Olive, J., Wollman, F.A., Bennoun, P. and Recouvreur, M.: Ultrastructure of thylakoid membranes in C. reinhardtii: evidence for variations in the partition coefficient of the light-harvesting complex-containing particles upon membrane fracture. Archives of Biochemistry & Biophysics **208** (2), 456-467 (1981).

Periasamy, A., Wodnicki, P., Wang, X.F., Kwon, S., Gordon, G.W. and Herman, B.: Time-resolved Fluorescence Lifetime Imaging Microscopy using a picosecond pulsed tunable dye laser system. Review of Scientific Instruments. **67** (10), 3722-3731 (1996).

Perrin, F.: Polarisation de la lumière de fluorescence. Vie moyenne des molécules dans l'état excité. J. de Physique, VIe série **7**, 390-401 (1926).

Perrin, F.: La fluorescence des solutions - Induction moléculaire - Polarisation et durée d'émission - Photochimie. Annales de physique, 10e série **12**, 169-275 (1929).

Perrin, F.: Fluorescence. Durée élémentaire d'émission lumineuse. In "Librairie Scientifique Hermann" (Paris) (1931).

Perrin, J.: Fluorescence et induction moléculaire par résonance. Comptes rendus **184**, 1097-1100 (1927).

Piston, D.W., Sandison, D.R. and Webb, W.W.: Time-resolved fluorescence imaging and background rejection by two-photon excitation in laser scanning microscopy. Proc. SPIE **1604** (Time-resolved Laser Spectroscopy in Biochemistry III), 379-389 (1992).

Piston, D.W., Marriott, G., Radivoyevich, T., Clegg, R.M., Jovin, T.M. and Gratton, E.: Wide-band acousto-optic light modulator for frequency domain fluorometry and phosphorimetry. Rev. Sci. Instrum. **60**, 2596-2600 (1989).

Polívka, T., Herek, J.L., Zigmantas, D., Åkerlund, H.E. and Sundström, V.: Direct observation of the (forbidden) S-1 state in carotenoids. Proceedings of the National Academy of Sciences of the United States of America **96** (9), 4914-4917 (1999).

Polívka, T., Zigmantas, D., Sundström, V., Formaggio, E., Cinque, G. and Bassi, R.: Carotenoid S-1 state in a recombinant light-harvesting complex of photosystem II. Biochemistry **41** (2), 439-450 (2002).

Pringsheim, P.: Über die Abweichungen von der Stokesschen Regel bei der Erregung von Joddampffluoreszenz. Z. Physik **7**, 206-216 (1921).

Raman, C.V. and Nagendra-Nath, N.S.: The diffraction of light by high frequency sound waves: parts I and II. Proc. Indian Acad. Sci. **2A**, 406-412 and 413-420 (1935).

Raman, C.V. and Nagendra-Nath, N.S.: The diffraction of light by high frequency sound waves: parts III, IV and V. Proc. Indian Acad. Sci. **3A**, 75-84; 119-125 and 459-469 (1936).

Rees, D., Noctor, G., Ruban, A.V., Crofts, J., Young, A. and Horton, P.: pH-dependent chlorophyll fluorescence quenching in spinach thylakoids from light treated or dark-adapted leaves. Photosynth Res **31**, 11-19 (1992).

Renger, G.: Photosynthetic water oxidation to molecular oxygen: apparatus and mechanism. Biochimica et Biophysica Acta - Bioenergetics **1503** (1-2), 210-228 (2001).

Renger, G., Eckert, H.J., Bergmann, A., Bernarding, J., Liu, B., Napiwotzki, A., Reifarth, F. and Eichler, H.J.: Fluorescence and spectroscopic studies of exciton trapping and electron transfer in photosystem II of higher plants. Australian Journal of Plant Physiology **22** (2), 167-181 (1995).

Rigler, R. and Elson, E.S.: Fluorescence Correlation Spectroscopy: Theory and applications. Chemical Physics (Springer Verlag: Heidelberg), pp. 500 (2001).

Roelofs, T.A., Lee, C.H. and Holzwarth, A.R.: Global target analysis of picosecond chlorophyll fluorescence kinetics from pea chloroplasts: A new approach to the characterization of the primary processes in photosystem II alpha- and beta-units. Biophysical Journal **61** (5), 1147-1163 (1992).

Schneckenburger, H., Konig, K., Kunzi-Rapp, K., Westphal-Frosch, C. and Ruck, A.: Time-resolved in-vivo fluorescence of photosensitizing porphyrins. Journal of Photochemistry & Photobiology. B - Biology **21** (2-3), 143-147 (1993).

Schneider, P.C.: Schnelle bildgebende Messung von Fluoreszenzlebensdauern im Phasenbereich. PhD-Thesis, Fakultät für Physik & Max-Planck-Institut für biophysikalische Chemie, Abteilung Molekulare Biologie, Georg-August-Universität, Göttingen, pp. 146 (1997).

Schneider, P.C. and Clegg, R.M.: Rapid acquisition, analysis, and display of fluorescence lifetime-resolved images for real-time applications. Review of Scientific Instruments **68** (11), 4107-4119 (1997).

Siebrand, W.: Nonradiative processes in molecular systems. In "Dynamics of molecular collisions", W.H. Miller [ed.], Modern theoretical chemistry Series Vol. 1, Part A (Plenum: New York), pp. 249-302 (1976).

Sjöback, R., Nygren, J. and Kubista, M.: Absorption and fluorescence properties of fluorescein. Spectrochimica Acta Part A-Molecular Spectroscopy **51** (6), L7-L21 (1995).

So, P.T.C., French, T., Yu, W.M., Berland, K.M., Dong, C.Y. and Gratton, E.: Time-resolved fluorescence microscopy using two-photon excitation. Bioimaging (3), 49-63 (1995).

Spencer, R.D. and Weber, G.: Measurements of subnanosecond fluorescence lifetime with a cross-correlation phase fluorometer. Ann. N.Y. Acad. Sci. **158**, 361-376 (1969).

Steffen, R., Christen, G. and Renger, G.: Time-resolved monitoring of flash-induced changes of fluorescence quantum yield and decay of delayed light emission in oxygen-evolving photosynthetic organisms. Biochemistry **40** (1), 173-180 (2001).

Stern, O. and Volmer, M.: Über die Abklingungszeit der Fluoreszenz. Physik. Zeitschr. **20**, 183-188 (1919).

Stirbet, A., Govindjee, Strasser, B.J. and Strasser, R.J.: Chlorophyll *a* fluorescence induction in higher plants - Modelling and numerical simulation. Journal of Theoretical Biology **193** (1), 131-151 (1998).

Stokes, G.G.: On the change of refrangibility of light. Philosophical Transactions of the Royal Society of London, part II, 463-562 (1852a).

Stokes, G.G.: Ueber die Veränderung der Brechbarkeit des Lichts. Poggendorff's Annal. **87**, 480-490 (1852b).

Straub, M. and Hell, S.W.: Fluorescence lifetime three-dimensional microscopy with picosecond precision using a multifocal multiphoton microscope. Applied Physics Letters. **73** (13), 1769-1771 (1998).

Strickler, S.J. and Berg, R.A.: Relationship between absorption intensity and fluorescence lifetime of molecules. Journal of Chemical Physics **37** (4), 814-822 (1962).

Sytsma, J., Vroom, J.M., de Grauw, C.J. and Gerritsen, H.C.: Time-gated fluorescence lifetime imaging and microvolume spectroscopy using two-photon excitation. J. Microsc. **191**, 39-51 (1998).

Teale, F.W.J.: Phase and modulation fluorometry. In "Time-resolved fluorescence spectroscopy in biochemistry and biology", R.B. Cundall and R.E. Dale [eds.], NATO ASI Series A: Life Sciences Series Vol. 69 (Plenum Press: London), pp. 59-80 (1983).

vandeVen, M. and Gratton, E.: Time-resolved fluorescence lifetime imaging. In "Optical microscopy: Emerging methods and applications", B. Herman and J.J. Lemasters [eds.] (Academic Press: New York), pp. 373-402 (1992).

Vasil'ev, S., Irrgang, K.D., Schrötter, T., Bergmann, A., Eichler, H.J. and Renger, G.: Quenching of chlorophyll *a* fluorescence in the aggregates of LHCII: Steady state fluorescence and picosecond relaxation kinetics. Biochemistry **36** (24), 7503-7512 (1997).

Velthuys, B.R.: Electron-dependent competition between plastoquinone and inhibitors for binding to photosystem II. Federation of European Biochemical Society (FEBS) Letters **126**, 277-281 (1981).

Verveer, P.J., Squire, A. and Bastiaens, P.I.H.: Global analysis of fluorescence lifetime imaging microscopy data. Biophysical Journal **78** (4), 2127-2137 (2000).

Vogel, M., Rettig, W., Sens, R. and Drexhage, K.H.: Structural relaxation of rhodamine dyes with different N-substitution patterns: A study of fluorescence decay times and quantum yields. Chem. Phys. Lett. **147** (5), 452-460 (1988).

Wahl, P.: Nanosecond pulse fluorimetry. In "New techniques in biophysics and cell biology", R. Pain and B. Smith [eds.] Vol. 2 (Wiley: New York), pp. 233 (1975).

Wang, X.F., Uchida, T. and Minami, S.: A fluorescence lifetime distribution measurement system based on phase-resolved detection using an image dissector tube. Applied Spectroscopy **43** (5), 840-845 (1989).

Wang, X.F., Uchida, T., Coleman, D.M. and Minami, S.: A two-dimensional fluorescence lifetime imaging system using gated image intensifier. Appl. Spectrosc. **45**, 360-366 (1991).

Wang, X.F., Periasamy, A., Herman, B. and Coleman, D.M.: Fluorescence lifetime imaging microscopy (FLIM): instrumentation and applications. Crit. Rev. Anal. Chem. **23** (5), 369-395 (1992).

Wawilow, S.J.: Die Fluoreszenzausbeute von Farbstofflösungen als Funktion der Wellenlänge des anregenden Lichtes. II. Z. Physik **42**, 311-318 (1927).

Webber, S.E.: The role of time-dependent measurements in elucidating static versus dynamic quenching processes. Photoch. Photobiol. **65** (1), 33-38 (1997).

Weber, G.: Polarization of the fluorescence of macromolecules. 1. Theory and experimental method. Biochem. J. **51**, 145-155 (1952).

Weber, G.: Resolution of the fluorescence lifetimes in a heterogeneous system by phase and modulation measurements. J. Phys. Chem. **85**, 949-953 (1981).

Weller, A. Pure Appl. Chem. **16**, 115 (1968).

Wentworth, M., Ruban, A.V. and Horton, P.: Chlorophyll fluorescence quenching in isolated light harvesting complexes induced by zeaxanthin. FEBS Letters **471** (1), 71-74 (2000).

Whitmarsh, J. and Govindjee: Photosystem II. In "Encyclopedia of Life Sciences (www. els. net)" (Nature Publishing Group; Macmillan Publishers Ltd.: England) (2001).

Wieb van der Meer, B., Cooker, G. and Chen, S.Y.S.: Resonance energy transfer - Theory and data (VCH-Verlag: New York), (1995).

Woo, M., Neider, J., Davis, T. and Shreiner, D.: OpenGL programming guide: The official guide to learning OpenGL; Version 1.2; OpenGL architecture review board. 3th ed. (Addison-Wesley: Reading, USA), (1999).

Wood, R.W.: The time interval between absorption and emission of light in fluorescence. Proc. Roy. Soc. A. **99**, 362-371 (1921).

Wraight, C.A.: Oxidation-reduction physical chemistry of the acceptor quinonecomplex in bacterial photosynthetic reaction centers: Evidence for a new model of herbicide activity. Israel Journal of Chemistry **21**, 348-354 (1981).

Yamamoto, H.Y., Nakayama, J.O.M. and Chichester, C.O.: Studies on the light and dark interconversions of leaf xanthophylls. Archives of Biochemistry & Biophysics **97**, 168-173 (1962).

Yamamoto, H.Y., Bugos, R.C. and Hieber, A.D.: Biochemistry and molecular biology of the xanthophyll cycle. In "The photochemistry of carotenoids", H.A. Frank, A.J. Young, G. Britton and R.J. Cogdell [eds.], Advances in photosynthesis Series Vol. 8, Govindjee [ed.] (Kluwer Academic Publishers: Dordrecht, The Netherlands), pp. 293-303 (1999).

Zouni, A., Witt, H.T., Kern, J., Fromme, P., Krauss, N., Saenger, W. and Orth, P.: Crystal structure of photosystem II from *Synechococcus elongatus* at 3.8 angstrom resolution. Nature **409** (6821), 739-743 (2001).

5.2 Figure index

5.3 Abbreviations

2D Two-dimensional; **3D** Three-dimensional; **A/D** Analog/Digital; **AGP** Accelerated Graphics Port (a specification for a 32-bit wide bus clocked at 66 MHz, enabling graphics cards to interface with the host computer memory and CPU faster than through PCI); **AMD** *Advanced Micro Devices, Inc.*; **ANSI** American National Standards Institute; **AOM** Acousto-Optical Modulator; **API** Application Programming Interface (a specific method prescribed by a computer operating system or application program by which a programmer can make requests of it); **ATA** Advanced Technology Attachment (the official name that American National Standards Institute group X3T10 uses for what the computer industry calls Integrated Drive Electronics, IDE); **ATI** *ATI Technologies Inc.*; **AVI** Audio Video Interleaved (a sound and motion picture file that conforms to the Microsoft Windows Resource Interchange File Format (RIFF) specification); **BNC** Bayonet Neil-Concelman or British Naval Connector (a connector for coaxial cables); **C** a structured, procedural programming language; **C++** an object-oriented programming language that supercedes the C language; **CCD** Charge-Coupled Device; **Chl** Chlorophyll; **CLUT** Color Look Up Table; **codec** Compression / Decompression; **CP** Chlorophyll-Protein complex; **CP29** a 29 kDa minor Chl-protein complex; **CPU** Central Processing Unit; **CRT** Cathode Ray Tube; **DAQ** Data Acquisition; **DCMU** 3-(3,4-dichlorophenyl)-1,1-dimethylurea; **DDR** Double Data Rate (a memory data transfer type that allows for data to be fetched on both the rising and falling edges of the clock thus doubling the effective transfer rate of the clock); **DLL** Dynamic Link Library (a program library that is linked to a program at runtime instead of compile time); **DMA** Direct Memory Access (capability provided by some computer bus architectures that allows data to be sent directly from an attached device to the memory on the computer's motherboard); $\mathbf{F_{max}}$ maximum Chl fluorescence level; $\mathbf{F_0}$ true initial minimum Chl fluorescence level; $\mathbf{F_{0meas}}$ initial measured Chl fluorescence level; $\mathbf{F_P}$ relative maximum (P, peak) of fluorescence transient curve; $\mathbf{f_1}$ fractional intensity of the first lifetime component in a two lifetime component system; $\mathbf{f_2}$ fractional intensity of the second lifetime component in a two lifetime component system; **FLI** Fluorescence Lifetime Imaging; **FLIF** Fluorescence Lifetime Image File; **FLIM** Fluorescence Lifetime-resolved Imaging Microscopy; **FLImage** custom designed software for rapid Fluorescence Lifetime Imaging; **FlimFast** custom designed software for rapid continuous Fluorescence Lifetime Imaging; **fps** Frames per Second; **GB** Giga Byte (1 GB = 1024x1024x1024 Bytes); **GPIB** General Purpose Interface Bus (a bus according to the IEEE-488.2 specifications, to connect and control programmable instruments, and to provide a standard interface for communication

between instruments from different sources); **GPU** Graphics Processing Unit; **HF** High Frequency; **HP** *Hewlett-Packard Inc.*; **HS** High Salt; **IDE** Integrated Development Environment; **IEEE** Institute of Electrical and Electronics Engineers; **IEEE-488.2** see GPIB; **I/O** In/Out; **LAN** Local Area Network; **LASER** Light Amplification by Stimulated Emission of Radiation; **LCD** Liquid Crystal Display; **LFD** Laboratory for Fluorescence Dynamics; **LHC** Light Harvesting Complex; ***Lhcbm1*** a major light harvesting polypeptide; **MB** Mega Byte (1 MB = 1024x1024 Bytes); **Mbps** Mega bits per seconds (unit of information transfer rate); **MCP** Micro Channel Plate; **MFC** Microsoft Foundation Classes; **MIP** multim im parvo ("many things in a small space"); **MS** *Microsoft Inc.*; **MTF** spatial Modulation Transfer Function; **MV** Methyl Viologen; **NIC** Network Interface Card; **NPQ** Non-Photochemical Quenching; **NTSC** National Television Standards Committee; **OJIPSMT** nomenclature of transient curve (O origin, J inflection, I intermediary hump, P peak, S quasi-steady state, M relative maximum, T terminal steady state); **OS** Operating System; **P** Peak (see OJIPSMT); **PAL** Phase Alternating Line; **PC** Personal Computer (commonly used to describe an "IBM-compatible" personal computer in contradistinction to an *Apple* Macintosh computer or UNIX based workstations); **PCI** Peripheral Component Interconnect; **PS** Photosystem; ***PsbS*** a 22 kDa protein involved in NPQ phenomenon (also known as CP22), the product of the PSII gene *psbS*; $\mathbf{Q_A^-}$ reduced one-electron acceptor-bound plastoquinone of PSII; $\mathbf{Q_B^-}$ singly reduced two-electron acceptor-bound plastoquinone of PSII; **qE** energy-dependent quenching; **qP** photochemical quenching; **qT** state-transition quenching; **qI** photoinhibitory quenching; **QVGA** video size standard 320x240; **RAID** Redundant Array of Independent Disks (originally redundant array of inexpensive disks; a way of storing the same data in different places on multiple hard disks thereby increasing storage size, speed and/or fault-tolerance); **RAM** Random Access Memory; **RF** Radio Frequency; **RGB** Red Green Blue; **RGBA** Red Green Blue Alpha; **ROI** Region of Interest; **RS-232** an interface between data terminal equipment and data communications equipment employing serial binary data interchange; **RS-422** Standard interface for multi-point connections between serial devices; **S** quasi-steady state (see OJIPSMT); $\mathbf{S_2}$ one of the redox states of the oxygen evolving Mn complex; **SDK** Software Development Kit (a set of programs used by a computer programmer to write application programs); **SDRAM** Synchronous Dynamic Random Access Memory (a random access memory data transfer type that synchronizes storage cells refresh with the clock); **SGI** Silicon Graphics Inc.; **SIMD** Single Instruction Multiple Data (microprocessor commands that lets one microinstruction operate at the same time on multiple data items); **T** Terminal steady state (see OJIPSMT); **TAP** Tris-Acetate Phosphate; τ lifetime of

fluorescence; τ_{phase} apparent single lifetime of fluorescence calculated from phase; τ_{mod} apparent single lifetime of fluorescence calculated from modulation; τ_1 first lifetime component of two lifetime component system; τ_2 second lifetime component of two lifetime component system; $<\tau>$ average lifetime of fluorescence; **TTL** Transistor-Transistor Logic (a type of electronic logic gate that demands a power rail which is very close to +5V, and uses a relatively high amount of current to drive their logic levels; below 1V for a logical '0' or 'low', and above about 3.5V for a logical '1' or 'high'); **UI** User Interface (the part of an application program that is visible to the user); **UIUC** University of Illinois at Urbana-Champaign; **UNIX** Operating system originated at Bell Labs in 1969; **VFW** Video for Windows; **WDM** Windows Driver Model (specification for unified device drivers for the Microsoft Windows 9x and XP operating systems); **Win32** Application Programming Interface (API) for the Windows operating system using 32 bit memory addressing; **WT** Wild Type; **VGA** Video Graphics Array; **VI** Virtual Instrument (a program module in LabVIEW).

5.4 Homodyne and heterodyne setups

In the heterodyne mode the phase is running through with the difference of both modulation frequencies (see sections 2.1.7 and 2.1.8). In the homodyne mode on the other hand one obtains a time independent signal at every location on the phosphor screen output of the image intensifier. In this case it is sufficient to integrate this time independent signal at a certain phase setting until a good signal to noise ratio is achieved, to read out this picture and shift the relative phase at a well defined amount and take a new picture with the same integration time. This method allows using every photon, which is produced at the output of the image intensifier and which reaches the camera, to build up the signal.

An instrument for lifetime imaging operated in heterodyne mode can achieve qualitatively exactly identical images as a homodyne setup (given identical hardware and samples). French (1996) for example uses a fast camera in a heterodyne setup, which allows the readout of four images per difference frequency period at a difference frequency of 32 Hz. He then software integrates many images at identical phase settings to reach a good signal to noise ratio. This requires long integration times, because in addition to the natural photon noise the readout noise of the camera plays an important role in this case. An advantage mentioned for this particular heterodyne setup is the small adulteration of the measured lifetimes caused by photobleaching because of the short acquisition time for each intensity image. But the same applies for a fast measurement with a homodyne instrument (as also has been shown by French (1996). Nevertheless he attributes an advantage to the heterodyne method in this case). The short acquisition time is no method inherent limit, but depends on the hardware used. With both methods, homodyne and heterodyne setups, fast measurements are possible, which reduces the effect of photobleaching on the measurement, but has its costs in the signal to noise ratio (and of course in both methods software integration in combination with short measurements can be used). A good compromise between acquisition time and signal to noise ratio has to be found in every case.

But also with a heterodyne setup the image acquisition can be adjusted so that each image is acquired with optimal signal to noise ratio. This can be done by selecting a longer period of the difference frequency and accordingly longer camera integration times. The homodyne method offers more comfort in this respect, because only the camera integration time needs to be adjusted.

But it has to be stated again, that if one uses the heterodyne setup in the way described by French, so that in principle all photons from the image intensifier are collected, there is

theoretically no difference between homodyne and heterodyne mode. For every special data acquisition and analysis technique, like for example the Normalized Difference (not discussed in this work, but see Schneider and Clegg 1997; Holub *et al.* 2000) in the homodyne mode, which allows to suppress and enhance special lifetimes in the image simply by changing the phase at the image intensifier, there is a corresponding method in the heterodyne mode and vice versa (in the heterodyne mode one would shift the pulse, triggering the image acquisition, instead of the phase).

The heterodyne mode has a clear advantage for non-imaging applications like lifetime measurements in cuvettes (Jameson *et al.* 1984), because the output signal can be electronically filtered with a narrow bandpass filter of the difference frequency in addition to the digitally Fourier filtering in the computer, which enhances the signal to noise ratio without additional time loss. But no camera with a good resolution exists at the moment, where the signal from every pixel would undergo electronical filtering during the readout. Therefore digital filtering in the computer has to be applied and it cannot be made use of this advantage of the heterodyne mode for imaging applications. Both modes use digital Fourier filtering and stay therefore equivalent. An instrument operating in the homodyne mode requires phase shift capabilities. The heterodyne setup in comparison does not need phase shift capabilities, but needs additional signal generation to obtain the cross-correlation frequency and pulse generation for the triggering of the image acquisition.

5.5 Apparent single lifetimes of systems with multiple lifetime components: Resolving two components with single frequency

Differing lifetime values from phase and modulation (as we measure for *C. reinhardtii*) can only be understood with two or more single exponential decay components. Measurements of the lifetime of Chl *a* fluorescence on *C. reinhardtii* in the time-domain have been analyzed with 3 components (Haehnel *et al.* 1983) to include the results of intermediate fluorescence levels. It was stated that at F_0 and F_{max}-levels the fluorescence decay was practically double-exponential.

In order to resolve a second lifetime component with measurements in the frequency domain, in general light modulation with at least two frequencies would be necessary.

Nevertheless we can deconvolve the separate times with certain assumptions as follows. If phase Φ and modulation M at one frequency and the lifetime of one component τ_1 are known, the second component τ_2 together with its amplitude a_2 are determined for a two component system (Weber 1981; see also Jameson and Gratton 1983; in imaging applications: Gadella Jr. *et al.* 1994; for a historical note: Jameson 2001):

$$\tau_2 = \frac{\beta + \omega\tau_1}{\beta\omega^2\tau_1 - \omega} \qquad \beta = \frac{M\cos\Phi - (1+\omega^2\tau_1^2)^{-1}}{M\sin\Phi - \omega\tau_1(1+\omega^2\tau_1^2)^{-1}}$$

$$f_2 = \frac{M\cos\Phi - (1+\omega^2\tau_1^2)^{-1}}{(1+\omega^2\tau_2^2)^{-1} - (1+\omega^2\tau_1^2)^{-1}}$$

where f_2 is the fractional contribution ($f_1 + f_2 \equiv 1$) to the steady state fluorescence made by the 2nd lifetime component. $f_s \equiv a_s\tau_s \big/ \sum a_s\tau_s$, where a_s is the s-th pre-exponential amplitude as given in (2.15).

In photosynthetic systems PSI in general contributes a short lifetime component of about 0.1 ns (see e.g., Gilmore *et al.* 2000), the intensity of which is constant during the transient induction curve. The intensities and lifetimes of all components of PSII are dependent on the irradiation. The long lifetime reaches 2 ns at F_{max} (cf. Holzwarth 1991). We therefore can get an idea of the lifetime components by assuming that a short lifetime component of 0.1 ns is present during each measurement. Table 1 shows the calculation of the second component for WT and NPQ-mutants from Fig. 21 and 22. The zeaxanthin accumulating mutant npq2 (in comparison to WT/npq1) always shows a shorter lifetime for the (long) lifetime component τ_2 in combination with a smaller fraction of this component. Zeaxanthin therefore quenches the Chl *a* fluorescence of PSII in *Chlamydomonas reinhardtii* by decreasing its quantum yield,

which is evidenced by a higher fraction of a short lifetime component. Apparent single lifetimes and average lifetime are 20-30 % shorter for npq2 (in comparison to WT/npq1). It may be pointed out that the rationalization given in Table 1 also accounts for the 25-35% reduction in fluorescence intensity for npq2 in comparison to WT/npq1 as a direct result of the lifetime difference. The intensity information can also be used for a better component estimation as will be discussed in the following section.

Model:	**Measured apparent single lifetimes of Chl *a* fluorescence**	**For a two lifetime component system with τ_1 = 0.1 ns**			
		Second lifetime component	**Pre-exponential amplitude/ Fractional intensity**	**Average lifetime** $\langle\tau\rangle=\Sigma\ f_i\tau_i$	**Calculated intensity** $I=\Sigma\ a_i\tau_i$
WT/npq1 (Fig. 21)	τ_{phase} = 1.11 ns τ_{mod} = 1.78 ns	τ_2 = 1.99 ns	a_2 = 10 % f_2 = 70 %	$\langle\tau\rangle$ = 1.42 ns	I = 0.30 ns
npq2 (Fig. 21)	τ_{phase} = 0.85 ns τ_{mod} = 1.44 ns	τ_2 = 1.69 ns	a_2 = 8 % f_2 = 61 %	$\langle\tau\rangle$ = 1.07 ns	I = 0.23 ns
WT (Fig. 22)	τ_{phase} = 0.96 ns τ_{mod} = 2.09 ns	τ_2 = 2.70 ns	a_2 = 5 % f_2 = 59 %	$\langle\tau\rangle$ = 1.62 ns	I = 0.23 ns
npq1 (Fig. 22)	τ_{phase} = 0.95 ns τ_{mod} = 2.52 ns	τ_2 = 3.55 ns	a_2 = 4 % f_2 = 58 %	$\langle\tau\rangle$ = 2.10 ns	I = 0.23 ns
npq2 (Fig. 22)	τ_{phase} = 0.73 ns τ_{mod} = 1.79 ns	τ_2 = 2.60 ns	a_2 = 3 % f_2 = 48 %	$\langle\tau\rangle$ = 1.30 ns	I = 0.19 ns

Table 1: Two lifetime component analysis

Apparent single lifetimes τ_{phase} and τ_{mod} from lifetime-resolved images of *C. reinhardtii* at F_P with an illumination intensity of 2500/2750 µmol photons m^{-2} s^{-1}, extracted by global pixel analysis of image regions (Fig. 21) or from fluorescence lifetime transients (Fig. 22). The second lifetime component τ_2 and its normalized fractional intensity f_2 (or pre-exponential amplitude a_2) were calculated (Weber 1981) for an assumed two lifetime component system where the first lifetime component is τ_1 = 0.1 ns. For this case the average lifetime $\langle\tau\rangle = f_1\ \tau_1 + f_2\ \tau_2$ and the integral of the intensity decay over time $I = a_1\ \tau_1 + a_2\ \tau_2$ (a value proportional to the fluorescence intensity under identical concentration conditions) are also given.

5.6 A global "possibility fit" for the analysis of fluorescence lifetime transients

For the fluorescence lifetime transient we measure simultaneously the fluorescence intensity, τ_{phase} and τ_{mod} at each time point of the fluorescence transient starting from the "P" level. Qualitatively the intensity in all cases seems to follow τ_{phase} (but not τ_{mod}). That evokes the question if the intensity curve (the transient) also quantitatively can be understood as the result of the measured lifetime changes. To answer this question a nonlinear least squares curve-fitting procedure has been applied, which globally fits intensity-, τ_{phase}- and τ_{mod}- curves and incorporates the Weber-algorithm described in the previous section (Appendix 5.5). Again one assumes the existence of only two lifetime components τ_1 and τ_2 (minimum requirement). The intensity curve can be fitted according to: Intensity = Matchfactor * ($a_1 \tau_1 + a_2 \tau_2$). During the fit the component τ_1 is varied[35] for each time point. Then τ_2, a_1 and a_2 are calculated from τ_1 and the measured τ_{phase} and τ_{mod} at this time point (Weber-algorithm). If the changes in intensity are the direct result of the changes in the lifetimes, a fit will be possible and a global matchfactor (valid for all time points) can be found. Application of such fitting procedure showed that it is possible to find a global matchfactor for the fluorescence lifetime transients (see Fig. 30). The intensity changes of the fluorescence lifetime transients therefore could be a direct result of the observed lifetime changes. But only in the case that a fit would not be possible, one would have direct evidence of non-lifetime related intensity changes (e.g. changes in the absorption cross section or state changes). Such changes still can play a role during the measurement (see discussion of the comparison of the lifetime transients of the mutants between each other in section 3.2.2.2). The fit does not exclude such possibility. The range of variability therefore is large in this method and if a fit is possible there is not only a single matchfactor. But for a fixed matchfactor there is only a single lifetime composition for each transient point. Therefore a fit with fixed matchfactor allows the determination of the possible changes in the lifetime composition under the assumption that the intensity changes are the direct result of the lifetime changes. A higher matchfactor forces the fit to a shorter lifetime composition. In combination with the known range of the lifetime composition of photosynthetic samples (see previous Appendix 5.5) the method allows to obtain information about the changes of the lifetime composition during the transient. (Without taking the intensity information into account and without applying a fitting routine, the calculation shown in Table 1 can also be performed for each point of the lifetime transient as a simple way to provide information on the composition behavior).

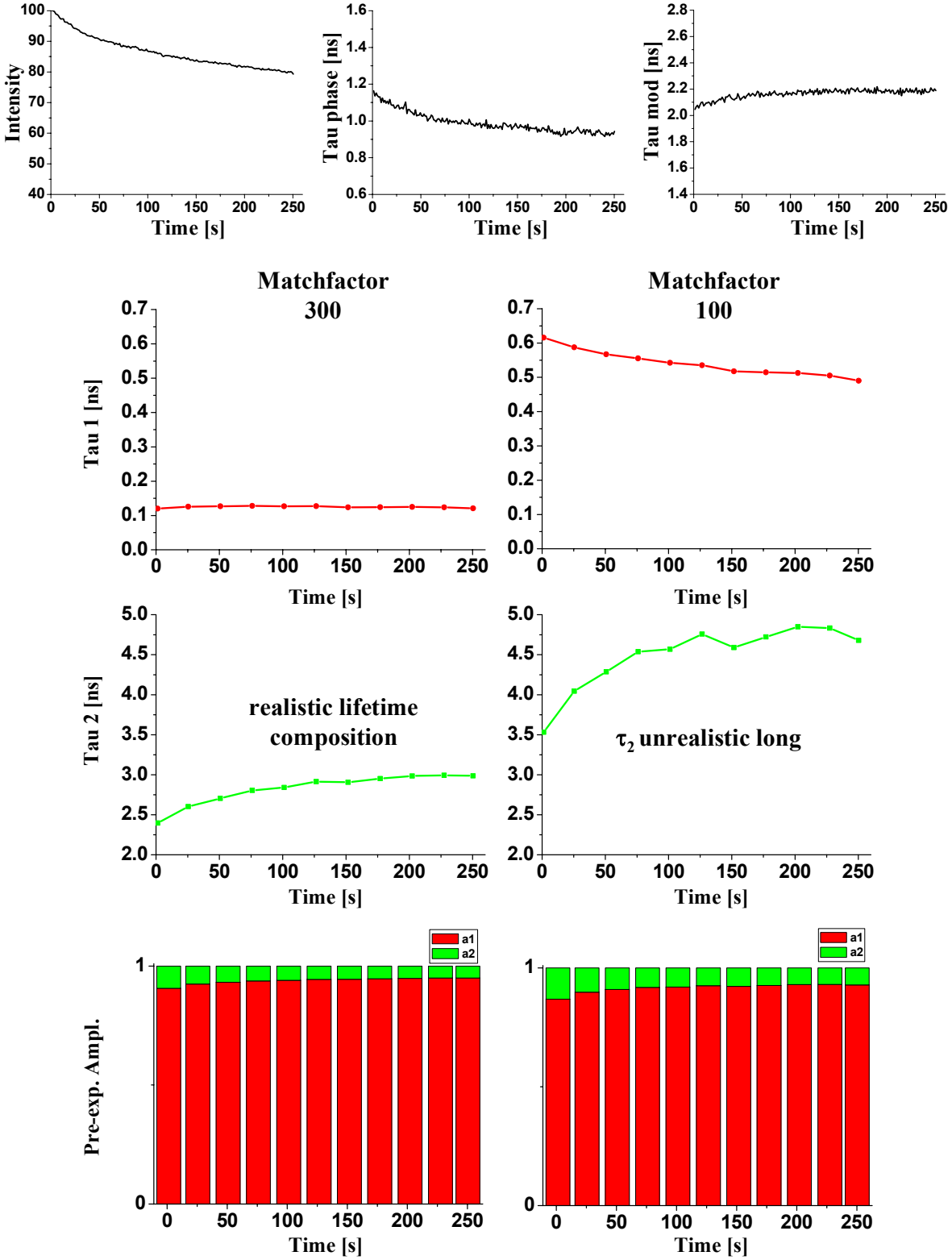

Fig. 30: Global "possibility fit" for a two lifetime component analysis of a lifetime transient
The fluorescence lifetime transient shown in the first line (WT, DCMU treatment; 2750 µmol (photons) m^{-2} s^{-1}) is analyzed with a nonlinear least squares curve-fitting procedure, which incorporates the Weber-algorithm. The fluorescence intensity is fitted according to: Intensity = Matchfactor * (a_1*τ_1 + a_2*τ_2). For each time point in the graphs, τ_1 is varied and used for the calculation of τ_2, a_1 and a_2 from the measured τ_{phase} and τ_{mod} (Weber-algorithm). The results from fits at two differently fixed matchfactors (300 and 100) are shown. For a fixed matchfactor there is only a single possible lifetime combination for each time point, which is determined by the fit. Therefore the fit of the data is perfect in both cases. At matchfactor 100 the second lifetime component displays unrealistic long lifetimes in comparison to known literature values. At matchfactor 300 realistic values for both lifetime components are displayed.

The fit showed (see Fig. 30; Matchfactor 300) that it is possible to understand the decrease in intensity and τ_{phase}, but increase in τ_{mod} of the fluorescence lifetime transient as the result of a constant 0.1 ns component τ_1 and a second component (about 2 ns), which increases in lifetime during the transient, but only in combination with a decreasing pre-exponential amplitude of this component.

5.7 Acknowledgments

I would like to thank:

Professor Dr. Robert M. Clegg for his advice during our time at the Max-Planck-Institute for Biophysical Chemistry in Göttingen and during the first years of his professorship at the University of Illinois at Urbana-Champaign, where this work has been carried out. His knowledge and scientific insight in the field of fluorescence has been a great source of inspiration.

Professor Dr. Govindjee, who encouraged my interest in photosynthesis and whose lifelong experience and knowledge in this field have been the motor for our successful collaboration, which I enjoyed very much (I will keep Rabinowitch's and your multimeter in honor).

Professor Dr. Gernot Renger for his friendly and unselfish agreement to be my advisor at the Technischen Universität Berlin, for writing a judgment of the thesis and for introducing me to interesting works in the field of photosynthesis, of which I had not been aware before. His help finally made the Ph.D. possible.

Professor Dr.-Ing. Hans Joachim Eichler from the Technischen Universität Berlin for participating in the judgment committee and writing a judgment of the thesis and Professor Dr. Karola Rück-Braun from the TU for leading the judgment committee.

Professor Dr. Enrico Gratton, who offered us with the LFD (Laboratory for Fluorescence Dynamics) a well equipped and interesting place to work, which he was leading with enthusiasm, never ending new ideas and great humor.

Professor Dr. David M. Jameson, whom I can not thank enough for our successful tRNA collaborations and a lot of fun during his regular visits in Urbana; especially for flying me to Hawaii and letting me forget the cornfields for a while; for introducing me to some unknown works of Professor Dr. Gregorio Weber and offering me the right atmosphere to study them: In Weber's armchair in his (at this time still existing) office in Urbana.

This work would not have been possible without the work of Christoph Gohlke, who wrote the computer programs for this project. His professional programming skills have not only optimized speed and functionality of the instrument during the years of development, but have created user interfaces, which are pieces of beauty by itself. But not only for his unreserved help and collaboration he deserves my special thanks, rather for his friendship.

Dr. Manfredo J. Seufferheld for our very fruitful collaboration on the Chlamy project, his enthusiasm and understanding, whenever things were not working out as they were planned.

Dr. Peter Schneider for our collaboration on fast fluorescence lifetime imaging on 5-aminolevulinic acid-induced protoporphyrin IX in cells. His pioneering work on rapid lifetime imaging has laid the foundation for the instrument presented in this work. And his enthusiasm has always been very motivating during our time in Göttingen.

Dr. Martin vandeVen for our collaboration on imaging of apple fruit skin and his constant help during his time at ISS.

Dr. Theodore Hazlett, who next to his own work in an amazing way manages to help all users and staff of the LFD, I would like to thank for his help with thousand things in the lab.

My collaborators John C. Croney, Takahisa Ishii, Prof. Dr. Steven E. Seifried, Dr. Marc Tramier for great times in Urbana and Hawaii.

I would like to thank all the people from the LFD, whom I had the pleasure to meet during my stay in Urbana, especially Dr. Osman Akcakir, Dr. Luis Bagatolli, Dr. Nicholas Barry, Dr. Sabrina Beretta, Sophia Breusegem, Dr. Christof Buehler, Dr. Albert Cerussi, Anna Celli, Tania Chakrabarty, Dr. Yan Chen (who perhaps might show me her wedding pictures some day), Melanie A. B. Cheng, Dawn Dallas, Jee Hyun Choi, Sarah Clark, Dr. Lucia D'Amico, Dr. Chen Dong, Dean A. Eckhoff, John Eid, Prof. Dr. Sergio Fantini, Dr. Mattia Filiaci, Dr. Maria Angela Franceschini, Seth Gammon, Dr. Kerry Hanson, Dr. Katarina Kis-Petikova, Dr. Don C. Lamb, Ziggy Majumdar, Prof. Dr. William Mantulin, Dr. Antonios Michalos, Maria Minchenko, Dr. Joachim Müller, Dr. Adelina Paunescu, David Posson, Dr. Timothy Ragan, Glen Redford, Qiao Qiao Ruan, Dr. Susana Sanchez (whose sense of humor and beauty I am missing very much), Prof. Dr. Paul R. Selvin, Greg Snyder, Dr. Alain Sillen, Prof. Jason Sutin, Prof. Dr. Peter So, Dr. Frank Stühmeier, Abdel K. Tahari, Elliot Tan, Dr. Vladislav Toronov, Dr. Martin P. Wolf, Dr. Ursula Wolf, Julia K. Wright, Dr. Mahalakshmi Yeditha, Dr. Weiming Yu.

Vanessa Arnold for bearing me as a roommate and showing me the beautiful things of our (wide open) surrounding.

Dr. María Alejandra Tricerri for her love and understanding, which has been my strongest source of joy and happiness; and I am most thankful that my place is still at her side and her place at my side.

Wally Holzner not only for teaching me how to machine, but also for his generous gift of a 1985 Mazda 626 and for introducing me to what in the states is called “American culture”.

I thank Prof. Dr. Krishna Niyogi for his generous gift of the xanthophyll-cycle mutants and Prof. Dr. Gerard Marriott for his loan of a Zeiss Axiovert 135 microscope. The work was supported by a grant of the National Institutes of Health (NIH, PHS 5 P41 RRO3155) and the personal funds of Horst and Ursula Holub.

5.8 Curriculum Vitae

Personal Information

Name:	Oliver Holub
E-mail:	ollihol@web.de
Website:	http://lfd.uiuc.edu/staff/holub/
Date and Place of Birth:	1 November 1970, Hanover, Germany
Citizenship:	German
Marital status:	Single

Education

1977 – 1979	Elementary school of the Brothers-Grimm-School, Hanover
1979 – 1981	Elementary school of Wennigsen
1981 – 1983	Orientierungsstufe Wennigsen
1983 – 1990	Matthias-Claudius-Gymnasium (High school), Gehrden Degree: Allgemeine Hochschulreife (Abitur) 8.5.1990
1990 – 1991	Basic military service at Neustadt am Rübenberge and Hanover Bothfeld

Academic Education

1991 – 1996 **Studies of Physics**
Georg-August-University of Göttingen
Pre-diploma 15.10.1993 (Grade: 'Very good')
Georg-August-University of Göttingen &
Max-Planck-Institute for Biophysical Chemistry, Göttingen
Department of Molecular Biology, Director: Prof. Dr. Thomas M. Jovin
Degree: Diploma in Physics (**Dipl. Phys.**) 31.10.1996 (Grade: 'Very good')
Topic of diploma thesis: "Orientation dependency of Förster Fluorescence Resonance Energy Transfer between similar dye molecules in double-stranded DNA"
Supervisor: Prof. Dr. Robert M. Clegg
University supervisors: Prof. Dr. Erwin Neher and Prof. Dr. Rainer Blatt

1997 – 2002 **Doctorate of natural sciences**
Georg-August-University of Göttingen &
Max-Planck-Institute for Biophysical Chemistry, Göttingen
08/97 – 08/01 University of Illinois at Urbana-Champaign, USA
Department of Physics, Laboratory for Fluorescence Dynamics,
Director: Prof. Dr. Enrico Gratton
Technical University of Berlin
Max-Volmer-Institute for Biophysical Chemistry and Biochemistry
Degree: **Ph.D.** (**Dr. rer. nat.**) 2003
Topic of Dissertation: „Fluorescence lifetime imaging at video rate - a new technique in photosynthesis research"
Supervisor: Prof. Dr. Robert M. Clegg
University supervisor: Prof. Dr. Gernot Renger

Publications

- **Fluorescence lifetime imaging (FLI) in real-time - a new technique in photosynthesis research**. Oliver Holub, Manfredo J. Seufferheld, Christoph Gohlke, Govindjee and Robert M. Clegg. Photosynthetica 38(4) 581-599, 2000.
- **Fluorescence Lifetime-resolved Imaging. Measuring lifetimes in an image. Why do it? How to do it. How to interpret it**. Robert M. Clegg, Oliver Holub and Christoph Gohlke. Methods in Enzymology, Volumes on Biophotonics, 2002. Submitted.
- **Binding of ethidium to yeast tRNA^{Phe} : A new perspective on an old Bromide**. Marc Tramier, Oliver Holub, John C. Croney, Takahisa Ishii, Steven E. Seifried and David M. Jameson. Journal of Fluorescence; Special issue "Seventh International Conference on Methods and Applications of Fluorescence Spectroscopy, Imaging and Probes", Amsterdam, The Netherlands, September 16-19, 2001.

Endnotes

[1] k_F is the Einstein-coefficient for spontaneous emission A_{21}.
[2] For a fascinating introduction into the pre-war literature of photoluminescence along its original sources, see Nickel (1996; 1997; 1998). Jabłoński published his energy diagrams in (1933; 1935). Nickel shows that Perrin (1929; 1931) deserves credit for it and even goes so far to talk of "Perrin diagram" and "Lewis-Kasha diagram", because Lewis and Kasha (1944) named their own diagram after Jabłoński.
[3] The slow nucleic movements can be neglected against the fast electric movements during absorption, which allows to use the adiabatic (Born-Oppenheimer) approximation. The Franck-Condon principle (Franck 1925; Condon 1926; Franck 1927; Condon 1947) then states that electronic transitions occur at unchanged nucleic coordinates in the Franck-Condon state, which does not have to be the equilibrium state of the new electronic state. The nuclei of the molecule then follow the new forces, which act on them, and relax from this higher vibrational state into their new ground state in a time much shorter than the lifetime of this state. The probability of a transition from the ground state into a Franck-Condon state is dependent on the difference of the nucleic coordinates of the two vibrational excited states before and after relaxation.
[4] As nearly always there are exceptions for a rule. Anti-Stokes fluorescence is the emission of fluorescence light, which has a shorter wavelength than the excitation light. This deficiency in energy balance is compensated by the internal heat energy of the luminescent molecules either by hot-band (higher vibronic states) fluorescence or hot-band absorption (Pringsheim 1921; for introduction see Nickel 1996). Spectral overlaps between excitation and emission spectrum are not uncommon even at temperatures of 300 K. In this case red-edge excitation always leads to the emission of anti-Stokes photons, but on average still more light energy is transformed into thermic energy than the other way, so that the center of mass of the fluorescence spectrum is at longer wavelength than the one of the excitation spectrum. This is the more general formulation of Stokes rule, which is always valid.
[5] There are major interactions of the fluorescent molecule with the surrounding solvent shell that affect the shape of the spectrum. The solvent dipoles will orient themselves around the fluorophore's ground state dipole to minimize the interaction energy. When the fluorophore is excited, the excited state dipole is often much different than the dipole moment of the ground state. The changed charge distribution in the molecule can result in dramatic changes in the proton affinity of the molecule, which results in reorientation processes of the solvent shell. During all of these processes the molecule loses energy (Stokes shift between absorption and emission spectrum). The polarity of the solvent is especially important. In polar solvents the surrounding molecules cannot adjust instantaneously to the new excited state dipole. During the relaxation time, in which the solvent dipoles are rearranging to minimize the interaction energy, the fluorophore emits a photon and returns to the ground state. If the solvent relaxation time is much faster than the fluorescence lifetime, then there is complete relaxation of the excited state (maximal Stokes shift); if the solvent relaxation time is much slower than the fluorescence lifetime, then there will be little or no solvent relaxation during the lifetime and no red shift. When solvent relaxation time and fluorescence lifetime are on the same order, then the spectrum will broaden and the time dependent spectral shifts can be observed.
[6] In this context one should also mention Vavilov's law (Wawilow 1927), which states that the quantum yield of a fluorescence does not depend on the wavelength of the exciting light.
[7] In some cases thermal reoccupation of S_1 from T_1 by ISC is possible. The following emitted fluorescence is called E-type delayed fluorescence (E for eosin), which is spectrally identical to prompt fluorescence, but has a long lifetime (corresponding to the lifetime of the triplet state).
[8] Indirect lifetime measurements were also obtained around this time. Two methods shall be mentioned here. Especially Perrin's equation $\frac{r_0}{r} = 1 + \frac{k_B \tau}{V_h} \cdot \frac{T}{\eta}$ allowed lifetime determinations by steady-state (not time-resolved) polarization measurements. Perrin's equation expresses the linear relation between the reciprocal of the measurable polarization anisotropy $1/r$ against T/η (T is the temperature and η the viscosity of the solution). r_0 is the limiting anisotropy of the fluorophore, k_B Boltzmann's constant and V_h the effective molar hydrodynamic volume of the molecules $V_h = N_A(4\pi/3)r^3$, where r is the radius of a sphere, whose volume is approximately equal to the molecular volume of the dye. Perrin's equation in the form given here is modified from its original version (Perrin 1926) only by the use of the more convenient polarization anisotropies r (Jablonski 1957, 1960), which are additive for different fluorescent species (Weber 1952), instead of the polarization degree P.
A second method for indirect lifetime measurements was also already applied by Perrin (Perrin 1926, 1929). Einstein (1917) had derived the fundamental relationship between the transition probabilities for induced absorption B_{12} (transition from lower state 1 to upper state 2) and emission B_{21} and that for spontaneous emission A_{21}. He showed that the spontaneous emission probability was directly proportional to the corresponding absorption probability and to the third power of the frequency of the transition. Therefore Perrin could make use of the following relation between lifetime and absorption spectrum:

$\frac{1}{\tau_0} = A_{21} = 8 \times 2303\, \pi\, c\, \tilde{\nu}_{21}^{\,2}\, n^2\, N_A^{-1} \frac{g_1}{g_2} \int_{linewidth} \varepsilon\, d\tilde{\nu}$, written here in the notation of Strickler and Berg (1962). A_{21} is the Einstein transition probability coefficient (the rate constant) for spontaneous emission from an upper state 2 to a lower state 1; c is the speed of light in a vacuum; $\tilde{\nu}_{21} = \nu_{21} / c$ is the frequency of the transition in cm^{-1}; n is the refractive index of the medium; N_A is Avogadro's number; g_1 and g_2 are the degeneracies of lower and upper state, respectively; ε is the molar extinction coefficient; the integration extends over the absorption band; τ_0 as introduced in (2.3) is the maximum possible mean lifetime of state 2 (the lifetime if spontaneous emission is the only deactivation process). The formula is strictly applicable only to atomic transitions with sharp absorption band and if absorption and emission occur at the same wavelength. Nevertheless it can be used for first lifetime estimations. In case of a structureless and symmetric absorption band the integral can be further simplified: $\int_{band} \varepsilon(\tilde{\nu})\, d\tilde{\nu} \approx \varepsilon_{\max} \cdot \Delta\tilde{\nu}_{fwhh}$; here $\Delta\tilde{\nu}_{fwhh}$ denotes the full width at half height of the absorption band. The estimation of the intrinsic lifetime from the absorption spectrum can then be written: $\frac{1}{\tau_0} \approx 2.89 \cdot 10^{-9}\, n^2\, \frac{g_1}{g_2}\, \tilde{\nu}_{\max}^2\, \varepsilon_{\max}\, \Delta\tilde{\nu}_{fwhh}$

Strickler and Berg (1962) were able to derive a modification of the formula, which allows lifetime determination of organic molecules from their absorption and fluorescence emission spectra with an accuracy of a few percent: $\frac{1}{\tau_0} = 8 \times 2303\, \pi\, c\, n^2\, N_A^{-1} \left\langle \tilde{\nu}_f^{-3} \right\rangle^{-1} \frac{g_1}{g_2} \int \varepsilon\, d\left(\ln \tilde{\nu}\right)$, where $\left\langle \tilde{\nu}_f^{-3} \right\rangle$ denotes the mean value of the reciprocal of the third power of the emission spectrum: $\left\langle \tilde{\nu}_f^{-3} \right\rangle = \frac{\int \tilde{\nu}_f^{-3}\, I\left(\tilde{\nu}_f\right) d\tilde{\nu}_f}{\int I\left(\tilde{\nu}_f\right) d\tilde{\nu}_f}$; here $I\left(\tilde{\nu}_f\right)$ denotes the wavelength-dependent intensity in the fluorescence emission spectrum, measured in terms of relative numbers of quanta at each frequency, rather than in the usual energy units.

[9] In the following section we will talk of "fluorescence", although the mathematical treatment in its generality includes any form of luminescence.

[10] It is obvious that at certain levels distributions need to be used for a correct lifetime description even if a single discrete lifetime component should be the physical reality. This is dictated first by the measurement error and second – if one can manage to reduce the measurement error to this level – by inherent distributions demanded by Heisenberg's uncertainty principle (uncertainty in photon energy and time of excitation). But both of these points are of no importance in the everyday experimental laboratory praxis. Even complex fluorescence decay characteristics measured in high-precision fluorometrically studies can in general be described by three or four exponential components (and a variety of fluorophores displays a single exponential decay in solution). It is of no use to construct models involving high numbers of exponential components, which cannot be distinguished from models using less exponentials in the frame dictated by the measurement error. Especially biological samples measured at room temperature display temporally changing heterogeneities of their physical and chemical conditions, which soon set a limit to the still useful component number. Therefore the number of lifetime components S in many cases does not correspond to the molecular species. It furthermore evokes the question if discrete lifetime components are the correct physical description for samples with heterogeneous conditions. For molecules, which for example can explore a variety of conformational states, or for sterically conditioned small fluorescence changes due to fluorophore movements, one would expect a large number of only slightly different lifetimes. Therefore lifetime distributions in certain cases can supply the better description, which was shown first for proteins (Alcala *et al.* 1987a, b, c). Nevertheless, even if one knows about the molecular distributions, one still might use discrete lifetimes as long as they provide a sufficient description of the experimental data. Practically lifetime distributions become important if a discrete analysis results in two or more only slightly different lifetime components, which cannot be fitted unambiguously or reproducible.

[11] The theoretical description of lifetime measurements using the phase and modulation method has been presented by Duschinsky (1933a; 1933b). A geometrical formulation of it can be found in (Jameson *et al.* 1984). Of importance are further the descriptions given in (Spencer and Weber 1969) and (Weber 1981). The theoretical description has been summarized for imaging applications by Schneider, Jovin and Clegg in its general form (Clegg and Schneider 1996; Clegg *et al.* 1996; Schneider 1997) and for the case of sinusoidal excitation (1997), which is of special interest for the operation of the instrument described in this work.

[12] Although the full theoretical description of the phase and modulation method for any excitation function can't be treated here in detail, a short outline shall be given. If the intensity of the excitation light is a periodic function of time with the fundamental frequency $f = \omega / 2\pi$, then it may be expressed as a Fourier series (in

complex notation, $i = \sqrt{-1}$): $E(t) = \sum_{n=-\infty}^{\infty} E_n \; exp\,(i\,n\,\omega\,t)$, where E_n is the amplitude of the n^{th} harmonic frequency component $n\omega$. These amplitudes are complex numbers of the form $E_n = |E_n| \; exp\,(i\,\phi_n^E)$ with real magnitudes $|E_n|$ and phases ϕ_n^E , which are temporally constant and depend on the special form of the excitation *E(t)*. As an intensity, the excitation *E(t)* furthermore is not negative and a real quantity, therefore $E_{-n} = E_n^* \;\Rightarrow\; \phi_{-n}^E = -\phi_n^E$. The special case of pure sinusoidal excitation is then obtained from *E(t)* by summation from *n* = -1 to 1:

$$E_{\sin}(t) = |E_0| + |E_1|\,[\exp\,(i(\omega\,t + \phi_1^E)) + \exp\,(-i(\omega\,t + \phi_1^E))] = |E_0| + |E_1|\;2\cos(\omega\,t + \phi_1^E)$$

For the case of a single lifetime component, solving $dN(t)/dt = E(t) - N(t)/\tau$ with the Fourier series *E(t)* gives the steady-state solution $N(t) = \sum_{n=-\infty}^{\infty} \frac{E_n\,\tau}{1 + i\,n\,\omega\,\tau}\; exp\,(i\,n\,\omega\,t)$. In this expression the amplitude of the n^{th} harmonic component $E_n\,\tau/(1 + i\,n\,\omega\,\tau)$ can be written in polar notation in the form $A_n\; exp\,(-i\,\Phi_n)$, where $A_n = \frac{E_n\,\tau}{\sqrt{1 + (n\,\omega\,\tau)^2}} = E_n\,\tau\,M_n$ and $\tan\Phi_n = n\,\omega\tau$. The extension of this general description to multiple lifetime components is straightforward (see e.g. Clegg and Schneider 1996). Phase Φ_n and modulation M_n in principle can be experimentally determined for each frequency component *n*. While the fundamental frequency component (sinusoidal excitation) suffices for determinations of a single lifetime component, higher harmonic components accordingly allow the determination of multiple lifetime components. But practically such a procedure requires longer measurement times to reach the accuracy for resolving the harmonic components; further samples are needed, which do not change during the measurement time. These requirements are often not met by biological samples.

[13] For optimizing the signal from a particular component, Teale (1983) states that the frequency must maximize the product of phase Φ and modulation *M*, i.e. the condition $\frac{d}{d\omega}(\Phi \cdot M) = \frac{d}{d\omega}\left(\frac{\arctan(\omega\tau)}{\sqrt{1 + (\omega\tau)^2}}\right) = 0$, which is the case for $\omega\tau \approx 1.16$. But for highest sensitivity the condition should be formulated:

$$\frac{d}{d(\omega\tau)}\left(\frac{d}{d(\omega\tau)}\Phi \cdot \left|\frac{d}{d(\omega\tau)}M\right|\right) = \frac{d}{d(\omega\tau)}\left(\omega\tau\left(\frac{1}{1 + (\omega\tau)^2}\right)^{5/2}\right) = 0$$

, which is the case at $\omega\tau = 1/2$.

[14] Measurements employing reflected excitation light practically are connected with certain drawbacks, which are discussed in more detail in the section about the calibration of the instrument (3.2.1.2). Reflections on all optical components give rise to interference patterns over the whole image. While a global image analysis over these patterns allows reproducible calibration, it was found that phase and modulation of the reflected light did not absolutely correspond to the signal from a sample with a lifetime of zero ns.

[15] It might not be obvious why the gain modulation should differ from pixel to pixel. But cathode modulated image intensifier can show an iris effect, which is an inhomogeneous distribution of the modulation signal over the image (see 3.1.1.5).

[16] The identical analysis can also be performed for the heterodyne detection. In this case one considers *K* time images spaced by $2\pi/(K\,\Delta\omega)$ s instead of the *K* phase delayed images spaced by $2\pi/K$ radians in the homodyne case.

[17] In the case of excitation of Chl *b* and some carotenoids, the excitation energy is rapidly transferred to Chl *a* molecules, because of their energetically lower first excited singlet state. As a consequence, the energy that escapes the antenna system as fluorescence comes almost entirely form Chl *a*.

[18] As this short literature review shows, the phenomenology of NPQ is very complex. It is very well possible that multiple mechanisms at different locations are involved in NPQ. Therefore a conformational change occurs at one or multiple locations. It can not be excluded that there exist further locations, which participate in NPQ, but do not involve a conformational change.

[19] The npq2 cells had 20% higher measured $F_{0\,meas}$ values than WT/npq1 cells. Due to the higher zeaxanthin concentration in this mutant, one rather would have expected a quenching of $F_{0\,meas}$. The reason for this difference is not known (for discussion see Govindjee and Seufferheld 2002). The F_0 fluorescence intensity has multiple origins (85-90% from PS2 centered at 685 nm and 10-15% from PS1 centered at 712 nm at room temperature). If some antenna should be dissociated from the reaction center core, this would lead to a decrease

in energy transfer to the reaction center core and to apparently increased F_0. Lifetime measurements allow a comparison between the mutants, which is independent of any F_0 normalization. At this point it should be further remarked that all intensity data shown in the experimental part of this work has not been normalized.

[20] A system, hardware or software, is called real-time if it can respond in a predictable, timely way to external events (such as a hardware trigger, a newly acquired image or a request by a human operator). A hard real-time system is guaranteed to handle all events in a predictable way (a late response might cause the system to fail) while a soft real-time system can tolerate some late response. In case of an imaging application the external event is a new image ready to be read out from the CCD chip. For a video-rate (26 fps) image acquisition and visualization system to be classified as hard real-time, it would need to be able to acquire, process and display the newly incoming images within less than 38 ms under any circumstances. If the system occasionally fails to respond within that time (such that a frame drop occurs), it would be classified as soft real-time. Video cameras and frame grabbers are usually designed to be hard real-time capable. Windows based personal computer systems however do not meet general hard real-time requirements. Windows NT was designed as a general purpose operating system running dozens of processes and threads in parallel. While it offers real-time thread priorities it does not guarantee low-latency responses to events, predictable time-based scheduling, or explicit CPU or resource management. Therefore the fluorescence lifetime imaging system presented in this paper has to be considered soft real-time.

[21] A video is commonly referred to as a time sequence of images (frames). Displayed successively at a high rate, individual frames cannot be distinguished any more by a human viewer. The video broadcasting standards PAL and NTSC consider frame rates of 25 respectively 30 fps (frames per second) to be sufficient for display on CRT displays. Hence rates of 25 fps and higher are classified as video-rate.

[22] The filters allow a very good suppression of the other laser lines of more than 10^{-6}. They are installed in a manually rotatable filter wheel (New Focus, Santa Clara, CA, USA).

[23] It should be pointed out that the used AOM is not a Bragg-cell (or traveling-wave modulator), which is also often named AOM. In the Bragg-cell also a sound wave (with a carrier frequency) is send through a crystal, but gets absorbed at the adjacent crystal side. Light is hitting the acoustic wavefronts not perpendicular, but in an angle and intensity modulation is obtained by additional amplitude modulation of the traveling acoustic carrier wave. The Bragg-cell is not useful to obtain light modulations up to100 MHz as they are necessary for lifetime measurements.

[24] Although all back reflections from the optical surfaces (laser filters and crystal block) have been blocked wherever possible, rest reflections might still slightly affect the zeroth diffractive order more than the higher orders.

[25] With a velocity of sound in flintglass of about 4000 m/s and a frequency of 40 MHz for the sound wave (corresponding to the 40 MHz used for driving the AOM, resulting in 80 MHz light modulation) one calculates a wavelength of 100 μm for the standing wave in the crystal (this defines the spacing *d* of the "diffraction grating"). The crystal block has a height of 1 cm. Therefore the number of the halfwaves in the glass block is 200. This makes a difference of 200 kHz to the next resonance frequency. The light modulation therefore can be chosen in steps of 200 kHz.

[26] For the AOM as a special diffraction grating the angle θ_n , under which the constructive interference of the *n*-th order can be found, is very small $\theta_n = n * \lambda / d$. This gives for an optical wavelength of 500 nm and d=100 μm (see previous footnote) $\theta_n \approx n * 5$ mrad. Therefore the clear separation of the diffractive orders requires a light path in the order of meters. But it should be stated at this point, that in principle a construction is possible, which does not require a long light pass at all. The beam of the selected order is coupled (by a single lens) into a single mode fiber, which has a core diameter of 5 μm. The small fiber core could in principle be used for the selection of the diffractive order in combination with a very short light path.

[27] This applies for the system as it is sold by *Pointsource* (and as used in this work). But their connectorized optics, which can be attached to FC connectors, allows a cheaper construction, which we have tested and which nevertheless works fine. A single mode fiber can be connectorized with FC connectors on both ends (one end can be polished in a slight angle to prevent backreflections of the incoming laser beam) instead of the fixed optics on one side as sold by the company. Then two of their connectorized optics can be attached and provide a working system similar to the one sold by the company. *Pointsource* guarantees a throughput efficiency of ≥ 70 %. Depending on the quality of the FC connectorization, the throughput of the self-configurated fiber can be lower.

[28] Especially in combination with the long optical path, laser pointing instabilities can result in changes at the coupling optics, which can give rise to large changes at the fiber output. We did not observe this problem with the used argon-ion laser, but have seen it with other laser setups before. The resulting changes at the fiber input coupler have to be large. It should be mentioned on the other hand, that single mode fibers in many applications are used especially to improve the beam pointing error of laser setups, because the output is independent from small laser beam drifts with time at the coupler.

[29] The lifetime of most fluorophores is independent of the illumination intensity. Therefore in most applications the differences in the illumination intensity will not affect the measured lifetimes and will not show up in the

lifetime images. For the experimental setup the more important point is that the illumination intensity does not change during the time of measurement. The use of a single mode fiber instead of a multimode fiber ensures this point. But even for samples, for which the illumination light intensity does effect the lifetime measurement (as it is the case for photosynthetic samples), the Gaussian illumination profile does not constitute a problem. The profile can be exactly determined and then the illumination intensity of every image point is known. The dependency of the lifetime from the excitation intensity is then automatically measured in each image.

[30] Slight tilting of the emission filter removed the reflections. But the spectral properties of all interference filters are "angle-sensitive" and will therefore change if used in tilted position. One therefore has to make sure not to exceed drastically the typical play in filter positioning provided by the microscopic setup. Another simple way to remove the reflections is the removal of the emission filter from the filter slider. It can be placed for example in front of the image intensifier. But such procedure on the other hand removes the comfort of fast filter changes provided by the filter slider.

[31] IFR acquired Marconi Instruments in 1998 and therefore sells nowadays the well-known Marconi series of signal generators.

[32] Many fluorescence lifetime measurements on photosynthetic systems employ direct time domain techniques. It is important to realize that in the time domain, intensity changes during the measurement also give rise to similar artifacts affecting both amplitude and lifetime composition.

[33] For the single purpose of fluorescence lifetime transient measurements relatively simple, cheap and more rapid instruments can be constructed, which use a modulated photomultiplier instead of image intensifier and camera.

[34] The cell cycle of *Chlamydomonas* seems to be regulated by what has been called an "hourglass" category of biological timers (Donnan and John 1983; Harris 1989, pp. 121). Light and dark periods function as a stimulus for cell division commitment points and the cell cycle is regulated by photosynthetic activity. If one is subjecting a light-grown culture to the dark overnight, one will get small cells of identical size at the next day (Harris 1989, pg. 37).

[35] The first lifetime component has been arbitrarily chosen to be the variable. Variation could be also performed in one of the other parameters – with the same result: if one parameter is chosen, the others are determined by the Weber-algorithm.